UNIVERSITÀ DEGLI STUDI DI PADOVA

DIPARTIMENTO DI INGEGNERIA INDUSTRIALE

CORSO DI LAUREA IN INGEGNERIA CHIMICA E DEI PROCESSI INDUSTRIALI

Tesi di Laurea Magistrale in Ingegneria Chimica e dei Processi Industriali

The role of the substrate porosity, Cu loading and redox state of $CuO/CeO_2/Al_2O_3$ catalyst in the CO Preferential Oxidation in H_2-rich mixtures

Relatore: Prof. Paolo Canu
Correlatrice: Ing. Benedetta Oliani

Laureando: MIRKO SCANFERLA

ANNO SCOLASTICO 2021-2022

Abstract

The Preferential Oxidation of carbon monoxide (CO-PROX) reaction is meaningful processes for CO removal in trace amounts from a reformate stream rich in H_2 to be further utilized in Fuel Cell applications. Catalysts based on transition metal oxides (e.g $CuO/CeO_2/Al_2O_3$) were identified as potential candidates for CO-PROX in H_2-rich reformate gas thanks to their high activity towards CO oxidation and their crucial role in the reduction or replacement of platinum-group metal (PGMs)-based catalysts.

In this work, six catalytic material were provided by National Center for Scientific Research "Domokritos" (NCSRD) as a part f an active collaboration. The catalyst were synthesised with two methods(ADP and EISA), which differ in the methodology employed for the deposition of CuO-Cu on the surface of the catalytic substrate. ADP catalysts differed according to the loading of copper oxide (15,20 and 30%), while EISA catalysts were calcined at different temperatures (400,550 and 900°C). A fixed GHSV value ($20000h^{-1}$) and a specific thermal ramp (up to 280°C) were taken into account for the verification of the catalytic activity.

Activity experiments in a standard plug-flow reactor showed that 20% CuO loading has the highest performance among the ADP samples, with a maximum CO conversion of 80% at 185°C and 100% selectivity for CO oxidation up to 170°C. However, the 20% sample synthesized with EISA and calcined at 900°C showed the highest activity among all the samples, with 90% of CO conversion at 210°C and H_2 conversion lower than 0.5% from 250°C. A weak deactivation of the 20% $CuO/CeO_2/Al_2O_3$-ADP sample was obtained as higher temperatures were needed to achieve the same performance of the fresh catalyst.

In the operational range of the reaction, the catalyst is subjected to a continuous cycle of reduction and oxidation, due to the high presence of hydrogen (a strong reducing agent) and the fact that the most stable form of the catalyst is the oxidized state. This redox cycle causes the catalyst to consume some of the oxygen in the mixture and thus reduce the possible conversion of CO WGS reaction cannot take place for temperature below to 155°C because the catalyst is not active towards the hydrogen oxidation.

Riassunto

La reazione di ossidazione preferenziale del monossido di carbonio (CO-PROX) è un processo significativo per la rimozione delle tracce di monossido di carbonio presenti in un flusso di riformato ad elevato contenuto di idrogeno, il quale può essere ulteriormente utilizzato in diverse applicazione, come le celle a combustibile. I catalizzatori basati su ossidi di metalli di transizione (come ad esempio il catalizzatore utilizzato in questo lavoro, $CuO/CeO_2/Al_2O_3$), sono stati identificati come potenziali candidati per la reazione di CO-PROX su gas riformati ad elevato contenuto di H_2, grazie alla loro elevata attività verso l'ossidazione del CO e al loro ruolo cruciale nella riduzione o sostituzione dei catalizzatori basati su metalli nobili (come i PGM), o catalizzatori a base di oro.
Questo lavoro ha previsto una collaborazione attiva tra l'Università degli Studi di Padova ed il centro di ricerca "National Center for Scientific Research "Domokritos" (NCSRD)", con sede centrale il Grecia. Il centro di ricerca ha fornito sei materiali catalitici da loro sintetizzati. I catalizzatori sono stati sintetizzati con due metodi (ADP e EISA), che differiscono nella metodologia impiegata per la deposizione di CuO-Cu sulla superficie del substrato catalitico. I catalizzatori ADP si differenziano in base al carico di ossido di rame (15, 20 e 30%), mentre i catalizzatori EISA sono stati calcinati a diverse temperature (400, 550 e 900°C).
Per la verifica dell'attività catalitica sono stati presi in considerazione un valore GHSV fisso (20000^{-1}) e una rampa termica specifica (fino a 280°C).
Gli esperimenti di attività in un reattore plug-flow standard hanno mostrato che il 20% di carico di CuO ha il rendimento più alto tra i campioni ADP, con una conversione massima di CO dell'80% a 185°C e una selettività del 100% per l'ossidazione di CO fino a 170°C. Tuttavia, il campione del 20% sintetizzato con EISA e calcinato a 900°C ha mostrato la più alta attività tra tutti i campioni, con il 90% di conversione di CO a 210°C e una conversione di H_2 inferiore allo 0,5% da 250°C. Una debole disattivazione del campione 20%-$CuO/CeO_2/Al_2O_3$-ADP è stata ottenuta poiché sono state necessarie temperature più alte per ottenere le stesse prestazioni del catalizzatore fresco.
Nell'intervallo operativo della reazione, il catalizzatore è sottoposto a un ciclo continuo di riduzione e ossidazione, dovuto all'elevata presenza di idrogeno (un forte agente riducente) e al fatto che la forma più stabile del catalizzatore è lo stato

ossidato. Questo ciclo redox fa sì che il catalizzatore consumi parte dell'ossigeno nella miscela e riduca così la possibile conversione di CO La reazione WGS non può avvenire per temperature inferiori a 155°C perché il catalizzatore non è attivo verso l'ossidazione dell'idrogeno.

Contents

List of Figures IV

List of Tables VIII

Introduction 1

1 Fuel Cell and Preferential Oxidation of Carbon Monoxide: State of the Art 3
- 1.1 Fuell Cells: innovative device to energy production 3
  - 1.1.1 Impurities of Fuel Cells Feedstock 6
- 1.2 Hydrogen enrichment stages required for fuel cell purpose 8
  - 1.2.1 Water Gas Shift Reaction 9
- 1.3 Preferential Oxidation of Carbon Monoxide 11
  - 1.3.1 General consideration relating the CO-PROX reactions . . . 11
  - 1.3.2 Catalysts for the Preferential Oxidation of Carbon Monoxide 13
  - 1.3.3 Reaction mechanism between noble metal and transition metal based catalyst 17
  - 1.3.4 Effect of the gas feed components on CO-PROX reaction . . 19

2 Experimental setup, procedures and methods 23
- 2.1 Procedure and experimental setup used for CO-PROX try-out . . . 23
- 2.2 Instruments and equipment used in the experimental setup 25
  - 2.2.1 Mass flowmeters 25
  - 2.2.2 Four-way solenoid valve 26
  - 2.2.3 Quartz tube reactor 27
  - 2.2.4 Gas-chromatograph Aligent HP-7820 29
  - 2.2.5 Direct thermo-conductivity detector (TCD) 32
  - 2.2.6 Micro Gas-chromatograph Variant CP-4900 33
  - 2.2.7 FT-IR IRTracer-100 Shimadzu 35
  - 2.2.8 Oxygen Sensor 36
- 2.3 Catalysts 37
- 2.4 Experimental procedures and data processing 39

2.4.1 Experimental procedures used for catalytic test 39
2.4.2 Processing of the experimental data and parameters calculated 44

3 Results and discussion 49
3.1 Equilibrium in CO-PROX reactions 49
3.1.1 Conclusion 52
3.2 Activity of $CuO/CeO_2/Al_2O_3$-ADP with different CuO loading . . . 53
3.2.1 Observations on the thermal behavior 54
3.2.2 Catalytic activity test of A-550-15 56
3.2.3 Catalytic activity test of A-550-20 60
3.2.4 Catalytic activity test of A-550-30 62
3.2.5 Conclusion 64
3.3 Activity of $CuO/CeO_2/Al_2O_3$ synthesized by EISA method 65
3.3.1 Catalytic activity test of E-900-20 65
3.3.2 Catalytic activity test of E-550-20 68
3.3.3 Catalytic activity test of E-400-20 70
3.3.4 Conclusion 71
3.4 Comparison of catalytic performance according to synthesis method 72
3.4.1 Conclusion 74
3.5 Specific features and effect of catalyst oxidation state on CO-PROX reaction 74
3.5.1 Effect of material aging on catalytic performance 76
3.5.2 Effect of the catalyst oxidation state on the activity 77
3.5.3 Presence of WGS reaction in the CO-PROX mechanism . . . 81
3.5.4 Catalytic activity tests at high GHSV 84
3.5.5 Conclusion 86
3.6 Catalytic tests carried out with isotherms protocols 88
3.6.1 Isotherm test performed on oxidized catalyst 88
3.6.2 Isotherm test on reduced catalyst 91
3.6.3 Conclusion 95
3.7 Temperature Programmed Reduction and Oxidation 95
3.7.1 Temperature Programmed Reduction (TPR) 96
3.7.2 Temperature Programmed Oxidation (TPO) 98
3.7.3 Conclusion 100

4 Conclusions 101

Future works 105

Bibliography 107

Appendix 113

List of Figures

1.1 PEM Fuel Cell schematic representation [37] 4
1.2 Quantitative representation of fuel cell material costs [16] 6
1.3 Polarization curve at different operating temperatures and carbon monoxide concentration in supplied hydrogen [20] 7
1.4 Conceptual illustration of catalutic performances of different types of catalyst for CO-PROX reaction [24] 14
1.5 CO conversion of CO-PROX reaction catalyzed by Pt.based catalyst with different substrate morphology [17] 15
1.6 Activity of unprompted and promoted Pt/CeO_2 for CO-PROX reaction:on the right, the catalytic activity of promoted catalyst, while on the left the catalytic activity of the unprompted catalyst [1] . . . 15
1.7 Different reaction pathways of CO-PROX over different catalysts:(a) competitive Langmuir-Hinshelwood mechanism over noble metal/inert suppo(b) no-competitive Langmuir-Hinshelwood mechanism over noble metal/reducible metal oxide, and (c) Mars-van Krevelen mechanism over TM based catalyst [33] 18
1.8 H_2-TPR profile of the bare support and the three CuO/CeO_2 catalyst [2] 20

2.1 Representative scheme of the experimental plant used to carry out the tests 24
2.2 Bronkhorst mass flow controller (in the left), real setup of gas flow regulation (on the right) 26
2.3 four-way solenoid valve 27
2.4 Central part of tubular reactor with controlling and monitoring thermocouples 28
2.5 Gas-chromatograph Aligent HP-7820 30
2.6 Example of chromatogram obtained with Gas-chromatograph Aligent HP-7820 during a CO-PROX analysis 31
2.7 Micro Gas-chromatograph Variant CP-4900 33
2.8 Example of chromatogram obtained with micro-gas-chromatograph Variant CP-4900 during a CO-PROX analysis 34

2.9 FT-IR IRTracer-100 Shimadzu 36
2.10 Alphasense O2-C2 oxygen sensor 37
2.11 Experimental setup employed for catalytic activity tests 40
2.12 Temperature program applied to pre-treatment and reaction phase during catalytic activity tests 41
2.13 Temperature program applied to pre-treatment and reaction stages during the analysis performed to identify the catalyst oxidative state and its performance during CO-PROX reaction 43
2.14 Experimental setup employed for TPR and TPO analyses 43
2.15 Temperature program applied to pre-treatment and TPR stage of analysis 44

3.1 Equilibrium molar fraction as a function of temperature, P = 1atm and y^0 as reported in Table 2.7 50
3.2 Delta of reaction as a function of temperature, P = 1atm and y^0 as reported in Table 2.7 51
3.3 Reagents conversion as function on temperatures, P = 1atm and n_{tot}^{in} = 100 moles 53
3.4 Trends of monitored temperature(green line), controlled temperature (orange line), set-point temperature (yellow dashed line) and oven power (red line) during catalytic activity test on ADP catalyst at different CuO loading 54
3.5 Temperature variation and CO conversion as function of temperature. Test:3 Cat: A-550-20 55
3.6 Temperature variation and oven power as function of controlled temperature. Test:3 Cat: A-550-20 56
3.7 Dry species molar fraction and monitored temperature as function of time. Test:4, Cat: A-550-15 57
3.8 Dry species molar fraction as function of monitored temperature. Test:4, Cat: A-550-15 58
3.9 (*a,b,c*) Reagents conversion profile as function of temperature, and (*d*) Selectivity of CO towards CO_2 as function of temperature. Test:4; Cat: A-550-15 59
3.10 Dry species molar fraction as function of the monitored temperature. Test:3, Cat: A-550-20 60
3.11 (*a,b,c*) Reagents conversion profile as function of temperature; (*d*) Selectivity of CO towards CO_2 as function of monitored temperature. Test:3, Cat: A-550-20 61
3.12 Dry species molar fraction as function of the monitored temperature. Test:2, Cat: A-550-30 62

3.13 (a,b,c) Reagents conversion profile as function of temperature; (d) Selectivity of CO towards CO_2 as function of temperature. Test:2, Cat: A-550-30 63
3.14 Comparison of conversion and selectivity profiles between A-550-15, A-550-20 and A-550-30 as function of temperature 64
3.15 Dry species molar fraction and monitored temperature as function of time. Test:37, Cat: E-900-20 66
3.16 Dry species molar fraction as a function of monitoerd temperature. Test:37, Cat: E-900-20 66
3.17 Reagents conversion as function of controlled temperature. Test:37, Cat: E-900-20 67
3.18 Dry species molar fraction and monitored temperature as function of time. Test:36, Cat: E-550-20 69
3.19 Dry species molar fraction as function of monitored temperature. Test:36, Cat: E-550-20 69
3.20 Dry species molar fraction as function of the monitored temperature. Test:11, Cat: E-400-20 70
3.21 Comparison between the reagents conversion for all the tested EISA catalyst as a function of monitored temperature. Test:11 Cat: E-400-20, Test:36 Cat: E-440-20, Test:37 Cat: E-900-20 71
3.22 CO conversion profile as function of monitored temperature. Comparison of ADP and EISA catalyst which provide the best catalytic performance. (green line) Test:37, Cat: E-900-20, (blue line) Test:3, Cat: A-550-20 72
3.23 CO conversion profile as function of monitored temperature. Performance comparison between catalyst calcined at the same temperature. (green line) Test:36, Cat: E-550-20, (blue line) Test:3, Cat: A-550-20 73
3.24 Comparison of catalytic performance as a function of catalyst aging. (◇) Test:2, (○) Test:15, (□). Stage considered: cooling, Test:31, Cat: A-550-20 76
3.25 Dry species molar fraction as a function of the monitored temperature. Stage considered: cooling, Test:22, Cat: A-550-20 78
3.26 Conversion profiles and monitored temperature as a function time. Stage considered: cooling, Test:22, Cat: A-550-30 79
3.27 Comparison between conversion obtained with completely pre-reduced and pre-oxidized catalyst. Stage considered: cooling, (○) Test:22, (□) Test:24, Cat: A-550-20 80
3.28 Variation of species concentration as function of time and temperature. Stage considered: cooling, Test:22, Cat: A-550-20 81

3.29 H_2-OX and CO-OX reagents conversion as function of monitored temperature. Stage considered: cooling, (○) Test:14, (□) Test:12, Cat: A-550-20 83
3.30 (a) Trends of monitored temperature(green line), controlled temperature (orange line), set-point temperature (yellow dashed line) and oven power (red line) as function of time. On the right Test:3 (low value of GHSV), on the left Test:31 (high value of GHSV), Cat: A-550-20; (b)Temperature variation and CO conversion as a function of the monitoring temperature. Test:31, Cat: A-550-20 85
3.31 Comparison of reagents conversion profile as function of monitored temperature. (a) heating stage, (b) cooling stage. (○) GHSV=40000 h^{-1} Test:31, (□) GHSV=20000 h^{-1} Test:3; Cat: A-550-20 87
3.32 Species delta of concentration normalized to O_2 consumption and monitored temperature, as a function of time. Test:23, Cat: A-550-20 89
3.33 Reagents conversion profile as a function of time and monitored temperature. Test:23, Cat: A-550-20 90
3.34 Measurement of hydrogen peaks with 50 % and 51%, as a function of time 91
3.35 Width of confidence intervals in terms of percentages compared to the mean as a function of the number of measures 92
3.36 Reagent conversion profile as a function of time and monitored temperature. Test:30, Cat: A-550-20 94
3.37 Consumed molar flow rate of H_2 and CO during TPR analysis as a function of monitored temperature. (orange and green line) Test:32, (blue line) Test:33, Cat: A-550-20 97
3.38 Profile of molar flow rate of O_2 consumed as a function of monitored temperature, Test:10, Cat: A-550-20 98
3.39 Profile of molar flow rate of O_2 consumed as a function of monitored temperature, Test:24, Cat: A-550-20 99

List of Tables

1.1 Electrochemical reactions occurring at the anode and cathode depending on fuel cell type [37] 5
1.2 syngas output compositions from thermal processes [32, 12] 8
1.3 Equilibrium constant of CO-PROX reactions [10] 12

2.1 Geometrical parameters of quartz glass tube used along experimental tests 28
2.2 Thermal conductivity of the analysed gases calculated at 250°C, [14] 30
2.3 Analytical method for Gas-chromatograph Aligent HP-7820 32
2.4 Analytical method for micro-gas-chromatograph Variant CP-4900 which does not consider water identification peak 35
2.5 Analytical method for micro-gas-chromatograph Variant CP-4900 which consider water identification peak 35
2.6 Catalyst used during for activity screening step 38
2.7 Experimental parameters used in catalytic activity tests 40

3.1 Experimental conditions for the catalytic test over A-550-15 56
3.2 Experimental conditions for the catalytic test over A-550-20 60
3.3 Experimental conditions for the catalytic test over A-550-30 62
3.4 Experimental conditions for the catalytic test over E-900-20 65
3.5 Experimental conditions for the catalytic test over E-550-20 68
3.6 Experimental conditions for the catalytic test over E-400-20 70
3.7 Experimental conditions to test the catalytic activity of one reduced material. Cat: A-550-20 77
3.8 Experimental conditions concerning the test conducted to verify the catalytic activity towards the CO-OX reaction alone 82
3.9 Experimental conditions concerning the test conducted to verify the catalytic activity towards the H_2-OX reaction alone 82
3.10 Experimental conditions for the catalytic test performed with high GHSV on A-550-20 catalyst 84
3.11 Experimental conditions for reaction stage of catalytic isothermal test performed tarting from oxidized catalyst 88

3.12 Experimental conditions for reaction stage of catalytic isothermal test performed tarting from reduced catalyst 93
3.13 Mixture composition and heating rate used in TPR analyses 96
3.14 Mixture composition and heating rate used in TPO analyses 96

Introduction

Fuel cell represents an attractive tecnological solution for the generation of power along all the scale. The hydrogen stream feeding the fuel cell, produced through a reforming processes including a fist WGS enrichment stage can still contain a quantity of CO that poisons the active site of the fuel cell catalyst. A promising technological solution is based in the process of catalytic preferential oxidation of carbon monoxide (CO-PROX).
An effective catalyst for the CO-PROX reaction should exhibit high CO oxidation rate combined with high selectivity, with respect to the undesired hydrogen oxidation side reaction. The catalysts which have been proposed for this process are noble metal-based catalyst, gold-based catalyst and transition metal oxide based catalyst. It has recently been shown that on the TM-based catalyst, $CuO/CeO_2/Al_2O_3$ is a promising candidate for this process and can shows higher activity, compared with the one of Pt-promoted and Au-based catalyst.
The purpose of this work are manifold. Firstly, it was decided to identify the activity of the previously mentioned catalyst, obtained from two different methods of synthesis, or rather two different method with which the active site was loaded on the catalyst substrate. In detail, it was identified how the amount fo active site affects the catalytic properties of the material, as well as the calcination temperatures. The second part of this work focused in identifying specific catalyst properties and how they affect the final performance of the material. Specific features of the material means its oxidative state and how it changes during the reaction process, the activity of the material towards the WGS reaction and its aging.
This thesis is based in three Chapters:

- Chapter 1: during the first period of the theis, a literature study focused on the fuel cell, the methods of hydrogen enrichment and particularity the CO-PROX reaction has been performed. This chapter contains a a description of fuel cells and their advantages and disadvantages. With regard to the disadvantages, an attempt was made to find out which is the most efficient methodology for the removal of carbon monoxide. The WGS and CO-PROX processes were then described. The mechanism, the catalysts that can be used and the effects that various factors have on the end result were then described for the CO-PROX reaction;

- Chapter 2: a complete description of the experimental setup used to carry out the tests, and a description of the analytical instruments, the experimental protocols, and the post-processing of the tests
- Chapter 3: all the results obtained from the activity test on ADP and EISA catalyst, the comparison between these two material and all the results concerning the catalyst oxidative state and the effect on the catalytic performance, as well as the aging of the catalyst, the possible presence of the WGS reaction and the effect of other parameter like GHSV on the catalyst are reported in this chapter.
- in the final part of this thesis the key conclusions of the work done and possible future work are defined. In the appendix of this paper a diary containing all the indications of the tests performed and reported in this thesis, and the matlab code used for the post processing of the PROX tests performed, is given.

Chapter 1

Fuel Cell and Preferential Oxidation of Carbon Monoxide: State of the Art

In the course of time, progress has always been associated with the growth of requirement of energy. In the last decades, the energy demand has grown significantly, going from 8.3 million of GWh in 1980 up to 18.9 million of GWh in 2006. However, these numbers are not comparable with an estimate made which predicted that energy demand could exceed 30 million of GWh in 2030. [38]
Currently, the energy needs are based on the combustion of fossil fuels and petroleum derivatives which, among other problems, contribute to the increase of greenhouse gases and thus to the rapid climate change. Considering these facts, the use of fossil raw materials for future energy production is not acceptable.
In order to fight climate change, in the last years the research has been focused on the environmental improvement of the existing technologies, but especially, on new technologies which in the near future could constitute a zero impact towards the release of greenhouse gases. In this last context, the most promising technologies use interfacial reactions such as electrochemical devices with very rich or pure mixtures in hydrogen as a power source. Among these devices, fuel cells represent the technology of greatest interest.

1.1 Fuell Cells: innovative device to energy production

The fuel cell is defined as an electrochemical device capable of converting energy from one form to another. In particular, this device is able to transform chemical energy possessed inside the fuel molecules being supplied (i.e its Gibbs Free Energy), directly into a work of electrical energy and heat, thought some oxidation-reduction

reactions [38]. According to what has been stated, fuel cell seems to be very similar to a usual galvanic cell, but unlike the latter, which it can provide only the energy that has been stored previously, this new electrochemical device theoretically is able to provide energy in unlimited mode as long as the fuel and oxidant are fed. The production of heat and energy upon introduction of fuel and oxidant could lead to think that fuel cell is similar to engines. As stated before inside the cell red-ox reactions take place, then unlike engines it does not combust the fuel giving out gases, but it galvanically burns fuel and produces water as scrap product. So the substantial differences that make a fuel cell different from a heat engine lie to the different type of reactions that take place inside it. In addition, due to its electrochemical reactions, this innovative device is not subject to the Carnot cycle, thus achieving high efficiency (up to 80%), and thus developing much higher energy compared to thermochemical unit. Moreover, the production of water as waste makes these systems suitable for energy production. Of relevance, fuel cells can also be used in commercial applications as energy source for vehicles or as city power generator. This is made possible because they have no mechanical bodies inside making them extremely quiet, and they allow easy independent scaling between power and capacity [35].

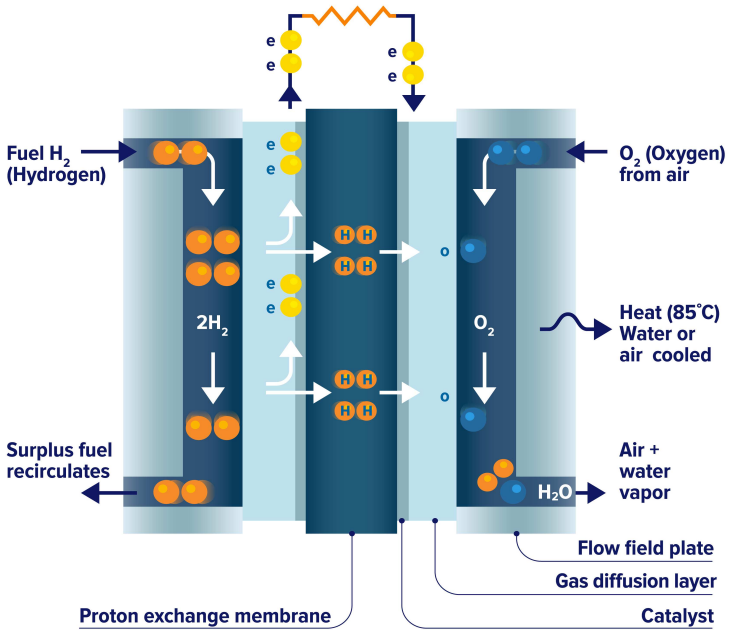

Figure 1.1: PEM Fuel Cell schematic representation [37]

The structure of a typical fuel cell is shown in Figure 1.1. This device consists of two electrodes, the anode and the cathode, which belong to a common electrochemical cell. An ion-conducting electrolyte, which functions as a current-carrying conductor, must be present between the two electrodes. The electrodes are electronically

connected by an external electric circuit, containing the electronic device that is to be electrically powered. The latter receives electricity by means of the current flow due to the potential difference created by the oxidation-reduction reactions occurring at the two electrodes. In particular, in a fuel cell, the fuel is oxidized at the anodic interface, accepting the electrons donated by the cathodic interface, where the oxidant, which is usually oxygen, is reduced. [37]
As mentioned above, chemical energy is converted through electrochemical reactions. These reactions involve different chemical species depending on the type of fuel cell, or more precisely on the fuel used inside the device. Nowadays in the industrial market there are several types of fuel cells. Their design depend to chemical compounds that are used and which reactions take place. The five mayor types of fuel cells are:

- Polymer electrolyte membrane fuel cell (PEMFC);
- Phosphoric acid fuel cell (PAFC);
- Solid-oxide fuel cell (SOFC);
- Montel Carbonate fuel cell (MCFC);
- Alkaline fuel cell (AFC).

Table 1.1 shows the overall reactions occurring in these fuel cells.

Table 1.1: Electrochemical reactions occurring at the anode and cathode depending on fuel cell type [37]

Fuel cell type	**Anode reaction**	**Cathode reaction**
PEMFC	$H_2 \rightarrow 2H^+ + 2e^-$	$1/2O_2 + 2H^+ \rightarrow H_2O$
PAFC	$H_2 \rightarrow 2H^+ + 2e^-$	$1/2O_2 + 2H^+ \rightarrow H_2O$
SOFC	$H_2 + O^{2-} \rightarrow H_2O + 2e^-$	$1/2O_2 + 2e^- \rightarrow O^{2-}$
	$CO + O^{2-} \rightarrow CO_2 + 2e^-$	
	$CH_4 + 4O^{2-} \rightarrow 2H_2O + CO_2 + 8e^-$	
MCFC	$H_2 + CO_3^{2-} \rightarrow CO_2 + H_2O + 2e^-$	$1/2O_2 + CO_2 + 2e^- \rightarrow CO_3^{2-}$
AFC	$H_2 + OH^- \rightarrow H_2O + 2e^-$	$1/2O_2 + 2e^- + H_2O \rightarrow 2OH^-$

Among the various problems, such as the slow cell start-up and the possible corrosiveness of the electrolyte used, the key disadvantages of fuel cells are related to the cost and presence of some impurities in the feed. Figure 1.2 qualitatively represents the expenditure of the most significant components of a generic fuel cell. Catalyst deposited on the electrodes surface is predominant charge compared to the others. This can be seen as a problem because the catalyst is the key to another problem: its deactivation. Most fuel cells employ platinum-based catalyst, which by its nature, is prone to deactivation and thus performance decay of electrochemical device. [28]

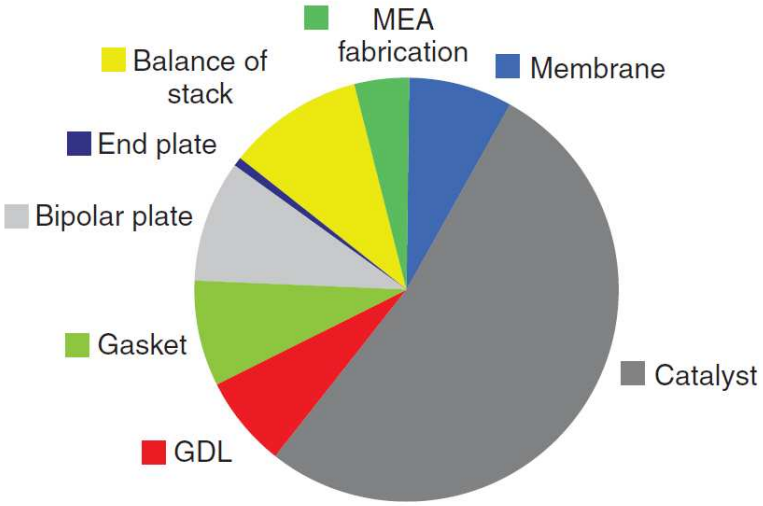

Figure 1.2: Quantitative representation of fuel cell material costs [16]

1.1.1 Impurities of Fuel Cells Feedstock

Speaking about fuel cells, it can be claimed that any compound that does not take part in the fuel cells reaction is regarded as impurity. The effect of different impurities differs considerably, both in severity and what parts of the fuel cell affected. Some pollutant, such as carbon monoxide and sulfur species, have been found to be harmful to the fuel cells performance even at trace concentration, while others, such as nitrogen and methane have a limited or no effect on the fuel cell [11, 36].The effects that impurities have on the catalyst are different and depend on the species itself. Some kind adsorb on the catalyst particles, blocking the catalytic sites to the intended reactants, sometimes referred to as poisoning of the catalyst. CO and S-species are examples of impurities that poison the catalyst in this way. Other catalyst poisons can interfere with the chemistry of electrochemical reaction when they adsorbed on the catalyst. Some metal cations, like CO_2^+ and Al_3^+, can affect the Oxygen Reduction Reaction (ORR) by shifting the equilibrium towards peroxide formation (H_2O_2). This latter breaks down into radicals that attack the ionomer causing membrane degradation and, possibly, its failure. Another possible effect of impurities occurs when the protons in the ionomer and/or the membrane are replaced by less mobile cation. This type of contamination is typical for alkaline metal ions (M^+ or NH_4^+), and causes a decrease in proton conductivity. Yet, another type of degradation occurs when impurities adsorb and deposit on fuel cell components, typically on the carbon components like GDL or catalyst support. These deposits can block the porous material, restricting gas flow in the fuel cell. [6, 27]

Carbon monoxide: a catalyst poison

In the previous paragraph it was mentioned that the presence of carbon monoxide, even in very small quantities, causes the poisoning of the catalyst. It is therefore interesting to understand what are the effects that this poison can cause to the fuel cell. Baschuk and Li. [7], as well as others (for instance K. Jiao et al. in [20]), have performed a study on the characteristics, mechanism and mitigation strategies of CO poisoning on Pt-based electrodes. The study was carried out on PEMFC, but these results can be extended to any cell-typologies that has platinum supported electrodes.
These studies have highlighted how the origin of its poisonous behavior is due to the strong adsorption of CO molecules on the surface of the catalyst, blocking the catalytic sites that under normal conditions would be used by hydrogen for its oxidation. By doing so, hydrogen molecules present in the feed are not oxidized because they are deposited on the CO surface vacations. Experiments evidenced that the CO poisoning effect is related to its concentration in the feed, as well as the cell operating temperature, CO exposure time and the characteristic catalyst deposited to the anode (i.e other metals linked with platinum). To explain better, in Figure 1.3 are reported qualitative performance decay trends as the CO concentration and operative density change. More specifically, a pollutant concentration of a few ppm results in a considerable decline in cell performance, especially at high current densities. The drop of performance is in turn boosted by the exposure time due to the increase of molecules accumulation on the catalyst surface. In contrast to pollutant concentration and exposure time, the increase in temperature discourages the adsorption of CO molecules onto the catalytic surface. To avoid catalyst poisoning, it would seem reasonable to work at high temperature. This is not always possible because some fuel cells must work at low-medium temperature to avoid internal material degradation. For instance,ade the proton exchange membrane, LT-PEMFC must operate at a temperature lower than 120°C.

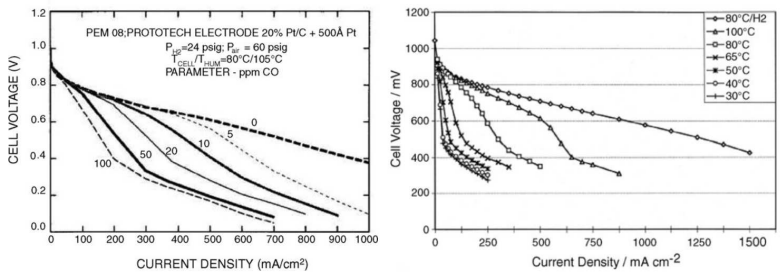

Figure 1.3: Polarization curve at different operating temperatures and carbon monoxide concentration in supplied hydrogen [20]

1.2 Hydrogen enrichment stages required for fuel cell purpose

In the previous section 1.1.1,it was pointed out that the fuel cell feed stream must have extremely high purity in order to avoid problems concerning poisoning and loos of performance in downstream processes. Therefore, it now seems reasonable to advance the discussion speacking about hydrogen production and hydrogen enrichment methodologies.
Most of the primary resources such as fossil fuels, as well as renewable energy sources and nuclear power could be used for hydrogen production. In particular, H_2 can be produced from any substance containing hydrogen atoms, such as hydrocarbons, water and even some organic matter. In addition, it can be readily produced from synthesized hydrogen carries such as methanol, ammonia and synthetic fuels.
Industrially, hydrogen can be produced from a variety of processes, including electrochemical, thermochemical and photo-electrochemical processes. In particular, thermochemical methods are normally used to derive hydrogen from hydrocarbons using natural gas, intermediate products of refining and coal as raw materials. Thermochemical production method are well established method: 96% of hydrogen is produced through these processes, whose 48% from methane steam reforming, 30% from partial-oxidation and auto-thermal reforming of intermediate products and 18% from gasification of coal. These processes enjoy good efficiency and amortizable costs, but at the same time with them it is not possible to directly recover hydrogen stream with high purity as outlet gas. To emphasize this, Table 1.2 reports the outlet composition of methane-steam reforming and coal gasification.
The remaining fraction of hydrogen production is fulfilled by electrochemical processes such as electrolysis. Through these galvanic processes, it is possible to obtain a very pure gas streams. Disadvantages of the latter are low efficiency and high production cost, if compared to traditional processes. All the thermochemical processes mentioned above are efficient for hydrogen production, but the amount of carbon monoxide contained within the gaseous stream is not suitable for many industrial processes and in detail is not appropriate for fuel cell purpose. Therefore, further purification processes like water gas shift and preferential oxidation of carbon monoxide are necessary to reduce the CO concentration to ppm levels.

Table 1.2: syngas output compositions from thermal processes [32, 12]

Process types	**Operative conditions**	**H_2**	**CO**	**CO_2**	**CH_4**
Methane-SR	T= 750°C	63.4%	20.4%	4.1%	12.2%
Biomass Gasification	T = 750-1200°C	40%	25%	25%	8%

1.2.1 Water Gas Shift Reaction

Water-Gas-Shift (WGS), which reaction is reported in Eq 1.1, is an intermediate reaction in hydrocarbon reforming process, and nowadays it is considered one of the most important reaction for hydrogen production. Similar to the preferential oxidation reaction, the capacity to break down the carbon oxide fraction at very low percentage makes the WGS reaction highly relevant at the industrial level. In particular, the scope of WGS is to produce hydrogen and carbon dioxide through the reaction between carbon monoxide and a steam stream.

$$CO + H_2O \rightleftharpoons CO_2 + H_2 \qquad \Delta\tilde{H}^{\circ}_{R} = -41.7\,\mathrm{kJmol^{-1}} \tag{1.1}$$

The WGS reaction occurs without change in the number of moles and it is thermodynamically limited with a equilibrium constant expressed by Eq 1.2.[30]

$$K_p = exp\Big(-\frac{\Delta G^0}{Rg * T}\Big) = exp\Big(\frac{4577.8}{T} - 4.33\Big) \tag{1.2}$$

Eq 1.2 emphasizes that as the temperature increases, the equilibrium constant decreases. This conclusion is also clear when considering the standard reaction enthalpies of WGS: the reaction is exothermic and therefore an increase in temperature disfavors the direct reaction. Then, in order to obtain higher CO conversion, it is desiderable to perform the WGS at low temperatures. Other state and industrial parameters which can influence the equilibrium of the reaction coul be the pressure, but it does not play a key role in the thermodynamics of this reaction because, since there is no change in the total number of moles. This late state parameter, inside an operative range between 0.1 and 0.5MPa, is not influenced. On the other hand the syngas production method can affect the equilibrium of this reaction. In particular, the amount of vapor introduced into the reactive system can have a positive effect on CO conversion: an excess of vapor can favor the forward reaction because it acts as a reaction inert. For what concern the syngas production method, the important parameter is the amount of hydrogen in the exiting stream: lover H_2 concentration improves the equilibrium and then the CO conversion. It is not possible to consider only thermodynamics because also kinetics limits this reaction, in fact if not catalyzed, the WGS reaction is relatively slow and therefore useless industrially. To increase the rate of reaction, different types of catalysts can be used, which must be active. The WGS catalyst activation occurs at a higher temperature respect the one required by thermodynamics, generating an operational inconsistency between thermodynamics and kinetics. In order to overcome this thermodynamic limitation maintaining quite high reaction rate, WGS can be performed in two subsequent stages: High Temperature Shift (HTS), carried out in a temperature range between 350 - 400°C and the follow stage, called Low Temperature Shift (LTS), performed with a temperature between 180 - 240°C. This industrial set-up allows to obtain at the outlet of the second reactor

a flow with a CO percentage lower than 0.1%.Two different types of catalyst must be used for the reaction stages: the high-temperature stage mainly required iron oxide or chromium oxide catalyst, while the lower-temperature stage mainly uses copper-based catalyst.
For the purpose of this thesis, the HTS stage is not important since the CO-PROX reaction, as will be seen in more detail in section 1.3, is carried out at relatively low temperatures, the one comparable with those of the low temperature WGS reaction.

Copper-based catalyst for WGS reaction

Until the 1950s, iron-based catalysts were used for both stages of WGS, resulting in limited performance. Limited activity of the iron based catalysts in lower temperature range motivated further investigations to develop an active catalyst combination for the lower temperature shift reaction [22]. Unsupported metallic copper or copper supported on Al_2O_3, SiO_2m MgO and Cr_2O_3 were investigated as a low temperature catalysts. In contrast to HTS stage catalyst, copper-based catalyst allow high selectivity to be achieved at low temperatures, reducing the number of undesirable secondary reactions. Their disadvantage lies in their instability and likelihood of sintering at low temperatures, as well as their easy poisoning in the presence of sulfurous gases.
Several studies have shown how the catalyst performance depends significantly on several operating parameters such as contact time, the amount of steam versus the one of carnon monoxide, also known as the S/C ratio, and the operating pressure. In particular, it was found that a high S/C ratio and low contact time favors the CO conversion and the selectivity od the carbon oxidation reaction. As well as the operating parameters, the catalyst preparation method has a significant impact on its activity, in fact, it influences its dispersion, the particle size and the interaction with the support.
Nowadays, WGS is industrially catalized by CuO-ZnO or $CuO/ZnO/Al_2O_3$, where the active site for the reaction is copper metal, ZnO represent the support and Al_2O_3 is used to help the dispersion. Another high-performance catalyst that could take the place of the previously mentioned catalyst is CuO/CeO_2. Compared to the other LTS-WGS catalyst, Cu-Ce catalyst exhibit high activity, and thermal stability.

As mentioned above, the stream leaving the LTS-WGS reactor has an average concentration of about 1%. This concentration is not suitable for catalysts used in fuel cells. Industrially, in order to obtain a suitable feed for these innovative devices, another method of gas purification, or rather, another method of gas purification, or rather, another method of enriching the stream in hydrogen by drastically decreasing the amount of carbon monoxide is employed. The processes being discussed

is called Preferential Oxidation of Carbon Monoxide. As the project of this thesis focused on investigating the CO-PROX reaction, the following paragraphs are devoted to it, in which its main principles will be explained.

1.3 Preferential Oxidation of Carbon Monoxide

The preferential oxidation of CO in H_2-rich streams dates to the 1960's, when it was recognized the practicability of a catalytic combustion process for the selective removal of carbon monoxide from hydrogen, target to purify H_2 for the Haber-Bosh process(*i.e.*ammonia synthesis). The process used a promoted catalyst containing 0.3-0.5% Pt, and it was able to oxidize 10000 ppm of CO without significantly oxidizing 70% H_2 (in dry based) present in the stream. The performance of this catalyst was significant because, in steady-state condition (50°C, 10000h^{-1} and 15-30 atm) it was able to reduce the CO concentration by up to 5 ppm. Before CO-PROX, industrial companies were employing the methanation process for removing carbon monoxide by converting it to methane. The deployment of Preferential oxidation has brought operating advantages, since by limiting the oxygen content in the feed there could be no danger of "reaction runaway". Although CO methanation is self limiting in the absence of CO_2, the potential for carbon dioxide methanation, especially when large quantities are present in the reformate, is a significant concern. However, PROX reaction has its challenges, a key one being (in practice application) to provide and maintain the appropriate level of oxygen (or air) to the reactor. Too little oxidizer results in too high a concentration of residual CO; too much O_2 results in exxes of hydrogen consumption, since all O_2 fed to the PROX reactor is generally consumed [9, 37]. Over the years, several studies have been conducted on the selective oxidation of carbon monoxide with promising results, leading to the process becoming important in the hydrogen production and the reformed gas industry. The research was not trivial because, as will be seen below, CO-PROX involves complex reaction mechanism and its performance depends in several factor and operational parameters[15].

1.3.1 General consideration relating the CO-PROX reactions

The aim of preferential oxidation of carbon monoxide is to selective oxidize CO, reducing its concentration to acceptable ppm levels without simultaneous oxidation of hydrogen present in the shifted reformate. Industrially, carbon monoxide in the exiting of WGS reactor is selectively oxidized in the PROX reactor over oxidized catalyst with externally supplied oxidizing agent. In more detail, the desired reaction to be achieved is shown in Eq 1.3, but since hydrogen is also present in the reactor feed stream, undesirable reactions can take place. These reactions are

shown in Eq 1.4. Therefore, preferential oxidation can be consider as a set of parallel and competitive reactions. In the reaction system represented in Eq 1.4, the first represents the oxidation of hydrogen to water, the second one is the Water Gas Shift reaction, already defined in section 1.2.1 of this chapter. The latter two reactions represent the methanation, namely the production of methane starting from hydrogen and carbon monoxide/carbon dioxide.

$$\text{CO-OX:} \quad CO + 1/2O_2 \longrightarrow CO_2 \qquad \Delta\tilde{H}_R^{298} = -282.98 kJmol^{-1} \tag{1.3}$$

$$\begin{array}{lll} \text{H-OX:} & H_2 + 1/2O_2 \longrightarrow H_2O & \Delta\tilde{H}_R^{298} = -244 kJmol^{-1} \\ \text{WGS:} & CO + H_2O \rightleftharpoons CO_2 + H_2 & \Delta\tilde{H}_R^{298} = -41 kJmol^{-1} \\ \text{CO-MET:} & CO + 3H_2 \rightleftharpoons CH_4 + H_2O & \Delta\tilde{H}_R^{298} = -206 kJmol^{-1} \\ \text{CO2-MET:} & CO_2 + 4H_2 \rightleftharpoons CH_4 + 2H_2O & \Delta\tilde{H}_R^{298} = -165 kJmol^{-1} \end{array} \tag{1.4}$$

H_2-OX, and the two methanation reaction are undesired reaction for two simple motivation: they use hydrogen as reactant and also bring down the selectivity of the process.
The preferential oxidation of carbon monoxide operates between the operating temperature of LTS-WGS and the reaction temperature of LTS-WGS: then from 80°C and 250°C. Operating conditions can be a starting point for some thermodynamic consideration. Inside this range of temperature, both hydrogen and carbon monoxide oxidation exhibit high equilibrium constant and thus they can be consider irreversible reactions. In contrast to oxidation reactions, the WGS reaction is not very favorable thermodynamically: inside the operating range, the equilibrium constant does not have high values. In addition, it can be assumed that the WGS reaction is not a limiting stage for the under consideration process because the characteristic reaction times are extremely long compared to the oxidation reaction times [10].

Table 1.3: Equilibrium constant of CO-PROX reactions [10]

T [°C]	50°C	100°C	150°C	200°C	250°C	300°C
CO-OX	10^{41}	10^{35}	10^{30}	10^{26}	10^{23}	10^{21}
H_2-OX	10^{41}	10^{36}	10^{32}	10^{28}	10^{26}	10^{24}
WGS	10^{4}	10^{3}	10^{2}	10^{2}	10^{1}	10^{1}
CO-MET	10^{22}	10^{17}	10^{14}	10^{11}	10^{9}	10^{7}
CO_2-MET	10^{17}	10^{14}	10^{11}	10^{9}	10^{7}	10^{6}

The nature of each individual reaction is closely linked to the reaction itself. In other words, for system, in which several reactions can occur simultaneously, consideration that could be valid for a single reaction may be longer be valid for a

system of several reactions. Therefore, considering the reactions that could be take place inside a PROX system, their mutuality could diversify the previous consideration. Purely thermodynamic consideration of a geniric CO-PROX system will be defined in Chapter 3.

1.3.2 Catalysts for the Preferential Oxidation of Carbon Monoxide

As already pointed out in the previous paragraph, the catalyst that is used to catalyze the PROX reaction can greatly affect the final species concentration in the exiting stream. Bearing in mind that several competitive reaction take place, among which, the most likely is the oxidation of hydrogen, the catalyst to be used must enhancing the CO oxidation and suppressing as far as possible undesirable reaction [28]. Catalyst for the selective oxidation of CO can be classified into three categories, according to the active metal used [8, 24]:

- Pt-group catalyst (PMG)
- Transition metal based catalyst (TM)
- Au-based catalysts

In Figure 1.4 different categories of CO-PROX catalysts are organized depending on their CO conversion as a function of the reaction temperature. This figure highlights that Au-based catalysts exhibits exceptionally high CO oxidation activity in the low-temperature range, whereas Cu-based catalysts, which belong to the TM catalysts, and promoted PMG catalyst show similar CO conversion levels at higher temperatures, with respect the first mentioned group. Instead, unprompted PMG catalysts usually show very low activities at temperatures below 100°C.

Platinum group metal catalysts

PMG catalysts generally comprise Pt, Rh, Ru, Ir and Pd-supported catalyst. Among these metals, platinum based catalyst are the most studied system for preferential oxidation of CO. It is acknowledged that this family of catalyst has been extensively studied. For instance, Kanlich et al.in [21] performed a kinetic study of the CO oxidation in a H_2-rich gas stream (1%CO, 1%O_2, 75%H_2 balanced in N_2) over Pt/Al_2O_3 catalysts. The authors proved that over 0.5%Pt/Al_2O_3, CO conversion was up to 80% even at 250°C. In particular, they also proved that in presence of hydrogen, the CO oxidation rate increased, and the optimum temperature range and O_2 concentration are about 200°C and 2.5 time higher the stoichiometric amount. Other studies evaluated the catalytic activity of Pt-based catalyst on different support. For instance, Gao et al. in [17] investigated how different morphology of the substrate influenced the catalytic activity of Pt/CeO_2. More in detail, the three morphology are cubic (c-), rods (r-) and octahedra (o-) and

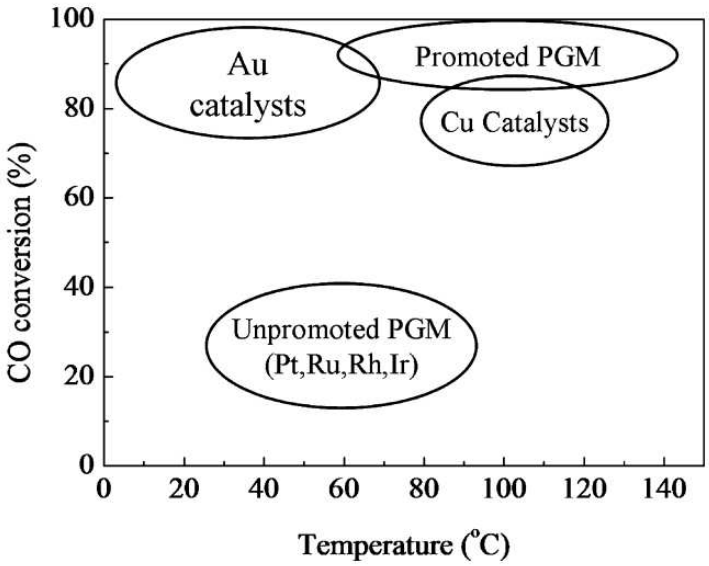

Figure 1.4: Conceptual illustration of catalutic performances of different types of catalyst for CO-PROX reaction [24]

they found that with Pt/r-CeO_2 the CO conversion achieved 80% in a temperature range between 60°C and 80°C, instead with Pt/c-CeO_2 the activity achieved the same level only at 100°C. On the other hand Pt/o-CeO_2 was not able to achieve the same catalytic activity even at higher temperature. However, some weak point that may hamper the implementation of unprompted Pt-based catalyst have been identified: they are able to work in a narrow operating window and with low selectivity towards CO oxidation. Especially, narrow operating window means that Pt-based catalyst can be efficiently used in a small temperature range and in presence of excess oxygen [39]. Other paper reported the performance of Ru-based catalyst as it is cheaper than other noble metals. Considering the study of Liu et al. in [24], they concluded that Ru/Al_2O_3 can be consider a good choice for CO-PROX reaction, although id it is active also for methanation reaction for both CO e CO_2, and therefore hydrogen consumption increases,compared to H_2 consumption with Pt-based catalyst.

As general conclusion, unprompted PMG catalysts are not considered as promising candidates for CO-PROX reaction, therefore in order to increase their activity, reducible metal oxides, that works as promoters, are added to them. Antoniassi et al. [1] conducted research on this types of catalyst. In particular their used $PtFe/CeO_2$ and they revealed how a small portion of promoters increases the catalytic activity of Pt/CeO_2, even at very low temperatures. Figure 1.5 and Figure 1.6 illustrate the consideration made above relating the Pt-based catalyst. In particular, Figure 1.5 highlights the catalytic activity of Pt/CeO_2 and how the substrate morphology influence the conversion, while Figure 1.6 emphasizes how the

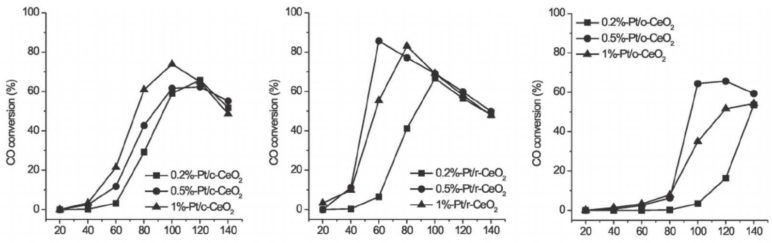

Figure 1.5: CO conversion of CO-PROX reaction catalyzed by Pt.based catalyst with different substrate morphology [17]

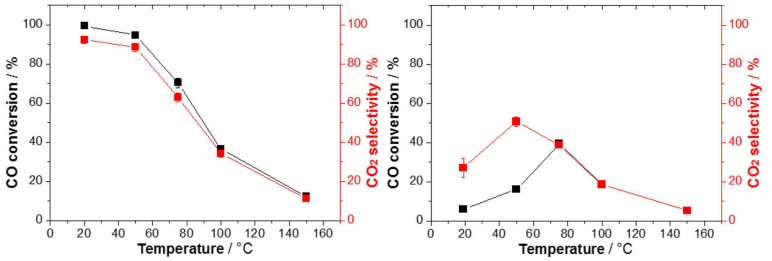

Figure 1.6: Activity of unprompted and promoted Pt/CeO_2 for CO-PROX reaction:on the right, the catalytic activity of promoted catalyst, while on the left the catalytic activity of the unprompted catalyst [1]

presence of a promoters increase the catalytic activity at low temperatures.

Transition metal oxide catalysts

The first studies reporting the presence of transition metal oxides (TM) in CO-PROX catalysts concerned its use as promoters of noble metal based catalysts. However, driven by the high cost of noble metal catalysts, the ones based in transition metal oxides have been researched as a cheap alternative. The first results of CO-PROX in $CuO\text{-}CeO_2$ catalysts were obtained by Avgouropoulos et al. in [5], based in the results of a previous work, where $CuO\text{-}CeO_2$ were examined for CO and CH_4 total oxidation. According to Avgouropoulos, with this catalyst it is possible to convert most of the supply CO directly to CO_2 at a temperature of 140°C approximately, and the WGS reaction does not occur. In addition, Marino et al.in [26] studied a wide range of transition metal catalyst (CO, Cr, Ni, Cu and Zn) supported on oxides with very different acid, basic and redox properties such as MgO, La_2O_3, SiO_2, Al_2O_3, CeO_2 and $Ce_{0.63}Zr_{0.37}O_2$. An important conclusion extracted was that, among the different metals investigated, only Cu presented high CO conversion and selectivity to CO_2, making Cu-based catalysts the most suitable for CO-PROX purpose. In addition, the authors found that Cu supported on Ceria and on $Ce_{0.63}Zr_{0.37}O_2$ showed similar activity to PMG catalyst and were

very selective in the 50-150°C temperature range. In particular, Copper-supported catalysts revealed very good activity for CO-PROX and exhibited higher selectivity than Pt-supported catalysts and very high conversion levels. Intrigued by this high performance, the scientific community has been looking for system that can be able to further increase the activity of CuO-CeO_2. To do that, different synthesis routes have been adopted, the addition of promoters, as in the case of PMG catalysts, such as Fe, La, and Zn, or the addition of different textural supports, such as Al_2O_3.
As seen in the previous paragraph, the morphology of catalyst influence its final catalytic activity. It can be considered to be directly related to the preparation method and calcinations temperature. In particular, Avgouropoulos et al. [4] studied how the catalytic performance is affected by its preparation method. Avgouropoulos discovered that the maximum catalytic activity is related to urea-nitrates combustion and decreases with the following alternatives: (*i*) citrate-hydrothermal, (*ii*) co-precipitation, (*iii*) impregnation. He also assumed that the superior activity of the catalyst prepared by urea-nitrate combustion method is claimed to be related to the formation of well-dispersed copper oxide species with strong interaction with ceria and the absence of bulk CuO. As regard calcinations temperature, Avgouropoulos et al. [3] and Jong-Won Park et al. [31] found that catalyst activated at higher temperatures get less easily reduced and they catalytic activity is maintained or even enhanced in most cases. Then, the activation temperature play an important role by influencing, on the one hand, the degree of interaction between the active site and substrate and, on the other hand, the phenomena of syntering and surface area loss.

Gold-based catalyst

From a general point of view, TM-catalyst and Au-based catalyst exhibit a better activity and selectivity in a larger temperatures range with respect PMG catalyst. Supported gold catalyst are famous for their exceptionally high and unique activity for CO oxidation, even at low temperature (<100°C). A first study on gold-based catalysts was carried out more than 30 yeas ago by Haruta et.al [19]. He revealed that when gold is dispersed as particle with diameter smaller than 5nm, it exhibits surprisingly high activates in the oxidation of CO. In particular, Au-based catalysts are not usefull for CO oxidation only, but is very active also for other many reactions of both industrial and environmental importance, such as low-temperature catalytic combustion, partial oxidation of hydrocarbon, reduction of No to N_2, hydrogenation of unsaturated substrates.
More in detail, the unique catalytic nature if Au-supported catalysts depends on several critical factors, which is some cases are intimately related. These factors are: (*i*)gold particle size, (*ii*) oxidation state and morphology, (*iii*) the metal oxide support type and crystalline structure, (*iiii*) presence of promoters and (*iiiii*) the interaction between Au-particle and its substrate. In these aspects, the preparation

method and the activation procedure play a key role [25].
The importance of converting as much CO as possible has stimulated research into gold-based catalysts, with several tests being carried out on different types of support. The most active support are titania, ceria, alumina, zirconia, and other oxide such as Co_3O_4 and MnO_2.
In the recent years, two or more elements of different categories have been combined in order to profit from the synergetic effect of their combination. Example of these "hybrid" catalyst are Au-Cu, Pt-Cu or Pt-Au catalysts. In all these cases, the addition ofa second element resulted in enhance activity by different mechanism: for instance, as reported Laguna et al. [23], the presence of Au on CuO_x/CeO_2 catalyst led to higher CO oxidation activity at low temperatures, however for T>140°C the doped catalyst showed lower activity than the no-doped catalyst.

1.3.3 Reaction mechanism between noble metal and transition metal based catalyst

Several studies have revealed that CO-PROX reaction mechanism differs depending on the type of catalyst used. For instance, Jing et al. [33] have reported the reaction mechanism follows two different patterns depending on whether the catalyst is based on a noble metal, or a transition metal. More specifically, they have also defined that the mechanism also changes depending on the support used. The two patterns that the reaction mechanism follow are Langmuir-Hinshelwood and Mars-van Krevelen model.
In particular, a competitive Langmuir-Hinshelwood reaction mechanism has been proposed for catalyst that consist of noble metals and inert supports ($i.e SiO_2$ or Al_2O_3), non competitive Langmuir-Hinshelwood reaction mechanism for noble metal catalyst supported on reducible metal oxides and Mars-van Krevelen model for transition metal based catalyst. In the case of noble metal catalysts supported on inert materials, there is a competitive mechanism because the support does not take part in the reaction, namely, it cannot release oxygen to the reaction environment and therefore a competition for O_2 molecules between CO and H_2 occurs. In particular, at high temperature hydrogen oxidation reaction take place, while a low temperatures the carbon monoxide oxidation reaction occurs. Contrary to this first case, with active support and TM-based catalyst, the catalyst actively participates in the reaction because the oxygen reacting with CO and H_2 molecules is directly released by the catalyst [33]. A schematic representation of the three reaction mechanisms can be found in Figure 1.7.
For the purpose of this thesis, the CO-PROX reaction mechanism on CuO/CeO_2, is further investigated.

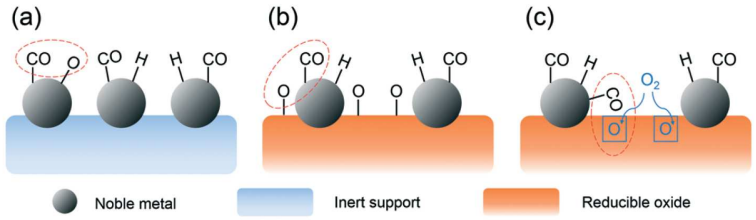

Figure 1.7: Different reaction pathways of CO-PROX over different catalysts:(a) competitive Langmuir-Hinshelwood mechanism over noble metal/inert suppo(b) no-competitive Langmuir-Hinshelwood mechanism over noble metal/reducible metal oxide, and (c) Mars-van Krevelen mechanism over TM based catalyst [33]

CO-PROX reaction mechanism over CuO/CeO_2 catalyst

As mentioned above, if catalyzed by CuO/CeO_2 catalyst, preferential oxidation of carbon monoxide follows the reaction mechanism defined by Mars-van Krevelen. In this facility, the CO adsorbs and instead of being oxidized by gas-phase O_2, it is oxidized by means the oxygen come from the lattice of the metal oxide. Upon removal of lattice oxygen species from the surface of the based metal oxide, the surface is left partially reduced, namely with oxygen vacancies. The gas phase O_2 co-fed with CO then replenished the removed oxygen atoms to regenerate the metal oxide, reacting an overall Red-Ox cycle [13].
With regard to the catalyst used in this thesis, several studies, such as the one conducted by Polster et al. [34], have reveled that the active phase is the oxidesed one ($i.e$ Cu^+). The formation and stabilization of this active phase would be promoted by means a Red-Ox equilibrium situated in the labile Cu-Ce interface. The whole process can be summarized as reported in Eq 1.5.

$$\begin{aligned}
&[1] && CO_g + O - Cu^+ \longrightarrow CO^* - O - Cu^+ \\
&[2] && CO^* - O - Cu^+ \longrightarrow CO_{2g} + V_O - Cu^0 \\
&[3\text{-a}] && O_{2g} + 2\left(V_O - Cu^0\right) \longrightarrow 2\left(O - Cu^+\right) \\
&[3\text{-b}] && Ce^{4+} - O + V_O - Cu^0 \longrightarrow Ce^{3+} + V_O - Cu^+ \\
& && O_{2g} + 2\left(Ce^{3+} - V_O\right) \longrightarrow 2\left(Ce^{4+} - O\right)
\end{aligned} \tag{1.5}$$

In particular, the first step reported in Eq 1.5 ($i.e$ [1]) highlights the chemisorption of carbon monoxide at the active sites, which can be either Cu^{2+} or Cu^+. Once CO has been adsorbed by active center, it forms higly active radicals, the carbonyl, which immediately react with the oxygen in the substrate to form carbon dioxide. Once the reaction has taken place, the final molecule is stable and is de-adsorbed by the active sites, releasing itself into the bulk. As can be observed from the second step in Eq 1.5 ($i.e$ [2]), the releasing of CO_2 causes the creation of a vacancy in the reaction site. This vacancy is restored through the oxygen molecules present in the

reaction mixture. This process, reported in the third step in Eq 1.5 (*i.e* [3]), may take place either directly in Cu_xO or via Ce-O-Cu labile entities, which constitute the direct or syhersistic mechanism for the lattice O recovery.
Up to This point, detailed issues are descriptive for pure CO oxidation process. However, in Preferential CO oxidation reaction there is a very excess of hydrogen in the reactant mixture, which is expected to get involved in the competitive process corresponding ti its oxidation. Luckily, CO is a better reducing agent than H_2, and then consequence of it, CO oxidation slhould take place at lower temperatures than $H2_2$ oxidation. This provides a CO selective temperature window corresponding to the difference between the on-sets for CO and H_2 oxidation reactions.

1.3.4 Effect of the gas feed components on CO-PROX reaction

Going back to section 1.3.1, the presence of different species in the reaction mixture could alter the catalytic performance, i.e to reduce or increase CO consumption. Generally, the reformate mixture entering the preferential oxidation process contains H_2, CO, CO_2 and H_2O. The largest fraction of this mixture is hydrogen, but percentage of carbon dioxide and water may be greater than 10%, and CO units are also present.

Effect of hydrogen

During the CO-PROX reaction, as reported in Eq 1.4, hydrogen can potentially react with O_2 to form water. At high enough temperature and over a suitable catalyst, it can also react with CO to form methane and more water. The oxidation of H_2 and its use in methanation reactions results in a reduction in both the conversion and CO to CO_2 selectivity. Although, at low temperatures and over most catalyst CO adsorption o is more favored with respect H_2, upon increasing the reaction temperature, hydrogen adsorption and oxidation becomes kinetically favored. This can take place even before the CO conversion values achieve 100%, depending on the catalyst used and the amount of O_2 co-fed.
Considering the catalyst studied in this thesis and the result obtained by Postel et al. [34], the active phase of Cu/CeO_2 is the oxidized phase. The strongly reducing environment created by the high percentage of hydrogen and the reaction temperatures could reduce the catalyst and thus decrease its catalytic activities. Truing to understand this catalyst reduction mechanism, Dìaz et al. [2], carried out a series of Temperature-Programmed Reduction (TPR). In particular, a polycristalline CuO/CeO_2 with a loading of 3%, 6% and 12% was used in this study. TPR test, which representation in shown in Figure 1.8, was performed with an atmosphere containing 10% of H_2 balanced in Ar. The results of this test are manifold. Firstly,

for each catalyst, a peak associated with its reduction was observed in the temperature range between 150°C and 250°C. In particular, the figure does not show a single peak: it can be considered as a set of three different peack. These may be related to a slight difference in the size of the metal oxide particles and the reduction of CuO in the bulk. It was also observed that increasing the copper content causes an increase in the reduction temperature and that the hydrogen consumed exceeds the amount required for the complete reduction of copper oxide. The higher hydrogen consumption may be associated with the partial reduction of the substrate at low temperatures, contrary to what was thought. Ultimately, the combination of the catalyst's active phase, the reducing environment of the mixture and the reaction temperature could favour the reduction of the catalyst above 150°C. A lower conversion of CO could be a consequence of this reduction because the catalyst may be less active and some of the reacting oxygen could be used by the catalyst for its oxidation.

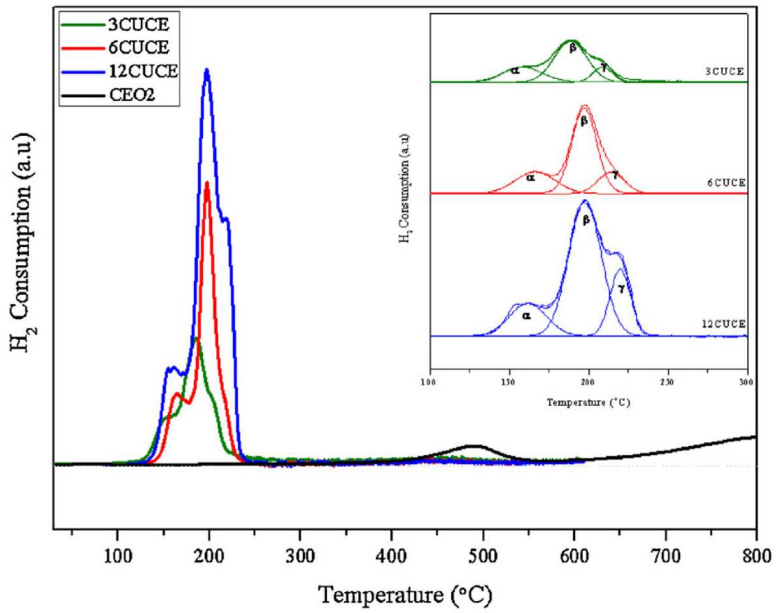

Figure 1.8: H_2-TPR profile of the bare support and the three CuO/CeO_2 catalyst [2]

Effect of water and carbon dioxide

The effect of addition of both carbon dioxide and steam in the CO-OX reaction mixture has not been widely studied. Results with respect the influence of these two gases on catalytic performance have been presented by Liu et al. [**?**], Gawade et al. [18], Wu et al. [40] and Monyanon et al. [29]. The final concept of all these article is the follow: the addition of steam and CO_2 to reaction mixture leads to a reduction in the performance of catalyst, whatever their typology. In particular, in

order of citation, the catalyst used for these papers are: CoO_x/CeO_2, CuO/CeO_2 and Pt-Au catalyst. In all catalyst, the addition of CO_2 and steam to the reaction mixture decreases their catalytic activity by 25-30%. This worsening is most noticeable at low temperatures ($i.e < 100°C$), while it can be neglected at relatively high temperatures.
Depending on the gas, the drop in catalytic activity differs: the presence of steam blocks the catalytic sites, preventing CO adsorption, and creates interactions between H_2O and CO molecules that favors the WGS reaction, while the presence of CO_2 creates carbonates or carboxylate that adhere to the catalytic site and favor both the methanation and R-WGS reaction. It is clear how the presence of CO_2 involves greater challenges for CO-PROX reaction because, as well as a decrease in catalyst performance, which is common to both gases, the presence of CO_2 encourages two highly undesirable reaction that consume hydrogen and produce carbon dioxide. Kim et al., through TPRs carried out with a mixture containing 10%H_2, 1% of H_2O and CO_2 balanced in N_2, showed that the presence of CO2 and H2O could benefit the oxidised phase during the reaction. In particular, the TPR performed showed that the presence of these two gases in the reducing mixture led to a decrease in the reduction peak and placed the reduction itself at higher temperatures.

Chapter 2

Experimental setup, procedures and methods

In order to achieve the scope of this thesis project,several experimental tests have been carried out.

2.1 Procedure and experimental setup used for CO-PROX try-out

A common procedure underlies all experimental analyses, which involves two consecutive stages. The former is an air pre-treatment stage in which, gradually increasing the temperature, a flow of air is directly conveyed to the catalyst, located inside the reactor. Through this operation, the catalyst is completely oxidized to its active form. The second part of this procedure is the actual reaction, in which the reactants flow, with a specific composition is sent to the reactor.
A laboratory plant has been used to carry out the required experimental tests. The se-up used is shown in Figure 2.1. This arrangement can be split in three different sections:

- A gas feed section;
- A reaction section, where a fixed bed reactor has been assembled;
- An analytical section;

As depicted in Figure 2.1, the gas have been pressurized to 200bar and kept inside cylinders. For safety reason, these pressurized containers are located outside the working area. Therefore, before arriving in the internal line, the gases are expanded though a pressure reducer to a pressure of 5bar. Internally, the flow regulation takes place through a first butterfly valve, which operates as an of-off control and a subsequent mass flowmeters which regulates the flow by means of an input signal sent by a software.

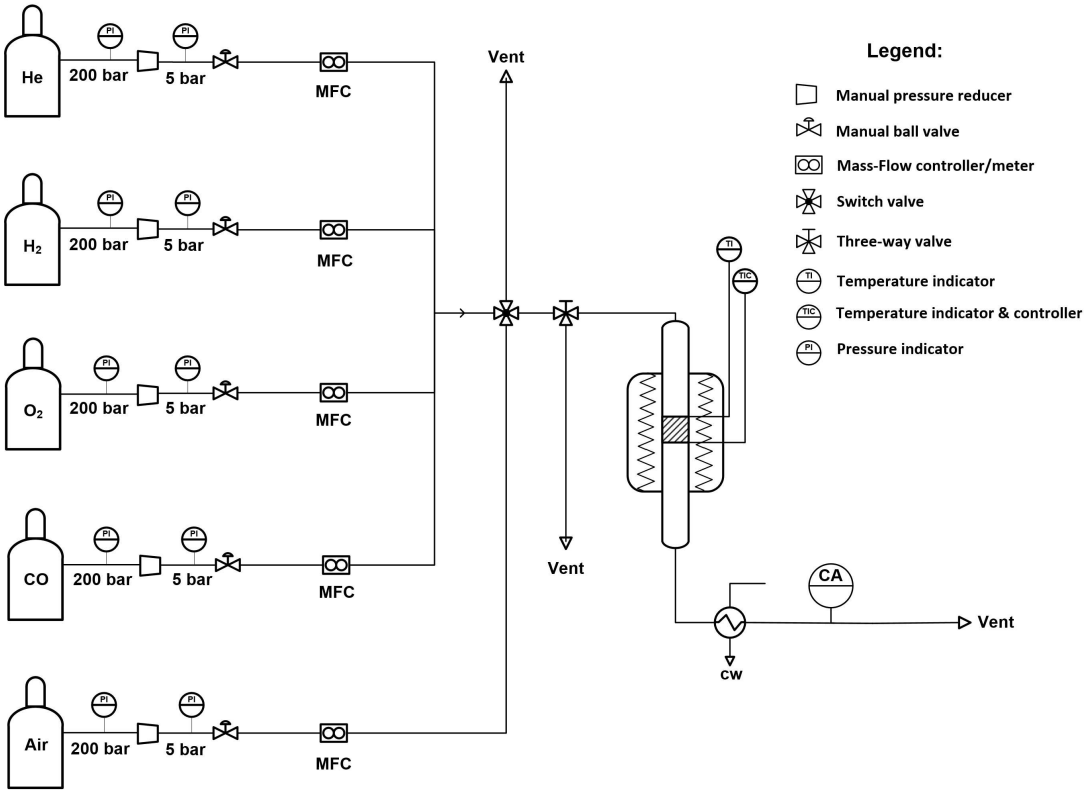

Figure 2.1: Representative scheme of the experimental plant used to carry out the tests

Afterwards to the section of the system regulating the gas flows, the reagent mixture and the air are sent to the 4-way valve. This valve, using an input signal defined by a control software, defines which flow, between the air and the reactants, should be sent to the reactor and which to the vent. After the 4-way valve (also called switch valve), another instrument is placed, which task is to regulate the flow of gas at the desired volumetric flow rate sending to the reactor. Precisely, the latter can be selected between a split valve or a peristaltic pump
The heart of this set-up is the reactor: a quartz tube of a predetermined size in which the catalyst and two thermocouples are placed. Respectively, these temperature transducers serve to control the temperature of the furnace and thus regulate its power, and monitor the temperature of the catalytic bed. Depending on whether water measurement is required or not, a condenser is used, *i.e* a heat exchange required to completely condense the vapors coming from the reactor. Finally, the analysis section must be present. It consists in a series of measuring instruments needed to derive useful information from the test being performed.

2.2 Instruments and equipment used in the experimental setup

In the following paragraphs, all the tools and equipment used will be described in detail. For a better understanding, it is convenient to recall the subdivision of experimental setup, and then to define which instrument and equipment belongs to each section. More precisely, in feed and reaction section, the most relevant interesting instruments and equipment are the mass flowmeters, the four-way valve and the reactor. On the order hand, a different consideration mist be mase for analytical section. Here one cannot define the most interesting equipment, instrument or device, but the one that have been used in each of the tests performed must be specified. In particular the instrument used during this work are:

- Gas-chromatograph Aligent HP-7820;
- Direct thermo-conductivity detector of Gas-chromatograph Aligent HP-6890;
- Micro Gas-chromatograph Variant CP-4900;
- FT-IR IRTracer 100 Shimadzu;
- Oxygen sensor Alphasense O2-C2;

2.2.1 Mass flowmeters

As mentioned before in section(2.1), several flowmeters were used to control the volumetric flow rate of the gases destined for the reactor. In particular, as it is possible to observe from the scheme reported in Figure 2.1, the flowmeters needed to complete the operation are five: one for the inert He, one for H_2, one for O_2, one for CO and the last for the air used in the pre-treatment.

Figure 2.2 explains a generic Bronkhorst's mass flowmeters. Inside this facility, a flow sensor is present, and it works according to the by-pass measurements and heat transfer principle. In particular, the control of flow is obtained by measuring the variation of temperature between the main and bypassed flow. Moreover, the flow controller takes into account the gas flowing through the line by means the specific heat of the gas itself since heat transfer is an intrinsic property of the gas. In order to have a reliable measurement of the volumetric flowrate, before starting the experimental campaign, the MFCs have to be calibrated. The calibration is performed by varing the operating set-point (*i.e.*from 5% to 95%) and measuring downstream the flowrate of a single reference gas (N_2). The correct set-point for different gases can be obtained by adjusting the reference calibration curve with a correction factor that depends on physical properties of the gases. During the experimental campaign, in order to respect the reliability of nitrogen correction method and the functionality of the MFCs over time, the calibration must be checked periodically. The rightmost picture in Figure 2.2 shows the assembly of mass flowmeters in the operating line.

Figure 2.2: Bronkhorst mass flow controller (in the left), real setup of gas flow regulation (on the right)

In addition, in Figure 2.2, it can be observed that in order to mix several gases and thus obtain the reaction mixture with the desired concentration, the flow leaving the flometers are mixed each with other through a T-junctions. The connection of several junctions constitutes a train. In order to facilitate the mixing of gases, the species with larger volumetric flow rate (H_2 and He in this case) have been connected upstream of the train, while the smaller in the downstream side of it.

2.2.2 Four-way solenoid valve

As already anticipated in the previous section, in order to facilitate switching between the two mixtures (the oxidizing and reacting one) used during the CO-PROX test, a four-way solenoid valve is installed in the feed section. The switching valve used during the analysis is presented in Figure 2.3. Through this device is possible to automatically change the gas flow. Its output channels can be selected through the action of a pneumatic actuator controlled by a software. The rotary valve is made of a chamber that has four equally spaced ports paired to each other with micro-metric internal lines and, depending on the ports coupling, two valve position can be identified (*i.e.* on and off). Internal connections can switch from one position to the other by using a two-position air actuator implemented with a solenoid valve assembly that pulses air at 5bar to the actuator to switch the port connections and redirect the gas flow. The solenoid valve is remotely controlled with electrical impulses regulated by a MATLAB executable program.

When CO-PROX test is performing, the air flow and reacting mixture are con-

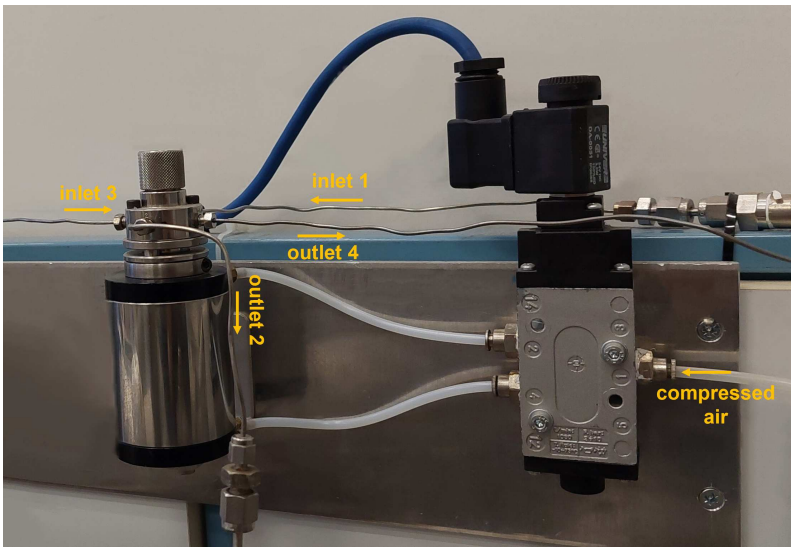

Figure 2.3: four-way solenoid valve

nected to inlet-1 and inlet-3 respectively. Before starting the analysis, the time, in seconds, needed for air pre-treatment and reaction stage must be entered in the control executable file. In particular, it has been defined that during the first phase of the analysis the valve position remain fix to off stance, in such a way that the oxidizing agent leaves through the output-2 channel and goes to the reactor, while the reaction mixtures is released to the vent passing through output-4 channel. At the end of the pre-treatment phase, the software commands the solenoid valve actuator to change its internal position and then from that moment the reactant mixture exits output-2 channel while air is released under hood passing through output-4 canal.

2.2.3 Quartz tube reactor

Previously, it has mentioned that before entering the reactor, the volumetric flow rate of the gases is regulated by means of a split valve or peristaltic pump. In detail, the split valve consists of a T-piece followed by a stem valve, while the peristaltic pump is a generic pump that uses alternating compression to regulate the fluid flow. In particular, tests have shown that by using the split valve, the volumetric gas flow rate changes slightly as the temperature varies. Conversely, when regulated with reciprocating pump, the gas flow is not affected by thermal action, then the reciprocating pump is the optimal choice. The selection of the most appropriate gas flow control system is very important, because the volumetric flow rate defines fundamental parameters of catalytic testing: GHSV and WHSV. These parameters will be more clearly defined in section 2.3 of this Chapter.
A typical catalytic reactor used in this work is outlined in Figure 2.4.It consists

of a quartz tube inserted into a programmable temperature furnace, with heats though an electrical resistance. Quartz is an outstanding reactor material because it is characterized by an excellent chemical inertia, a high melting temperatures and the ability to tolerate high temperature changes oer time and space. In particular, the geometry of this reactor, reported in Table 2.1, is very important for minimizing significant thermal and concentration gradient along the reactor itself.

Table 2.1: Geometrical parameters of quartz glass tube used along experimental tests

Parameter	**Symbol**	**Unit of measure**	**Value**
Internal diameter	d_{int}	[mm]	5.9 - 7.8
External diameter	d_{ext}	[mm]	7.9 - 10
Length	L	[cm]	60

Table 2.1 shows two different values for inner and outer diameters because two types of reactors have been used for this thesis work.
The operating reactor is a fixed bed, made of powders which is positioned inside the quartz tube, and it is kept by two quartz wool layers, upon and below the catalyst. The tube is then sealed with two steel fittings which allow the gas flow to pass through it, and the two thermocouples to be installed. The control thermocouple, with diameter of 1/8", is installed under the catalytic bed, in contact with the lower quartz wool bed, while monitoring thermocouple, which a diameter of 1/16", is introduced from the top side of the reactor and placed inside the catalytic bed. This choice allowed the controller to control the power of the oven, and therefore the operating temperature, without being influenced by the chemistry of the reaction.

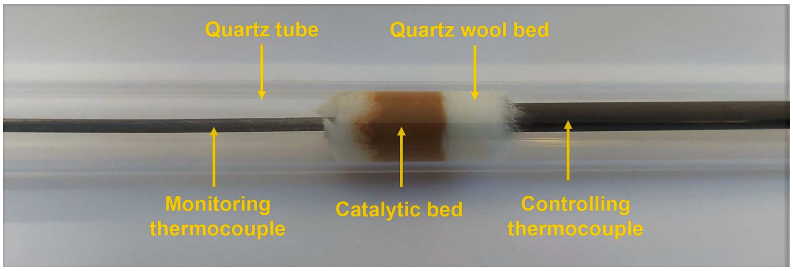

Figure 2.4: Central part of tubular reactor with controlling and monitoring thermocouples

Once assembled, the quartz tubular reactor is placed inside a cylindrical oven that heats it through an electrical resistance.A CFD simulation performed using Comsol software estimated that radial and axial temperature gradients are present inside

the furnace, causing a difference of hundreds of centigrade degrees. In particular, the simulation showed that the se-point temperature is only reached in the central part of the furnace. For this reason, the catalytic bed must be positioned in this area of the oven. Finally, since the furnace diameter is higher than the external diameter of the tubular reactor, it is insulated with quartz wool pieces, preventing also heat loses due to air currents generated by natural convention.
Operationally, the furnace is controlled by a PID-acting thermal regulator, named Omron, which controls the power required by the electrical resistance. Cx-Thermo's software, is directly related with Omron, and it allows the implementation of the desired temperatures polities via computers. On the other hand, the monitoring temperature, is recorded a Measurement Computer data acquisition device via a Matlab's executable.
For analyses in which it has not been required to measure the fraction of water produced , the mixtures leaving the reactor flows through a condenser which, operated at 3-4°C to condense the excess steam. The condenser is made of a glass tube which inserted inside an aluminum blok. The glass tube is closed by a special cap with two threads for the inlet and the putlet gaseous mixture respectively. The jacket between the metal block and the glass cylinder has two connection for the service fluid, that is water /glycol refrigerant mixture, thermostated by a water chiller.

2.2.4 Gas-chromatograph Aligent HP-7820

Looking again at Figure 2.1, it can be seen that the concentration analysis is located after the reaction section. Gas-chromatograph Aligent HP-7820 is one of the instruments used to determine the concentration of the species involved in the CO-PROX reaction. This instrument, represented in Figure 2.5, determines the concentration by means a chemical-physical adsorption. It may be possible because the species present in the feed mixture can be distributed between a mobile phase (more commonly called carrier) and the stationary one. In particular, the stationary phase is a polymer on an inert solid support,situated inside a piece of glass or metal tubing called column. This gas-chromatograph model is equipped with two different adsorption columns: Porapak Q (PPQ), able to separate CO_2, H_2O and light hydrocarbon and, a Molsieve (Molecular Sieve 5Å, MS5A), capable to separate permanent gases, such as O_2, H_2, CO and noble gas. Molsieve column can not accept some gases, like carbon dioxide and water because they would be adsorbed irreversibly, depleting the performance of the column. In order to overcome this problem, this device has a switching-valve able to isolate this last column. To identify and quantify the desired species, GC-7820 uses two detectors in series: a thermal conductivity detector (TCD) and a flame ionization detector (FID). Among these two, only the TCD has been utilized to carry out the tests because it detects all the species.

Figure 2.5: Gas-chromatograph Aligent HP-7820

The choice of the carrier is very important because, in order to have a good detection of each components, the difference between its thermal conductivity and the one of the species to measure has to be as high as possible. In particular, the thermal conductivity of the species involved in CO-PROX reaction are represented in Table 2.2. As can be observe in Table 2.2, the thermal conductivity of all species

Table 2.2: Thermal conductivity of the analysed gases calculated at 250°C, [14]

Gases	**Thermal conductivity [W/(m*K)]**
He	0.26062
Ar	0.02743
H_2	0.27534
O_2	0.04321
CO	0.03958
CO_2	0.03465

except hydrogen differs by an order of magnitude with respect the one of helium. For this reason, this inert gases has been chosen as carrier for this reaction. In contrast, since the thermal conductivity between hydrogen and helium are comparable one each other, the hydrogen determination is impaired by the choice of this inert a carrier. In practice, hydrogen concentration is still determined with adequate accuracy because its quantity in the fed is very high.

In this thesis work, this gas chromatograph has been used to detect the following

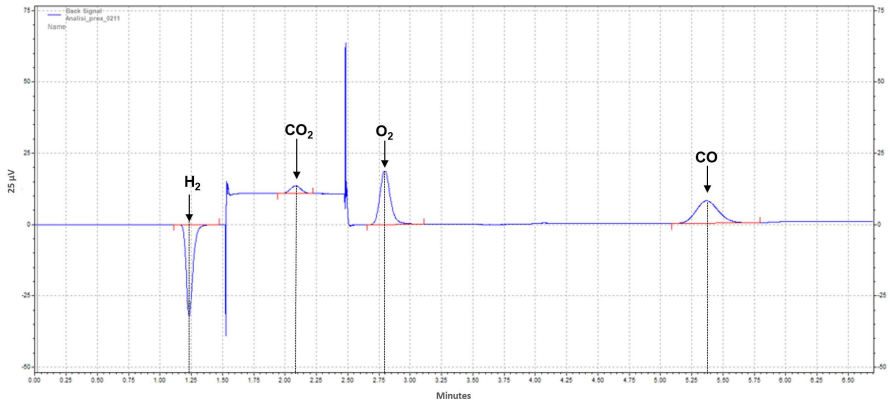

Figure 2.6: Example of chromatogram obtained with Gas-chromatograph Aligent HP-7820 during a CO-PROX analysis

chemical species: H_2, O_2, CO and CO_2. In particular, a chromatogram, such as the one reported in Figure 2.6 is used to both identify and quantify these species. More precisely, a chromatogram represents a series of peaks which are proportional to the amount of substance of each single species present in the reacting mixture. Respectively, qualitative and quantitative analysis are performed through the identification and calculation of each single peak area. Each spike is associated with a retention time (*i.e.*the time required for the species to elute with the carrier and then arrive at the instrument detector). This retention time can be optimized by adjusting both the temperature of the oven and the gas flow pressure inside the gas chromatograph. The definition of the latter together with the setting of the commutation time of 6-way valves is called analytical method. The analytical method used is shown in Table 2.3. The initial temperature (65°C) and the pressure (35psi) was set after several tests to get H_2, CO_2 and O_2 peaks at the right distance between the two valve switches. Subsequent pressure and temperature ramps were used to anticipate the CO release and thus achieve a shorter sequance and thus to perform more analyses for the same test.
The definition of analytical method as well as the first step of the post-processing has been carried out using Open-Lab commercial software.
The first phase of the analysis involves the determination of calibration lines of the gaseous compounds. They are obtained by analyzing a mixture with a known composition. This calibration is then used in the second part of post-processing, the one which uses a Matlab code, to correlate the peaks area to the concentration by means a linear equation.

Table 2.3: Analytical method for Gas-chromatograph Aligent HP-7820

Temperature

	Rate [°C/min]	Value [°C]	Hold time [min]	Total time [min]
Initial ramp		65	3.7	3.7
Ramp 1	60	90	1.3	5.4167
Ramp 2	70	110	1	6.7024

Pressure

	Rate [psi/min]	Value [psi]	Hold time [min]	Total time [min]
Initial ramp		35	3.7	3.7
Ramp 1	20	40	1.78	5.4167
Ramp 2	30	45	1	6.7024

6-way valve

Position	Time [min]
ON	1.5231
OFF	2.4771

2.2.5 Direct thermo-conductivity detector (TCD)

A fast response is not possible with a classical gas chromatograph. If it is necessary to obtain an immediate response, as in TPR analysis, the gas must not pass through stationary pahse, but it must be sent directly to the analysis detector. Gas-chromatograph Aligent HP-6890 has been used to carry out such measurement. This instrument has been adapted so that, if necessary, the detector could be used separately from the stationary phase. With this configuration, the detector compares the thermal conductivity of two gas stream (*i.e.* a inert flow gas and a mixture flow containg the same inert and the sample gas) and produce an electrical signal(µV) proportional to the difference in λ.
The detector cell is divided into two parts, one of them containing an electrically heated filament kept at constant temperature with a constant flow of the reference gas (such as Ar, He or N_2). As the analysis is carried out, the sample gas stream alternately flows across the filament and changes the thermal conductivity by changing the temperature. Therefore, the filament increases its temperature and produces a measurable voltage change. Within the reacting mixture, the two reducing gas are hydrogen and carbon monoxide. As already show in Table 2.2, the thermal conductivity of CO and Ar and the thermal conductivity of H_2 and

He are of the same order of magnitude. For this reason, when TPR with hydrogen has been carried out, Argon has been used as reference gas, whereas in CO-TPR used He as carrier. As already mentioned for GC-7820, a calibration of the species involved must be carrier out in order to construct a calibration straight line used to correlates voltage and gas concentration. Unlike the previous gas chromatograph, the TCD is sensitive to flow rate variation, so both calibration and test must be carried out at the same volumetric flow rate.

2.2.6 Micro Gas-chromatograph Variant CP-4900

Instrumental innovation has enabled the miniaturization of the packed columns that make up the stationary phase inside the gas chromatograph. Variant CP-4900 micro gas chromatograph, represented in Figure 2.7, is an example of this innovation. Contrary to classic gas chromatograph, the supply is a gas taken from the main line via a vacuum pump. This gas is then injected into the carrier flow and sent to the packed columns. Similar to the GC-7820, the micro gas chromatograph has two packed columns PPQ and MS5A, but unlike the former, in the latter instrument, the columns are installed in parallel. The species that the stationary phases are able to separate are all the same.

In contrast to GC-7820, this device uses back-flushing to prevent carbon dioxide

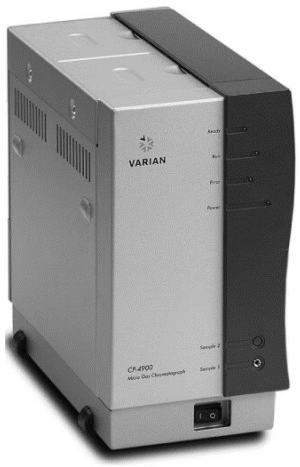

Figure 2.7: Micro Gas-chromatograph Variant CP-4900

and water from entering the zeolite column. In particular, a backflush system always consists of a pre-column and an analytical column. These two columns are coupled at a pressure point, which allow to invert the carrier gas flow direction through the pre-column at a present time.

In micro-GC, the detection of compounds in the reactor output mixture is performed by thermal conductivity detectors. In particular, this instrument uses two different detector, which are installed, through micro-connections at the end of the

two analysis columns. The presence of thermal conductivity detectors made possible to use helium as carrier.
In this thesis work, micro-gas chromatograph has been used to detect the following chemical species: H_2, O_2, CO, CO_2 and H_2O. In particular, the representation of the species separation performed with this instrument is shown in Figure 2.8. As

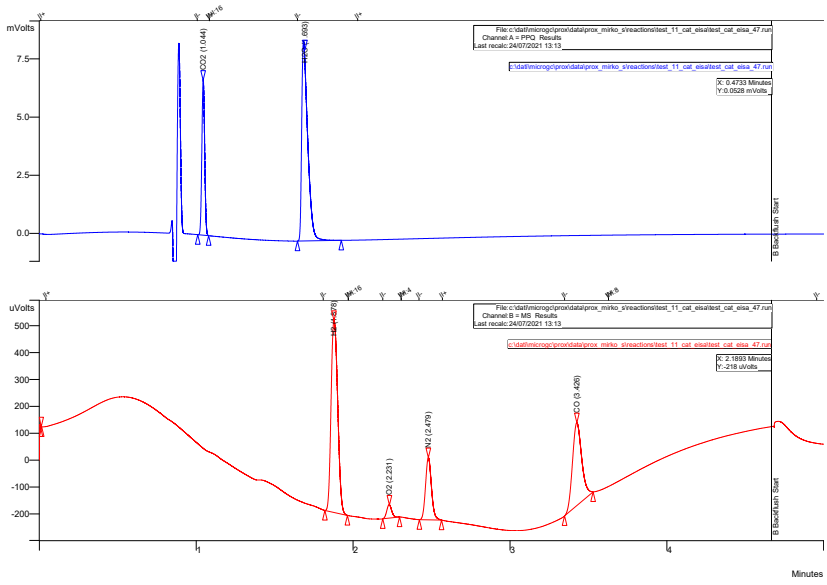

Figure 2.8: Example of chromatogram obtained with micro-gas-chromatograph Variant CP-4900 during a CO-PROX analysis

well as classical gas chromatograph, micro-gas chromatograph requires the definition of an analytical method for conducing species concentration analysis. The definition of the method in this case must be carried out for both columns.
Depending on whether the water was determined or not, two different analytical methods were used during the tests carried out in this work. In the following Table 2.4 and Table 2.5, these methods are shown. Unlike the method explained in section 2.2.4, this method defines the injection time and the sample time, through which it is possible to modify the peaks in term of height and resolution. The special features of this instruments is the possibility of measuring the water produced by hydrogen oxidation. This, as mentioned above, is possible thanks to the presence of pre-column and backflush. In addition, this technique speed up the analysis time, enabling the acquisition of more data during the tests carried out and thus have greater accuracy on the development of the reactions.

Table 2.4: Analytical method for micro-gas-chromatograph Variant CP-4900 which does not consider water identification peak

Parameters	Porapak Q (PPQ)	Molsieve (MS5A)
Column Temperature	100 °C	100 °C
Injection Temperature	100 °C	100 °C
Injection Time	100 ms	20 ms
Sample Time	20 s	20 s
Column Pressure	100 kPa	100kPa
Backflush Time		186 s

Table 2.5: Analytical method for micro-gas-chromatograph Variant CP-4900 which consider water identification peak

Parameters	Porapak Q (PPQ)	Molsieve (MS5A)
Column Temperature	80 °C	85 °C
Injection Temperature	70 °C	50 °C
Injection Time	100 ms	40 ms
Sample Time	10 s	10 s
Column Pressure	70kPa	100kPa
Backflush Time		140 s

2.2.7 FT-IR IRTracer-100 Shimadzu

IR spectroscopy is an analytical technique based on the interaction of electromagnetic radiation with the matter. When an organic molecule is hit by an infrared radiation, the energy transferred is converted into vibrational energy. The molecules absorb frequencies that are characteristic of their structure. Thus, the frequency of the vibrations is associated with a particular normal mode of motion and a particular type. The intensity at a given wavelength depends on the value of the dipolar moment of the bond and therefore on the relative electronegativity of the atoms involved in the bond. When the variation occurs, the molecule produces an oscillating electric field.
The analysis at the IR is carried out to perform qualitative and quantitative analysis of specific species in the product mixture. Specifically, the analysis are conducted with an FTIR spectrometer, IRTracer-100 of Shimadzu, which is represented in Figure 2.9. A FTIR spectrometer produces an infrared spectrum that can be visualized in a plot of absorbance intensity as a function of wave number (cm^{-1}). In this work, the device being considered has been used to analyze the exiting mixture during TPR with CO as reducing species and therefore, the compounds that FTIR should identify and quantify are CO and CO_2. In particular, the wave numbers of

Figure 2.9: FT-IR IRTracer-100 Shimadzu

these two molecules are 2073.3cm^{-1} and 2334.16cm^{-1} respectively.
In practice, the measurement is carried out using a detector, which analyzes the absorption of the mixture over time, placed after the FTIR sample cell, of 12cm in length that is crossed by the infrared radiation. The sample cell is equipped with infrared-trasparent windows, in KBr, at the both ends of the tube. The IR analysis is almost continuous and therefore allows precide indication on the characteristics of the mixture. The tests can last several hours, so the mixture is scanned every 40 seconds to allow long measure time.The instrument requires daily calibration, being sensitive to environmental changes that occur even during the same day.
FTIR works by associating the height of characteristic peaks with a certain concentration value of a species of the mixture. First of all, an initial background spectrum mu be acquired, indicative of the initial conditions presents in the cell. The background is obtained by fluxing a defined amount of inert flow rate into the chamber where the cell is located, to limit disturbances ofrom the atmosphere, especially on CO_2 and H_2O measurements. The variation of the mixture, determined on this spectrum,are analysed through the variation in the adsorption value at predetermined wave number.

2.2.8 Oxygen Sensor

To evaluate the oxygen consumed during Temperature Programmed Oxidation analysis, a oxygen sensor has been used, The most popular technology for measuring oxygen concentration are galvanic sensor. To track catalyst oxidation, Alphasese O2-C2, which is shown in Figure 2.10, has been used. In particular, Alphasese O2-C2 is a mass flow control galvanic sensor that operates like a metal/air battery:

the oxygen in contact with the cathode is reduced with water to hydroxil ions and a balancing reaction of lead oxidation to lead oxide happens at the anode. A current is generated, following the Faraday law, which is proportional to the rate of oxygen consumption, then the signal, which is in the range 0 to 3V (0 to 20.9%O_2) is sent to a PicoLog acquisition software, which reports the actual voltage. In particu-

Figure 2.10: Alphasense O2-C2 oxygen sensor

lar PicoLog is a data acquisition device, capable of transforming an input current signal into an output signal useful for the analysis being carried out. For the analysis performed, the oxygen concentration is the output signal. To obtain that, the sensor must be calibrated, namely a linear relation must be obtained between the current signal and the exact concentration of the mixture sent to the sensors.

2.3 Catalysts

The catalysts tested in this work have been provided by National Center for Scientific Research "Domokritos" (NCSRD). All of them consist of copper oxide supported on ceria and alumina catalyst ($CuO/CeO_2/Al_2O_3$), but they differ according to the synthesis method, or more specifically on the method used to load on the active site on the catalytic support. The catalyst used are shown in Table 2.6. It presents a first distinction according to the method of synthesis, and in addition, there is a further differentiation based to the copper loading and the temperature at which they were calcined.
In the next sections and in Chapter 3, $CuO/CeO_2/Al_2O_3$-ADP will be denoted with A-T_{calc}-%CuO loaded and $CuO/CeO_2/Al_2O_3$-EISA with E-T_{calc}-%CuO.
The catalytic support was synthesized by modifying a facile, highly reproducible and cost effective procedure described by Yuan et al in [42]. This synthesis method called "Evaporation Induced Self-Assembly" (EISA) involved the use of a non-ionic

Table 2.6: Catalyst used during for activity screening step

ADP	EISA
15%- $CuO/CeO_2/Al_2O_3$	$CuO/CeO_2/Al_2O_3$ (400°C)
20%- $CuO/CeO_2/Al_2O_3$	$CuO/CeO_2/Al_2O_3$ (550°C)
30%- $CuO/CeO_2/Al_2O_3$	$CuO/CeO_2/Al_2O_3$ (900°C)

triblock copolymer as a soft-template. In particular, the copolymer is dissolved in an alcohol solution in which various acids and salts were added and maintains under vigorous stirring. The formed final solution was then poured into a petri dish and then placed in an oven at a fixed temperature and for a fixed time. Finally, a calcined procedure was perfumed subjecting the material to a flow of air and gradually increasing the temperature up to a fixed value.
As said earlier, the catalyst employed in this work differs by the second stage of the synthesis procedure. In the case of ADP catalyst this preparation stage has been carried out by the University of Antwerp, in Belgium. This loading step is called Ammonia-Driven deposition Precipitation method and it follows what Xin et al. described in [41]. Specifically, this method involved stirring the substrate with a certain amount of copper-precursor and then adding an aqueous ammonia solution. This step was carried out in a stirred and isolated environment to prevent evaporation of the ammonia. The mixture was then dried and calcined at a specific temperature.

All the catalytic tests carried out in this work was performed at a specific value of Gas Hourly Space Velocity (GHSV). The GHSV, whose formula is given in Eq 2.1, is a parameter that identifies the value of the volumetric flow rate through a specific volume of catalyst. This factor is of considerable importance as it determines the contact time between the reagent flow and the catalytic powder. More specifically, low GHSV values make it possible to obtain a longer residence time between gas and catalyst particle, providing for greater catalytic activity. As the GHSV value increases, the gas-particle interactions decrease, resulting in a loer conversion.

$$GHSV = \frac{\dot{V}_{std\ cond}}{V_{bed}} \tag{2.1}$$

Most of the tests carried out used a GHSV of 20000h^{-1}, to allow the catalytic system to optimize the reaction. This GHSV value mate it possible to define a reference value for CO and H_2 conversion. In order to get closer to the industrial GHSV values, a test with a higher GHSV was carried out and the conversions obtained were compared.

2.4 Experimental procedures and data processing

As mentioned this thesis work involved several catalytic tests. Most of them concern preferential oxidation tests, for which the experimental procedure mentioned in section 2.1 has been used. To identify particular aspect of CO-PROX reaction and specific features of the catalyst used, other analysis have been performed. For these tests, which focus on identifying specific aspects of the reaction and the catalyst, the experimental procedure differs. However, all of them will be described in the following sections.
The tests performed, depending on their ultimate purpose, can be classified into different categories. In this section, these work points are defined, further specifying the experimental procedures used. Subsequently, the data post-processing phase of the tests is also explained. Finally, the main parameters identified and how they have been calculated are described.

2.4.1 Experimental procedures used for catalytic test

All the tests performed can be grouped into the following two macro categories::

- Activity screening of $CuO/CeO_2/Al_2O_3$ catalyst;
- Identification of reaction and catalyst specific properties;

Activity screening of $CuO/CeO_2/Al_2O_3$ catalyst

In this first category of test, all one-shot trials performed on different catalytic material are grouped together. In particular, the catalyst used in this first part of work have been described in the previous section of this chapter. Reflecting what was written in section 2.3, two different type of catalyst were employed in this thesis work and these catalysts were obtained through two different methods of active site deposition. It is possible to divide this category of tests into two different stages: in the first stage, catalyst prepared with the same loading method, called "Ammonia Driven deposition Precipitation" (ADP), but containing a different charge of copper oxide have been used; while in the second part, catalyst obtained using "Evaporation Induced Self-Assembly" (EISA) method to load CuO on the support, but calcined at different temperatures were studied. In particular, the first tests have been performed with the aim of testing whether a different loading of copper oxide affected the performance of the catalyst and, therefore selecting the best catalyst for future tests. Once the optimal ADP catalyst was identified, it became possible to compare the two catalyst families. In order to be consistent, and thus to be able to compare the results, the loading of copper oxide used in EISA catalyst is equal to the CuO loading of the catalyst with highest catalytic activity obtained by ADP method.

The specific experimental set-up (which will be called Setup-1) used to evaluate

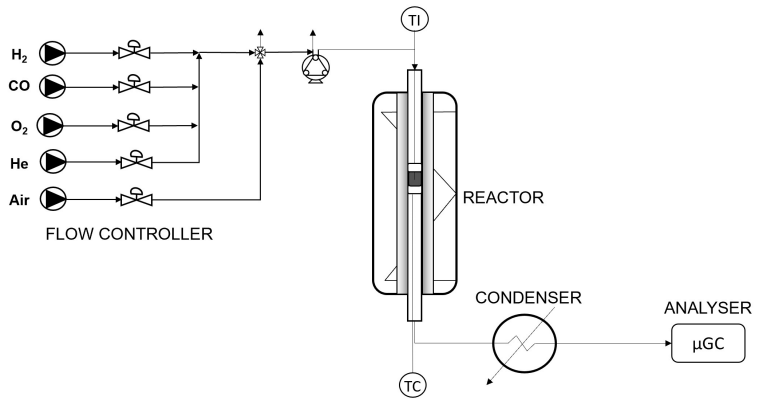

Figure 2.11: Experimental setup employed for catalytic activity tests

catalyst activity is illustrate in Figure 2.11. The reagent flow has been calculated assuming a total volumetric flow rate of 100ml/min. Then, the flow has been reduced to a specific value (defined below for each tests) by means a peristaltic pump. All catalyst have been previously screened to eliminate a certain range of particle size and the amount of catalyst with too fine grain size has been discarded. This operation is useful to avoid an increase in pressure drops inside the reactor and therefore the leakage between quartz tube and metal joint. To conclude, water produced by hydrogen oxidation reaction has not been measured in these tests. For this reason, a condenser has been placed at the reactor outlet. As shown in Figure 2.11, micro gas chromatograph or the gas-chromatograph GC7820 are used to determine the concentration of each species present in the exiting reactor flow. The micro gas chromatograph and the Aligent HP-7820 method defined for conducting these tests are shown in Table 2.4 and Table 2.3.
For what concern the experimental procedure, before running the analyses, the sample is pre-treated in an oxidative flow, to bring all the particles inside the catalytic bed to an oxidized state before the PROX activity test. Once the oxidation phase is complete, the reacting mixture is fed to the reactor. Both stage of the test are subject to a specific temperature program and they are carried out with a specific gas flow composition. The main experimental parameters used to carry out the tests are shown in Table 2.7

Table 2.7: Experimental parameters used in catalytic activity tests

Stage	**Air** [%]	$\mathbf{y}_{He}$ [%]	$\mathbf{y}_{H2}$ [%]	$\mathbf{y}_{O2}$ [%]	$\mathbf{y}_{CO}$ [%]	β [°C/min]	**GHSV** [h^{-1}]
Pre-treatment	100	-	-	-	-	5	20k
Reaction	0	47.6	50	1.2	1.2	2	20k

An important factor that must be decided before carrying out a test is the heating protocol of the furnace. Figure 2.12 and the β column in Table 2.7 show the thermal protocol chosen for these tests. In particular, for both stages of the test, furnace has been programmed to linearly heat and cool the reactor. In Figure 2.12, two different heating and cooling rates can be seen for pre-treatment and reaction stage. More specifically, in the first stage of this analysis an higher heating rate can be used because the concentration of the oxidizing agent is not monitored as the temperature changes. On the contrary, in the reaction phase the concentration of all the species is monitored and a lower heating and cooling rate must be used to ensure measurements that reflect a quasi-stationary system. In addition, two isotherms are kept at the end of each heating ramp. In the pre-treatment stage, the isotherm is needed to complete the perfect oxidation of all catalyst particle, while in the second stage, an isotherm is present to determine the time required to achieve a steady-state condition at high temperatures.

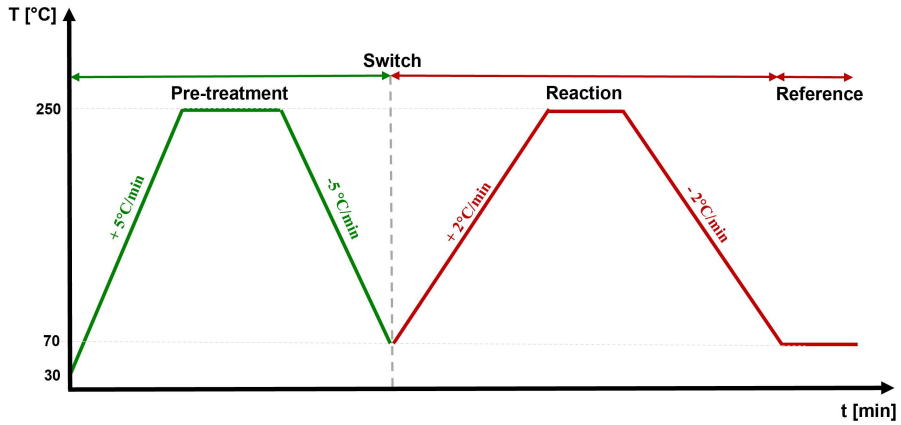

Figure 2.12: Temperature program applied to pre-treatment and reaction phase during catalytic activity tests

Several reactors have been used to test the catalyst. Depending on the amount available of powered material, the height of catalytic beds differs between the reactors. This latter parameter, as well as the reactor diameter and the volumetric gas flow rate, are important factors regarding the definition of "Gas Hourly Space Velocity" (GHSV) since affect the bed volume. So, in order to have the same GHSV, having different catalytic bed size, the volumetric flow rate differs between tests.
To identify the performance of catalyst synthesized by EISA method, a similar experimental procedure has been used. In particular, the composition of the reacting gas flow and the value of GHSV were were the same as ADP catalyst but, the controlled temperature in the pre-treatment and reaction stages was increased to 280°C and the temperature rate set for the reaction stage further dropped to 1°C/min. The temperature can be increased because the calcination temperature is higher and therefore the catalyst will not be sintered. In addition, by increasing

the temperature more information about the system can be identify. On the other hand, the temperature is not increased by much because the Carbon Monoxide Preferential Oxidation process does not require very high temperatures.

Identification of reaction and catalyst specific properties

The A-550-20 catalyst with the highest catalytic activity towards the carbon monoxide preferential oxidation reaction has been used for further tests. In particular, these trials have been performed to determine the following aspects:

- Presence of Water Gas Shift reaction in addition to H_2 and CO oxidation;
- Comparison of catalytic performance between fully oxidized and fully reduced catalyst;
- Comparison of catalytic performance between fresh and old catalysts;
- Change in the oxidative state of the catalyst during the reaction
- Temperature and reduction peak of the catalyst;
- Temperature and oxidation peak of the catalyst;

The methodology used to carry out the additional tests centered on verifying the first four bullet points is very similar to the one used to verify the activity of ADP and EISA catalysts. More specifically, as a results of consideration that will be outlined later on, it has been decided to take into account only the cooling stage, thus excluding the heating step.
The major difference in these new experimental procedures concerns the pre-treatment phase. For all tests centered on determining the state of the catalyst and its performance during the CO-PROX reaction using an oxidized catalyst, pre-treatment has been carry out by feeding a stream of air to the reactor. Conversely, whenever the reaction is carried out using a reduced catalyst, a reducing stream (5% of H_2 in helium) has been fed to the reactor.
Figure 2.13 shows the temperature protocol used in these analyses. Respect to the protocol defined in Figure 2.12, the reaction phase has a high-temperature isothermal stage. This stationary stage is required for the stabilization of the analysis instruments.

The experimental procedure and set-up takes a different format when the objective of the test regarding the identification of specific catalyst features, such as its reduction and oxidation profile and their respective temperature. In order to define these features, it is necessary to carry out a Temperature Programmed Reduction (TPR) and Temperature Programmed Oxidation (TPO). To perform these analyses, a mixture containing the selected reducing/oxidizing agent, balanced in inert must be sent to the reactor, and a specific heating program must be set to the furnace. In particular, the reaction mixture used to carry out all the tests defined

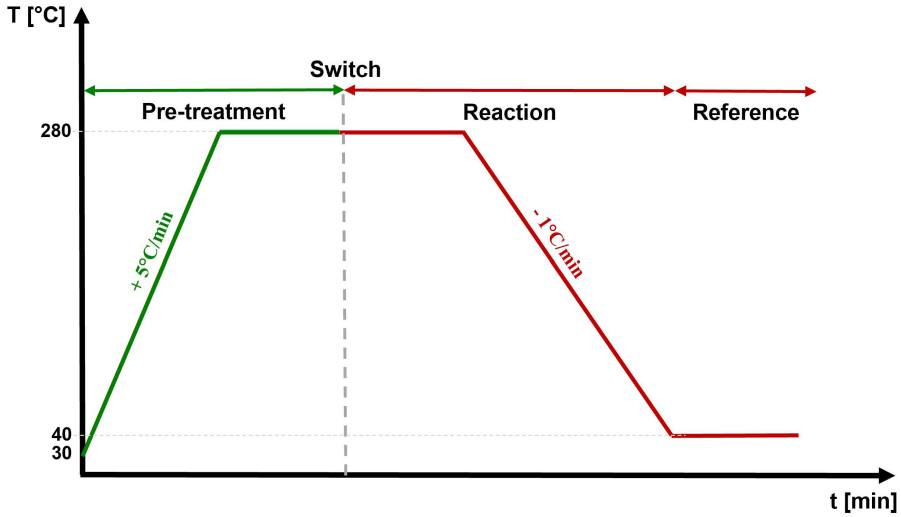

Figure 2.13: Temperature program applied to pre-treatment and reaction stages during the analysis performed to identify the catalyst oxidative state and its performance during CO-PROX reaction

earlier, contains hydrogen and carbon monoxide, both as reducing agents.In contrast, for TPO analysis a mixture of oxygen and inert is sent to the reactor.
Figure 2.14 shows the experimental set-up used for these trials (which will be called

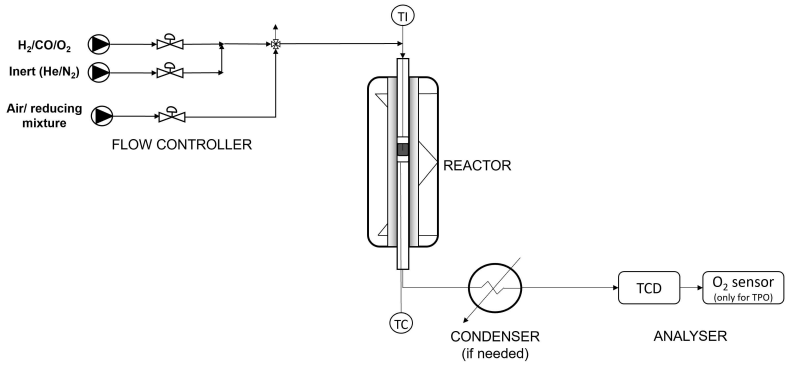

Figure 2.14: Experimental setup employed for TPR and TPO analyses

Setup-2). The main difference between the experimental set-up used between the test focused on verifying the catalytic activity and these ones lies in the analysis section. In particular, these tests require some instruments with a very high sampling frequency in order to detect any possible variation in the concentration of the species involved.
Similar to the analyses defined above, TPR can also be seen as a series of two stages

(see Figure 2.15): an oxidation step performed to bring the catalyst to its maximum oxidized level, and a subsequent actual TPR stage. In TPR stage, the first and second isothermal periods are required by the instrument to ensure a constant reference signal both at low and high temperature. A specular thermal protocol us used for TPO analysis. The difference again lies in the pre-treatment stage, where, in contrast to TPR, the catalyst have to be reduced.

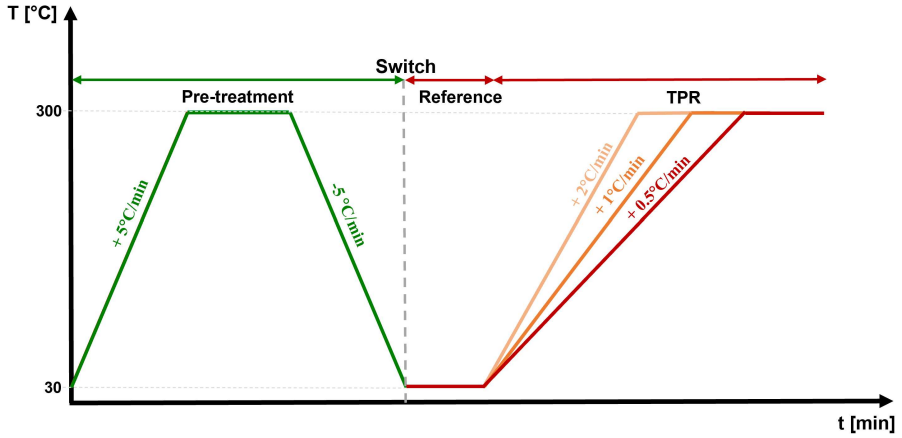

Figure 2.15: Temperature program applied to pre-treatment and TPR stage of analysis

2.4.2 Processing of the experimental data and parameters calculated

The output signals of each analytical instrument, have been employed to obtain useful information with respect the catalyst, as well as, to gain more information about the reaction mechanism of CO-PROX. More precisely, the experimental data obtained by analytical instruments have been processed with a tailored script of Matlab language, that allows to easily obtain the match between compositions, temperatures, time and pressure and then quantify important parameters like conversion, selectivity and variation of concentration. The script used in CO-PROX tests is able to: open the files *.Area* from the gas-chromatograph (Aligent HP-7820) and read the values of each area associated to a single peaks, open and read the file *.dat* from the Matlab executable for temperature and pressure acquisition and the files *.txt* from CX-Thermo software used by the thermal regulator. For all these data, the Matlab's code performs a synchronization of the variables using the time of the slower instruments (GC-7820) to perform the analysis, as a limiting factor. The total molar flow rate entering to the reactor has been calculated through the Ideal Gas Equation of State (IG-EoS) reported in Eq 2.2, where P is the ambient pressure,$\dot{V}_{tot}^{in}$ is the total volumetric flow rate entering in the reactor, Rg is the universal gas constant and T is inlet gas flow temperature, assumed equal to

the ambient one. The total molar flow rate is assumed constant during the whole process since diluted mixtures are used.

$$\dot{n}_{tot}^{in} = \frac{P\ \dot{V}_{tot}^{in}}{Rg\ T} = \dot{n}_{tot}^{out} = \dot{n}_{tot} \tag{2.2}$$

The species molar flow rate exiting from the reactor, is then calculated through the Matlab's code by means the product of the total molar flow rate and the mole fraction of each individual component obtained from the chromatogram areas.

$$\dot{n}_i = \dot{n}_{tot} * y_i^{out} \tag{2.3}$$

The species molar flow rates are useful because allow to calculate several helpful parameters such as conversion, selectivity, material balances errors and delta of concentration. More precisely, the conversion has been calculated on the reagents, such as H_2, CO and O_2 according to Eq 2.4-Eq 2.6:

$$X_{H_2} = \frac{\dot{n}_{H_2}^{in} - \dot{n}_{H_2}^{out}}{\dot{n}_{H_2}^{in}} \tag{2.4}$$

$$X_{O_2} = \frac{\dot{n}_{O_2}^{in} - \dot{n}_{O_2}^{out}}{\dot{n}_{O_2}^{in}} \tag{2.5}$$

$$X_{CO} = \frac{\dot{n}_{CO}^{in} - \dot{n}_{CO}^{out}}{\dot{n}_{CO}^{in}} \tag{2.6}$$

Conversion makes it possible to determine how much hydrogen and carbon monoxide has been consumed during the reaction. Since CO-PROX consist of several reaction in parallel, a further useful parameters is the selectivity, which explains how much of a given reagents can be converted into a given product. The selectivity considered is given in:

$$S_{CO/O_2} = \frac{\dot{n}_{CO}^{cons}}{\dot{n}_{O_2}^{cons}} * \left|\frac{\nu_{O_2}}{\nu_{CO}}\right| = \frac{\dot{n}_{CO}^{in} - \dot{n}_{CO}^{out}}{\dot{n}_{O_2}^{in} - \dot{n}_{O_2}^{out}} * \left|\frac{\nu_{O_2}}{\nu_{CO}}\right| \tag{2.7}$$

Another means of identifying what is happening during the process and thus understanding the mechanism of the CO-PROX reaction is to calculate the variation of concentration for both reactants and products. These parameters are calculated as:

$$\Delta x_{reactant} = y_i^{in} - y_i^{out} \tag{2.8}$$

$$\Delta x_{product} = y_i^{out} - y_i^{in} \tag{2.9}$$

Finally, the accuracy of the CO-PROX tests results has been estimated calculating the error on the closure of carbon and oxygen balance, reported in Eq 2.10 and Eq 2.11

$$Err_C = \frac{\dot{n}_C^{in} - \dot{n}_C^{out}}{\dot{n}_C^{in}} = \frac{(\dot{n}_{CO}^{in} + \dot{n}_{CO_2}^{in}) - (\dot{n}_{CO}^{out} + \dot{n}_{CO_2}^{out})}{\dot{n}_{CO}^{in} + \dot{n}_{CO_2}^{in}} \tag{2.10}$$

$$Err_O = \frac{\dot{n}_O^{in} - \dot{n}_O^{out}}{\dot{n}_O^{in}} = \frac{(2\dot{n}_{O_2}^{in} + \dot{n}_{CO}^{in} + 2\dot{n}_{CO_2}^{in}) - (2\dot{n}_{O_2}^{out} + \dot{n}_{CO}^{out} + 2\dot{n}_{CO_2}^{out})}{\dot{2}\dot{n}_{O_2}^{in} + \dot{n}_{CO}^{in} + 2\dot{n}_{CO_2}^{in}} \tag{2.11}$$

The experimental error depends from several factors such as the accuracy of the calibrations of the gas chromatograph and the presence of some species formed but not considered/measured. In particular, a positive values of these error suggest that some C or O fed are missing in the outlet. This consideration is particularly relevant to the oxygen material balance, because by not measuring the water produced by the reaction, the balance will be positive if water is produced (ss will see in the next chapter oxygen error achieve error higher than 50%). For what concern the carbon material balance, since no more species should be produced during the reaction, low values of err_C are considerable acceptable (low value means that the results are affect by only minimum experimental error).
The post-processing of TPR and TPO analyses is slightly different from the previous one. Here too, the Matlab's code opens the *.txt* files containing the temperature data of the control thermocouple and the *.dat* files containing the vector of the monitored temperature, but unlike the code used for the CO-PROX analyses, this script does not open the data of *.Area* file, but another *.dat* file obtained as a response from the Matlab executable (GC.exe), used to manage the direct thermo-conductivity detector. Considering the post-processing of a TPR analysis (for a TPO, the procedure is specular), once all files required have been opened, the code performs a data synchronization. Then, the vector containing the TCD signal is converted into a mole fraction of the reducing species by means of the TCD calibration.
To achieve the ultimate purpose of a TPR analysis, the factor that need to be determined are, the reducing agent quantity consumed and the temperature at which this consumption takes place. In order to obtain that, through Eq 2.2, the total molar flow rate is calculated (which again can be considered constant given the high dilution) and, then the molar flow rate of the reducing species is calculated by means Eq 2.3. The molar flow rate consumed over time is then calculated using Eq 2.12. In addition to the molar flow rate, the amount of hydrogen or oxygen of the reaction mixture consumed during TPR or TPO respectively can also be calculated. This calculation requires integration of the area of the reduction/oxidation peak. Integration is performed using a Matlab command which performs the following in Eq 2.13. Knowing the stoichiometry of the reduction and oxidation reaction of the catalyst, the amount of reduced and oxidized material in the catalyst can be

determined.

$$\dot{n}^{cons}_{H_2,CO} = \dot{n}^{in}_{H_2,CO} - \dot{n}_{H_2,CO}(t) \tag{2.12}$$

$$n^{cons}_{H_2,CO} = \int_{t_{in}}^{t_{fin}} \dot{n}^{cons}_{H_2,CO}(t)dt \tag{2.13}$$

Chapter 3

Results and discussion

This Chapter collects all the results obtained during this thesis work. More precisely, these findings include a first theoretical study, focused on the thermodynamic equilibrium achievable during the CO-PROX process, and a second experimental work, focused on catalytic aspects of CO-PROX and on the catalyst previously defined in paragraph 2.3.
For sake of clarity, the product composition profile will be mainly presented in dry form because all the water in the reaction mixture is assumed to be totally withheld by the condenser.

3.1 Equilibrium in CO-PROX reactions

Reflecting what has been said in section 1.3.1 the Preferential Oxidation of Carbon Monoxide is used to selectively oxidize CO (see reaction in Eq 1.3). Unfortunately, with a generic reacting mixture, other undesirable reactions emerge (reported in Eq 1.4).
Both the oxidation reactions, as well as the methanation ones, are exothermic and occur with a decrease in the moles number. Therefore, at low temperatures these reactions are competitive with each other and therefore CO_2, CH_4 and H2O should be expected among the reaction products. As the operating temperature increases, these reactions will gradually be disadvantaged and then, the resulting mixture will be richer in H_2, CO and O_2. For oxidation reaction, one particular aspect must be taken into account: in comparison with methanation reactions and WGS, the equilibrium constant of H_2 and CO oxidation are extremely high at any temperatures, and then such reactions should be favored at high temperatures yet. This makes it possible to suppose that CO_2 and water will also be present at higher temperatures.
The thermodynamic equilibrium has been calculated using the open-source NASA-CEA software , which uses the data documented in "NASA Glenn Coefficients for

Calculating Thermodynamic Properties of Individual Species" as a thermodynamic database.
To estimate the isothermal and isobar equilibria, the software required the following data of input:

- Temperature at which the equilibrium was to be calculated. This imput value has been varied from 50°C to 950°C with a steps of 50°C;
- Pressure, always at 1bar;
- Species fed and their mole fraction, which for this work are the one reported in Table 2.7;

The simulation reveled that more than 120 different species are included in this reaction mechanism. Most of these species are radicals and hydrocarbon up to C_4. In Figure 3.1, the molar fraction of the species involved in this thermodynamic

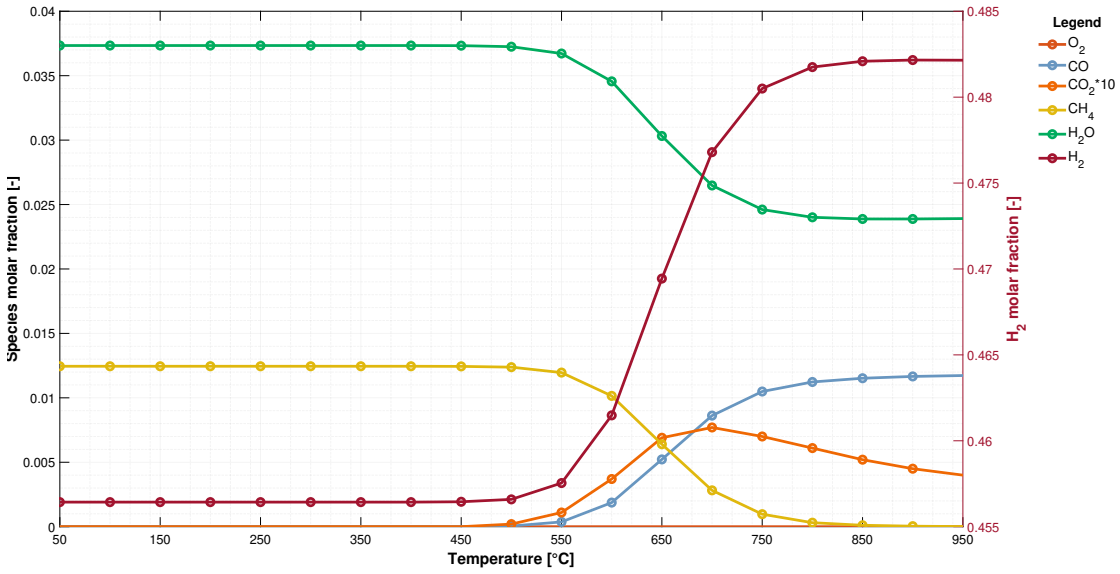

Figure 3.1: Equilibrium molar fraction as a function of temperature, P = 1atm and y^0 as reported in Table 2.7

equilibrium with a fraction higher than 5ppm are plotted. The picture can be subdivided into three temperature range. Below 450°C the total consumption of CO, O_2 and H_2 are observed. For what concern the products, only CH_4 and H_2O are formed. As the temperature increases, CO_2 and reagents molar fractions increase at the expense of methane and water. For temperatures above 850°C a plateau is observed: methane is no longer formed, CO_2 mole fraction decreases, and the amount of steam in the outlet mixture stabilizes.
A low temperatures, CO can be consumed either directly by methanation reaction, or through a chain mechanism involving an initial oxidation and a subsequent CO_2

methanation. To clarify the possible reactions, reference can be taken to concentration variation between equilibrium and feed illustrated in Figure 3.2. The figure indicates that the amount of steam produced is greater than the stoichiometry of H_2 oxidation reaction, and this discrepancy is due to methanation reaction. As for CH_4 production, this is attributable to CO methanation reaction. This statement is derived from the calculation between the actual consumption and the theoretical H_2 consumption due to its oxidation reaction. In particular, considering the methanation equation in Eq 1.4, it can be observed that when produced by CO methanation reaction, one mole of CH_4 requires the consumption of three moles of H_2; on the other hand, if the same amount of CH_4 is produced by Sebatier reaction (CO_2 methanation), the moles of hydrogen involved increase to four. For this reason, it may be stated that for temperatures below to 450°C, the CO oxidation reaction is not favored according to thermodynamics. As the temperatures

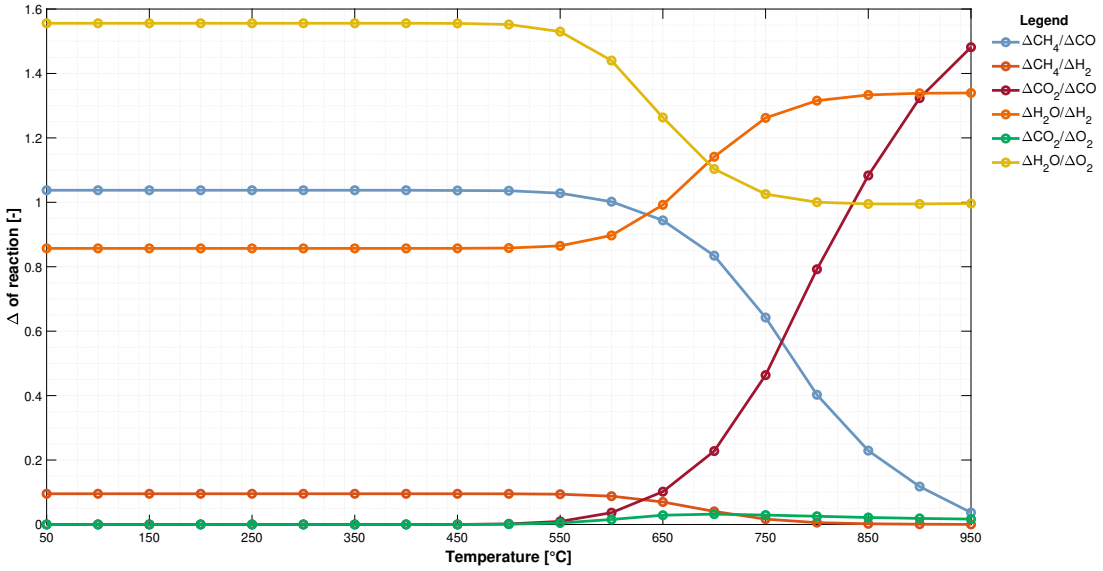

Figure 3.2: Delta of reaction as a function of temperature, P = 1atm and y^0 as reported in Table 2.7

rise, CO methanation reaction is less thermodynamically favored: H_2O production reaches values that approximately respect the stoichiometry of hydrogen oxidation reaction and a tiny fraction of CO_2 arise. However, it should be noted that the consumption of H_2 does not respect the stoichiometry of its reaction. Indeed, at high temperature, methanation reaction is disadvantaged, but still present, and this allows further hydrogen consumption.
The result of Figure 3.1 can be founding in terms of moles. To account for total moles variation, in the present case, the result would be the same since, as stated in section 2.4.2, the molar flow rate can be considered constant due to the high

dilution of the system. In particular, a material balance, on the inert species (represented in Eq 3.1) has been carried out to establish this statement. Then, Eq 3.2 enabled the evolution of the total number of moles, as the temperatures changes. Finally, the number of moles calculated with the inert material balance has been compared with the one considering constant number of moles. More specifically, the error between these two calculations has been estimated. This error, reveled a variation lower than 1% between the two calculation and, therefore the assumption of constant molar flow rate can be consider valid.

$$n_{He} = const = (y_{He} n_{tot})^{eq} = (y_{He} n_{tot})^{out} \tag{3.1}$$

$$n_{tot}^{eq} = \frac{n_{tot}^{in} y_{He}^{in}}{y_{He}^{eq}} \tag{3.2}$$

Knowing the total molar flow rate, the conversion of the system's reactants could be calculated through a preliminary determination of the molar flow rates of each species and the subsequent Eq 3.3 - Eq 3.5 .

$$X_{CO} = \frac{n_{CO}^{in} - n_{CO}^{eq}}{n_{CO}^{in}} \tag{3.3}$$

$$X_{H_2} = \frac{n_{H_2}^{in} - n_{H_2}^{eq}}{n_{H_2}^{in}} \tag{3.4}$$

$$X_{O_2} = \frac{n_{O_2}^{in} - n_{O_2}^{eq}}{n_{O_2}^{in}} \tag{3.5}$$

Figure 3.3 shows the reagents conversion profile. Carbon monoxide, by means of methanation reaction, fully react up to 450°C. Thereafter, its conversion dramatically drops because the equilibrium disadvantages this reaction at higher temperatures. The same behavior can be observed for hydrogen. Below to 450°C, H_2 is simultaneously consumed by CO methanation and H_2-OX , in fact in this thermal range hydrogen conversion is 12%, which is higher than 4.8% expected if only H_2 oxidation reaction took place. At higher temperatures, H_2 conversion decreases to 6% and remain constant until 950°C. At these temperatures, this H_2 conversion is due to the hydrogen oxidation reaction and some reaction that use a lower amount of hydrogen. On the other hand, O_2 conversion remains constant to 100% for any temperature. Comparing the conversion and molar fraction plots, can be stated that the O_2 consumption is only due to hydrogen oxidation reaction.

3.1.1 Conclusion

The thermodynamic analysis demonstrated how at temperature comparable to the operating condition at which tests PROX will be carried out, CO is fully consumed

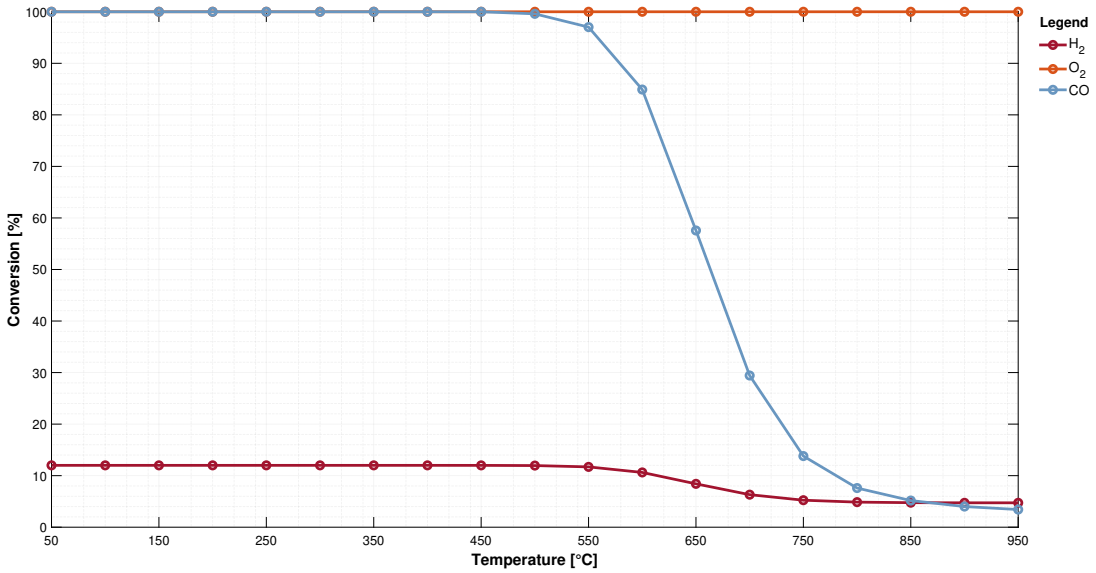

Figure 3.3: Reagents conversion as function on temperatures, P = 1atm and n_{tot}^{in} = 100 moles

in favor of the methane formation. This result should be consider very interesting, since no molecules of carbon monoxide would be present in the output flow. On the other hand CO methanation involves a significant consumption of hydrogen: H_2 is lost due to its oxidation reaction, together with the methanation reaction.
In short, conducting reactions under these conditions is not industrially profitable. For this reason, as already mentioned in the first chapter of this thesis, the CO-PROX process must be carried out in the presence of catalyst which must be highly selective towards the CO oxidation reaction, disadvantaging both the CO methanation and H_2 oxidation reaction. For this reason, all the these reaction must always be checked experimentally, particularly the CO methanation because it is the reaction that uses the largest amount of hydrogen.

3.2 Activity of $CuO/CeO_2/Al_2O_3$-ADP with different CuO loading

The main objective of this first part of tests carried out during this work, concerns the quantification and then the comparison of catalytic activity of $CuO/CeO_2/Al_2O_3$-ADP catalyst, as a function of two different factors: the loading of active site and the method used to synthesize the catalyst itself.
This section shows the results obtained from tests aimed to quantify the activity of

ADP catalysts. The experimental setup employed (Setup-1) and the experimental procedure have already been defined in section 2.4.1, specifying in Figure 2.12 the thermal protocol and in Table 2.7 the composition of the inlet gases and the value of GHSV used.

3.2.1 Observations on the thermal behavior

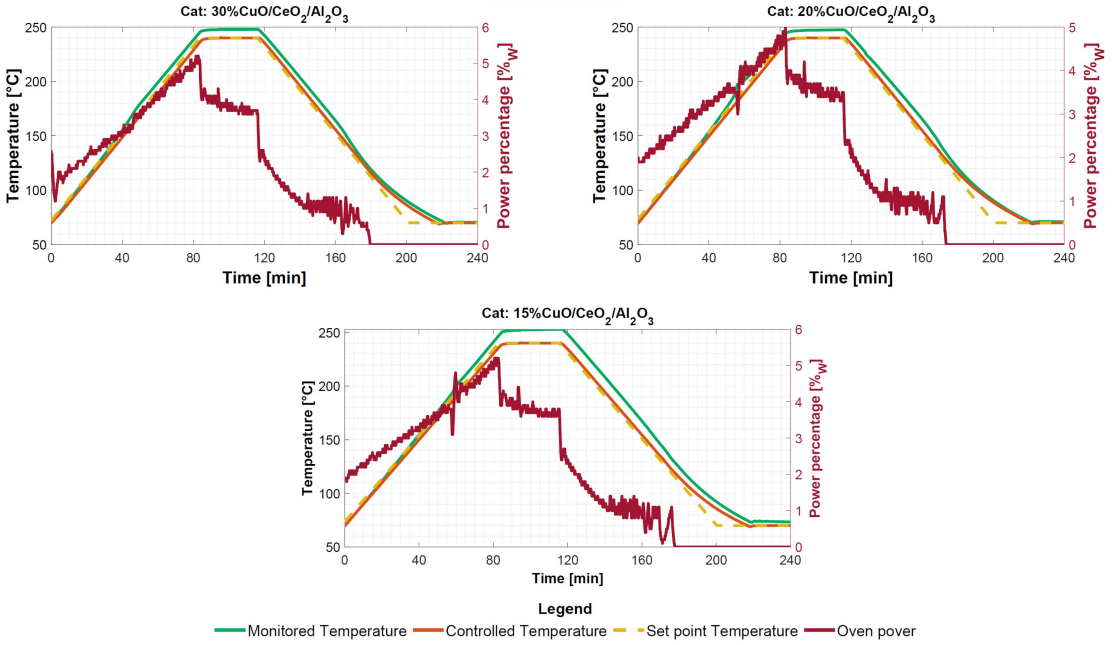

Figure 3.4: Trends of monitored temperature(green line), controlled temperature (orange line), set-point temperature (yellow dashed line) and oven power (red line) during catalytic activity test on ADP catalyst at different CuO loading

Before examining the catalytic performance of each ADP catalyst, the measured thermal profile, which is common to all the catalyst, can be seen in Figure 3.4. More precisely, the controlled temperature, the monitored temperature, the set-point temperature and the profile of oven power (red continuous line). In particular, up to 55 minutes, there is an overlapping between the oven temperature (*i.e* the controlled one) and the catalyst bed temperature (the monitored). This overlap indicates that up to this temperatures the catalyst is not active and therefore, any reaction takes place yet. The temperature at which the two Ts begin to separate depends on the catalyst; it seems to decrease as the loading of cooper oxide increase. In presence of A-550-30, the green line, with compared the orange one changes its slope, from around 130°C, while for A-550-20 and A-550-15, the temperature must be achieve 145 and 150°C. However, this temperature cannot

be used as a discriminator between the three catalyst because the difference between them is small and approximated. Remarkable difference between the three catalysts is shown in the heating power of A-550-20 catalyst. At 180°C there is a temperature peak which reinforces the gap between the two temperature, by almost 20°C (see Figure 3.5). This temperature jump demonstrates a rapid increase in the catalytic activity. The other two catalysts also show an increase in the monitored temperature, but the difference is not as marked as for A-550-20. For A-550-15, above 200°C, it is observed an almost constant temperature gap demonstrating that some exothermic reactions occur. However, in the isothermal section as well as in the cooling stage, the large difference between the monitored and controlled temperature is probably due to the presence of one or more exothermic reaction, and to the positioning of the two thermocouple. This observation results from the presence of ΔT even at low temperatures.

Figure 3.5 and Figure 3.6 confirm the cause of the peak present in the heating

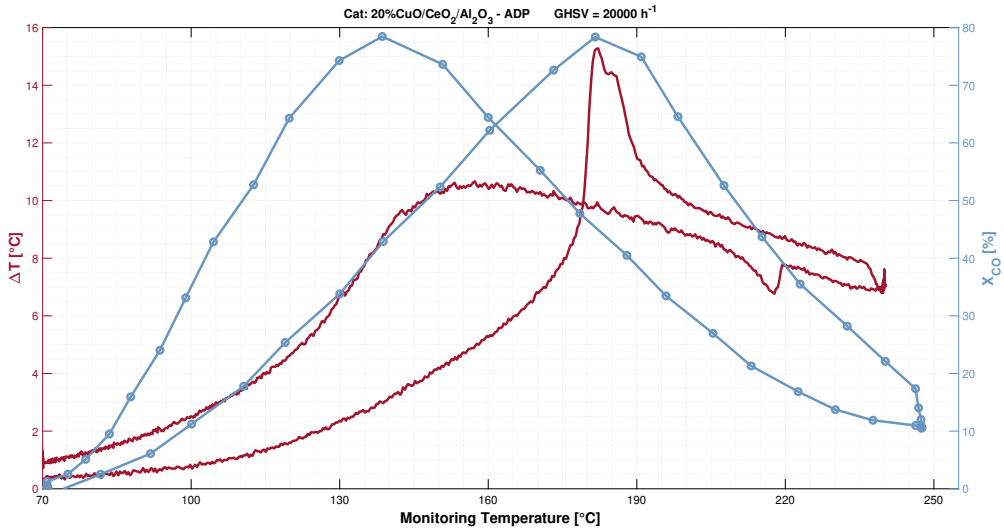

Figure 3.5: Temperature variation and CO conversion as function of temperature. Test:3 Cat: A-550-20

ramp in Figure 3.4 referring to A-550-20. The A-550-20 catalyst shows a maximum conversion value at the same temperature at which the temperature variation peak is shown. Figure 3.5 shows that the maximum temperature variation occurs at the temperature at which the maximum CO conversion is observed. In addition, the power of the furnace decrease at the same temperature. This implies a sudden generation of the heat due to the exotermic reaction. Figure 3.5 also shows a decrease in temperature variation in the cooling stage due to possible water condensation on the control thermocouple.

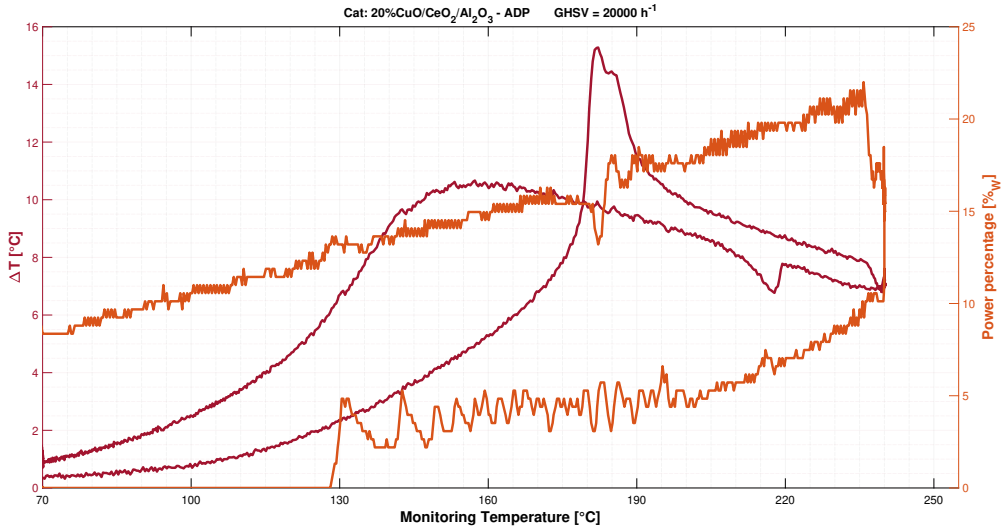

Figure 3.6: Temperature variation and oven power as function of controlled temperature. Test:3 Cat: A-550-20

3.2.2 Catalytic activity test of A-550-15

The experimental condition of this test are outlined in Table 3.1. The specific experimental conditions for this test are shown in the Test:4 row on the diary reported in the Appendix of this thesis. The profile of measured molar fraction and the

Table 3.1: Experimental conditions for the catalytic test over A-550-15

Heating/cooling rate [°C/min]	**T range [°C]**	$\dot{V}_{in}$ **[ml/min]**	**GHSV [h^{-1}]**	h_{cat} **[mm]**	$\varnothing_{particle}$ **[µm]**
2	70 - 250°C	38.482	20k	4	45 - 250

monitored temperature as a function of time is shown in Figure 3.7. Figure 3.7 is useful for obtaining temporal information about the system. It is possible to observe a delay between species concentration compared to the temperature. That is apparent at the beginning and end of the isothermal stage. A non-uniformity of the temperature along the axial direction of the catalytic bed. This delay prevailing in the final part of the isotherm, where a continuity of the species concentration value is observed, when in reality, it should drop whit the same profile obtained in the heating step. This effect may be due to delay between the output data of the micro-gas chromatograph and the monitoring temperature. The delay is greater than 8 minutes, and therefore a thermal inertia must be considered on the possible causes of this effect. This delay is detectable in every test performed with this instrument.

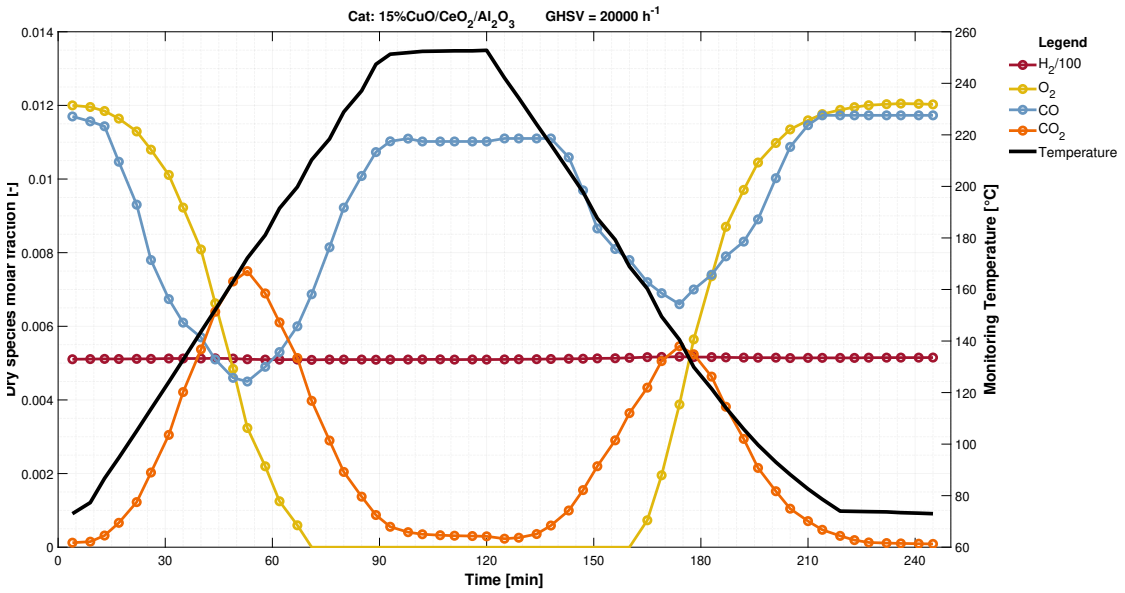

Figure 3.7: Dry species molar fraction and monitored temperature as function of time. Test:4, Cat: A-550-15

The profile of measured molar fractions as a function of the monitored temperature is depicted in Figure 3.8. The picture illustrates that at a temperature of 70°C, at the beginning and at the closing time of the test, the catalyst is not active and consequently, the mole fractions of the reactants reflect the feed one, while the reaction products molar fraction approaches zero. The catalyst activation can already be observed at low temperature. At around 95°C, the mole fractions of CO and O_2 decrease at the expense of CO_2. The trend of these molar fractions establishes that at these temperatures, the catalyst is active towards the CO oxidation reactions. As the temperature increases, the CO oxidation reaction consumes more and more reactant, reaching a maximum of CO consumption at around 175°C. However, at this temperatures, the molar fraction of O_2 reaches approximately 0.2%, much less than expected. The O_2 consumption provides some clarification of the reaction's behavior at these temperatures. Taking into account the CO oxidation reaction (Eq 1.3), for each mole of CO consumed, the reaction requires the consumption of half mole of O_2. For these reason, if at 175°C only this reaction took place, the O_2 consumed should be less than those measured. In particular, assuming that only CO-OX reaction takes place at 175°C, the mole fraction of O_2 in the outlet should be about 0.85%, but in practice its value is less than 0.35%. This shows that another reaction is taking place in competition with the CO oxidation. In particular, with the reactants available in the mixture and observing the concentration profiles, hydrogen oxidation reaction is a likely reaction although the large amount of H_2 does not allow to easily measure small variation. Above 175°C, a decrease in the

CO_2 mole fraction is observed, which shows that the catalyst decrease its activity towards CO consumption. At the same time, the mole fraction of O_2 continues to decrease, reaching its complete consumption at 210°C. At the highest temperatures, a stationary condition is observed: the activity of CO oxidation reaction is almost negligible, while the H_2 oxidation reaches its maximum levels.
During the cooling ramp, a behavior similar to the one observed during the heating part can be noted. Specifically, a new peak in CO consumption is observed. At this analysis stage, the temperature range at which the CO molar fraction differs from the reference fraction varies between 205°C and 78°C. In addition, the maximum amount of CO consumed is lower compared to the one present in the heating ramp. As with CO, the O_2 molar fraction profile differs with respect to the heating rate: here a total oxygen consumption is observed above to 169°C (in contrast to the 210°C of the heating stage).
Figure 3.9 shows the conversion of the reactants as a function of temperature. In

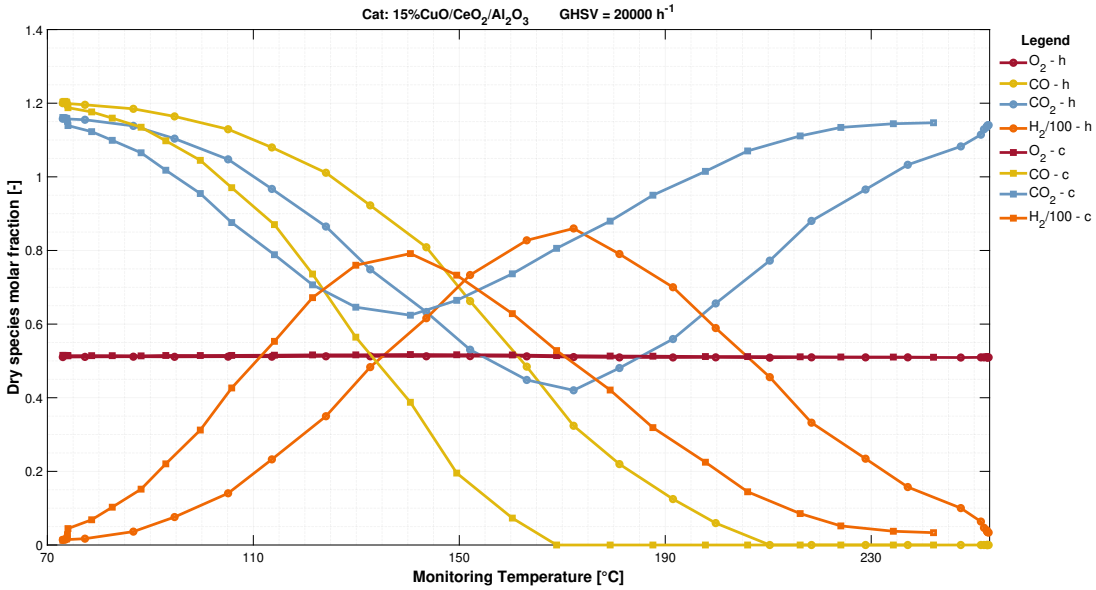

Figure 3.8: Dry species molar fraction as function of monitored temperature. Test:4, Cat: A-550-15

addition, selectivity is used for quantifying the CO consumed through its oxidation reaction.
Considering the heating stage represented in Figure 3.9-a, Figure 3.9-b and Figure 3.9-c, it is possible to define that at 175°C the catalyst converts at best around 60% of the total CO present in the reacting mixture. On the contrary, O_2 shows a total conversion above 210°C, since as mentioned earlier, oxygen is used by both oxidation reactions. With regard to H_2 profile, an initial smaller constant consumption is observed up to 150°C. At higher temperatures, a sudden increase in

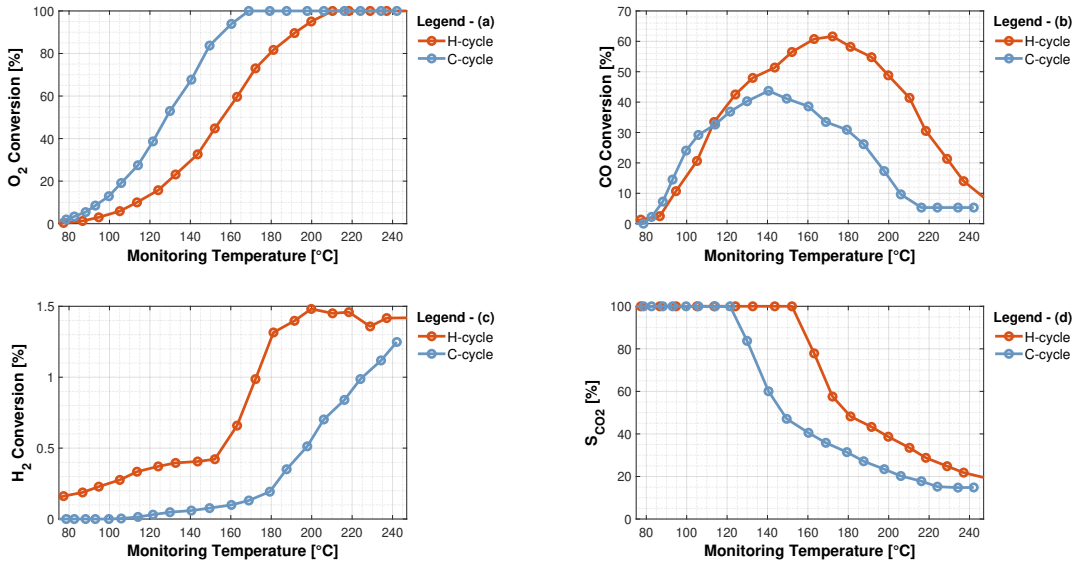

Figure 3.9: (a,b,c) Reagents conversion profile as function of temperature, and (d) Selectivity of CO towards CO_2 as function of temperature. Test:4; Cat: A-550-15

conversion occurs until a stationary value is reached at 200°C. In the cooling step the catalyst is less active toward CO-OX, with the CO conversion reaching a maximum of 43% at 140°C. The catalyst is also less active for H_2-OX, in fact the H_2 conversion presents a rapid decline, reaching a conversion below to 0.1% at 160°C. Figure 3.9-d shows that the selectivity of CO towards CO_2 reaches 100% for low temperatures. In section 2.4.2 this parameter is defined as the consumption of O_2 by CO in its oxidation reaction. A profile such as the one shown in the subplot being examined confirm what has been said previously: as the temperature changes, oxygen is used by both the other two species present in the reacting system. In particular, at low temperatures, oxygen is totally consumed by CO, whereas at higher temperatures this uniqueness decreases as the catalyst is more active for hydrogen oxidation reaction.
Subplots in Figure 3.9 show a hysteresis between the profiles. This hysteresis could be due to temperature non-uniformity in axial directions within the catalytic bed. Because of the exothermic reactions within the reacting system, internal temperature peaks can be generated. These temperature peaks does not have the time to stabilize with the heating/cooling rate being considered. The non-uniformity of the heat therefore leads to the thermocouple recording a non entirely accurate temperature.

3.2.3 Catalytic activity test of A-550-20

The experimental condition of the test are outlined in Table 3.2. The specific experimental conditions for this test are shown in the Test:3 row on the diary reported in the Appendix of this thesis. The species concentration profiles obtained from CO-

Table 3.2: Experimental conditions for the catalytic test over A-550-20

Heating/cooling rate [°C/min]	T range [°C]	$\dot{V}_{in}$ [ml/min]	GHSV [h^{-1}]	h_{cat} [mm]	$\varnothing_{particle}$ [µm]
2	70 - 250°C	38.316	20k	4	45 - 250

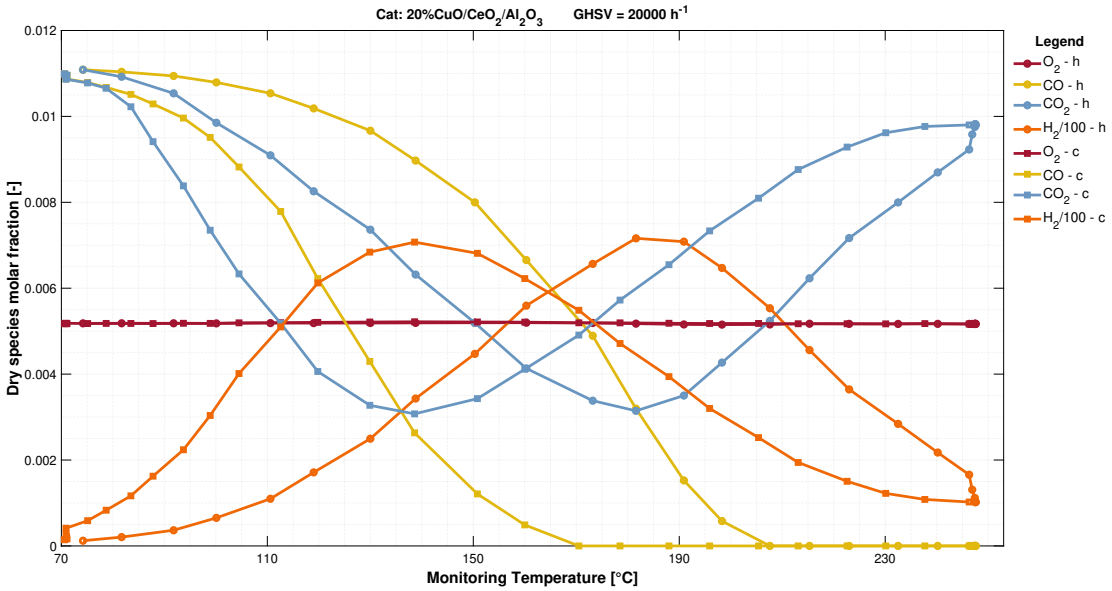

Figure 3.10: Dry species molar fraction as function of the monitored temperature. Test:3, Cat: A-550-20

PROX reaction carried out with ADP catalyst containing 20% of CuO, depicted in Figure 3.10, can be qualitatively compared with the profile shown in Figure 3.7. On the other hand, as the CuO loading changes, the profile change quantitatively. In particular, like the previous one, this catalyst allows CO to be consumed starting from 75°C and has a maximum consumption peak at approximately 185°C. In addition, CO is also partially consumed at high temperatures. Up to 160°C, the molar fraction of O_2 decays stoichiometrically with the CO concentration profile. For higher temperature and until its total conversion is reached, the O_2 trend slightly changes slope. Similar to the previous case, the change of oxygen profile slope is likely due to the competitive H_2 oxidation reaction.

With respect to A-550-15, the main difference can be seen during the cooling ramp: another peak in CO consumption is observed, and its height can be compared to the one present in the heating ramp of this test. In particular, in the cooling stage it can be noticed that CO starts again to be consumed below to 235°C and it has a peak at 160°C. From this temperature, the activity of the catalyst decreases until it reaches 70°C at which the catalyst is no longer active for any reaction.
Figure 3.11 show the reactants conversion profile and the selectivity of CO oxidation reaction. As can already seen from the analysis of the concentration profiles, this catalyst allows a higher conversion of carbon monoxide, reaching values of approximately 80% in both the heating and cooling stages. From hydrogen conversion profile, represented in Figure 3.11-c, it can be observed a consumption comparable to the one obtained from A-550-15, with conversion values lower than 0.8% up to 180°C and a maximum conversion of 1.5% at high temperatures. In addition, the conversion profile are almost equal between the heating and cooling ramps. In addition to the higher level of conversion, a higher activity of the catalyst towards the CO oxidation reaction can be noted. Considering the in Figure 3.11-d, the selectivity of CO towards its product maintains unit values up to 160°C. On the other hand, as with the catalyst containing 15% CuO, at higher temperatures the oxygen present in the mixture binds mainly to hydrogen.

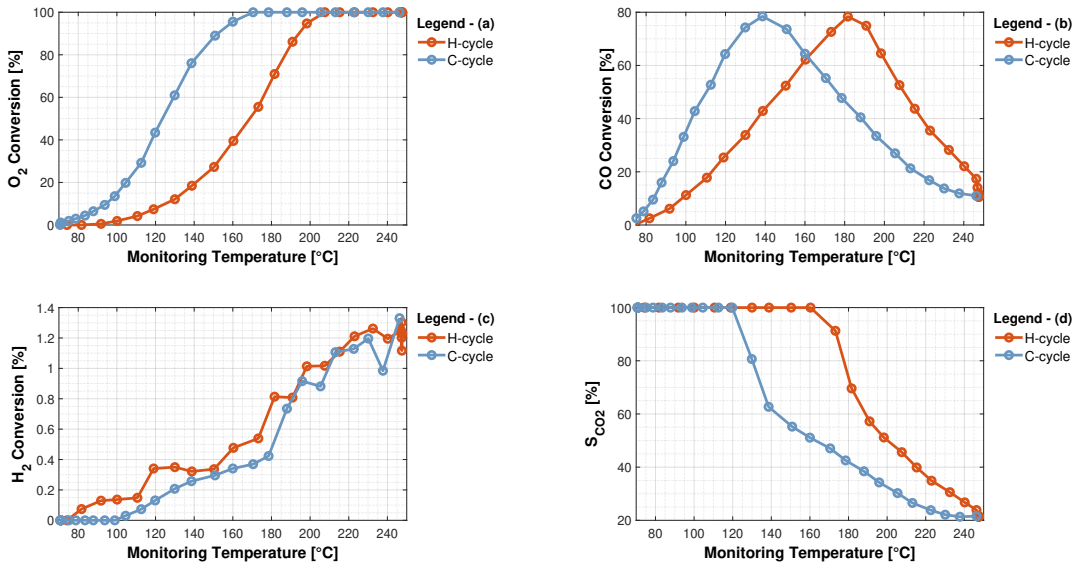

Figure 3.11: (a,b,c) Reagents conversion profile as function of temperature; (d) Selectivity of CO towards CO_2 as function of monitored temperature. Test:3, Cat: A-550-20

3.2.4 Catalytic activity test of A-550-30

The experimental condition for this test are outlined in Table 3.3. The specific experimental conditions for this test are shown in the Test:2 row on the diary reported in the Appendix of this thesis. Figure 3.12 and Figure 3.13 respectively

Table 3.3: Experimental conditions for the catalytic test over A-550-30

Heating/cooling rate [°C/min]	T range [°C]	$\dot{V}_{in}$ [ml/min]	GHSV [h^{-1}]	h_{cat} [mm]	$\varnothing_{particle}$ [µm]
2	70 - 250°C	47.022	20k	5	45 - 250

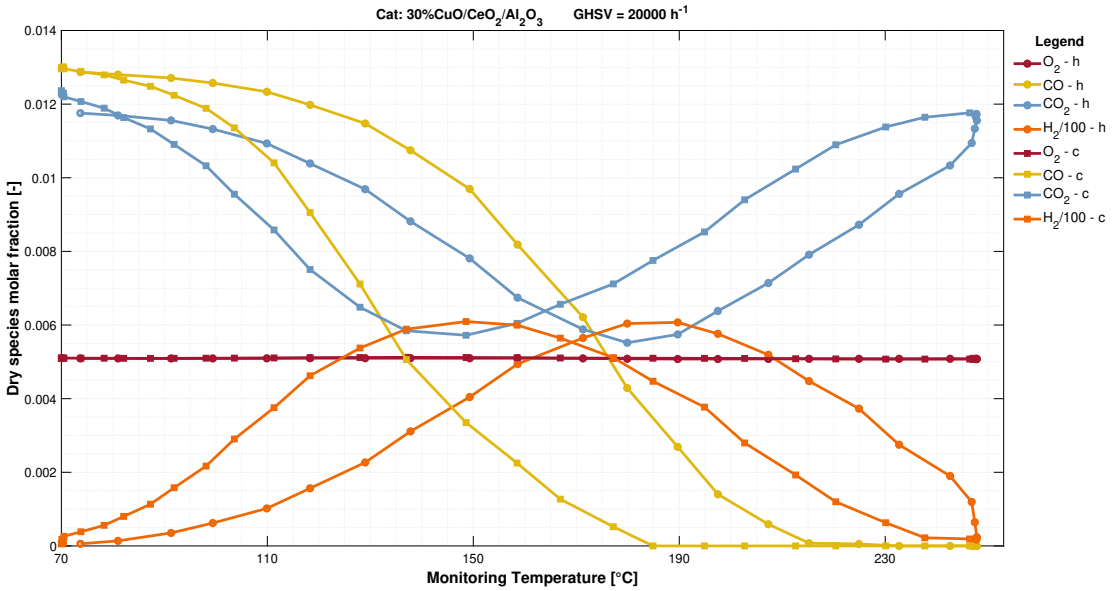

Figure 3.12: Dry species molar fraction as function of the monitored temperature. Test:2, Cat: A-550-30

show the mole fraction profiles of the species involved in the system as a function of monitored temperature, and the conversion and selectivity profiles of the carbon monoxide oxidation reaction as function of monitored temperature.
This catalyst is already active at 80°C since, as can be seen in Figure 3.12, the CO mole fraction starts to decrease slightly at this temperature. Considering the heating section, as the temperature increases, CO consumption increases and the maximum of CO conversion is reached at 180°C. The O_2 molar fraction profiles follows the pattern already seen in the previous charts, reaching its maximum conversion at 215°C. Similarly to the previous catalyst, a stationary state arises at higher temperature, in which the mole fraction of CO_2 is almost zero, which proves

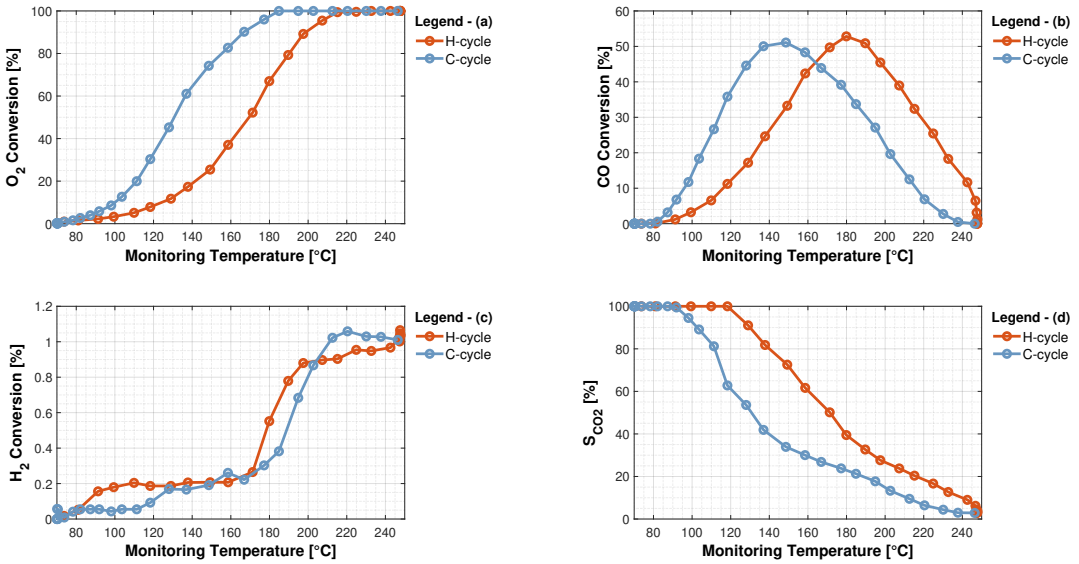

Figure 3.13: (a,b,c) Reagents conversion profile as function of temperature; (d) Selectivity of CO towards CO_2 as function of temperature. Test:2, Cat: A-550-30

how the catalyst has a low affinity for the carbon monoxide oxidation reaction at high temperatures,compared with its competitive reaction. In particular, in the heating stage, and at low temperatures, the H_2 conversion follows the same trend as that obtained by its previous catalysts, whereas as the temperature increases, the conversion shows a rapid increase to 1%, which remain a lower value than the conversion achieved by preceding catalysts.
For the cooling stage, profiles mirroring the heating stage can be observed, but shifted to a lower temperature, as seen before form all catalysts. More precisely, the second curve representing the CO consumption has a peak of maximum conversion at 150°C and quantitatively, this peak can be compared to the one obtained in the heating cycle. In addition, the catalyst is able to consume the CO present in the reacting mixture up to 80°C. The selectivity profile S_{CO/O_2} shown in Figure 3.13-d, provides mirroring information to that already provided in the previous tests. However, it is particularly noticeable that the changing slope of the curve, namely the decrease of O_2 consumption by CO, begins at lower temperatures. In addition, it can be seen that at high temperatures the profile reaches zero selectivity. This last observation implies that close to 270 and 280°C, CO is hardly consumed by its reaction.

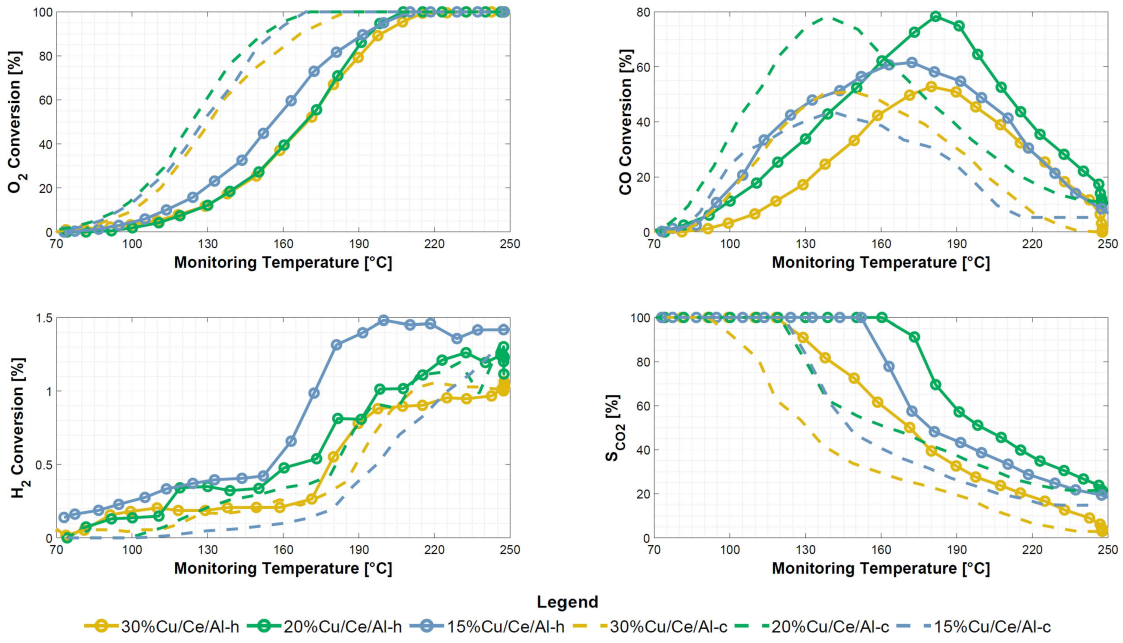

Figure 3.14: Comparison of conversion and selectivity profiles between A-550-15, A-550-20 and A-550-30 as function of temperature

3.2.5 Conclusion

Figure 3.14 compares the conversion profiles and the selectivity profiles obtained from all the above-mentioned ADP catalysts, as a function of operating temperature. This representation is useful to identify which loading of copper oxide the catalytic material must contain to provide maximum CO consumption, by minimizing the hydrogen loss. CO conversion is the parameter that discriminates the catalytic activity. From the Figure 3.14-b is clear that catalyst A-550-20 has a higher CO conversion with respect to A-550-15 and A-550-30. Furthermore, it can be noted how the conversion is not directly linked to the loading of copper oxide, because A-550-30 allows a lower consumption of CO with respect the catalyst with the smallest content of active site. On the contrary, it is possible to state how the CuO loading affects the conversion: the curves referring to the cooling stage compared to the heating one is clearly lower for the A-550-15, while is comparable for the other two catalysts. In terms of H_2 consumption, at high temperature A-550-15, with respect to A-550-20 and A-550-30, has an higher average conversion of 1.5%, while as the temperature decreases, this difference decreases and all the catalysts reach an average conversion value of 0.2%.
In addition, a comparison can be made between the experimental data and those considering purely thermodynamic aspect. In particular, it is clearly observed how these catalyst are highly selective towards the CO_2 with respect to methane; it can

be seen that the use of these catalysts considerably reduce the amount of hydrogen consumed (maximum 1.2% respect the 12.4% estimating thermodynamically), since they are not being selective towards methanation reactions, and then the only amount of H_2 consumed is referring to H_2 oxidation reaction.

3.3 Activity of $CuO/CeO_2/Al_2O_3$ synthesized by EISA method

To verify the catalytic activity of these last two catalyst, a set-up similar to Setup-1 has been used. From the instrumental point of view, the only difference concerns the replacement of the micro-chromatograph with the gas chromatograph (GC-7820). The thermal protocol employed in these tests is described in section 2.4.1. With regard to active site loading, EISA catalysts all contain 20% of CuO. For this reason the percentage of CuO is omitted in the name, but the calcination temperature is defined .

3.3.1 Catalytic activity test of E-900-20

The experimental condition of the test are outlined in Table 3.4. The specific experimental conditions for this test are shown in the Test:37 row on the diary reported in the Appendix of this thesis. Similar to the tests carried out with ADP

Table 3.4: Experimental conditions for the catalytic test over E-900-20

Heating/cooling rate [°C/min]	**T range [°C]**	$\dot{V}_{in}$ **[ml/min]**	**GHSV [h^{-1}]**	$\mathbf{h}_{cat}$ **[mm]**	$\varnothing_{particle}$ **[µm]**
1	40 - 280°C	17.610	20k	1	45 - 250

catalyst, this results shown a time delay between the trend of the molar fraction and the temperature. Figure 3.15 shows how the molar fraction of CO and CO_2 stabilizes to 0.825% and 0.5% respectively, approximately 10 minutes before to the temperature ramp reaches the isothermal stage. Moreover, at the end of the same stage, the mole fraction of CO does not start to immediately decrease, but about 50 min later. This could be a confirmation of what has already been said about ADP catalyst; the high catalytic activity of the reactions, but especially the CO oxidation reaction, leads to thermal inconsistencies within the bed which offset the thermocouple reading.
In addition, from this graph it can be seen that, after maximum CO consumption, the fraction of CO increases rapidly to a value of 0.8%.
Figure 3.16 reveals how this catalyst is already active at 70°C. Indeed at this tem-

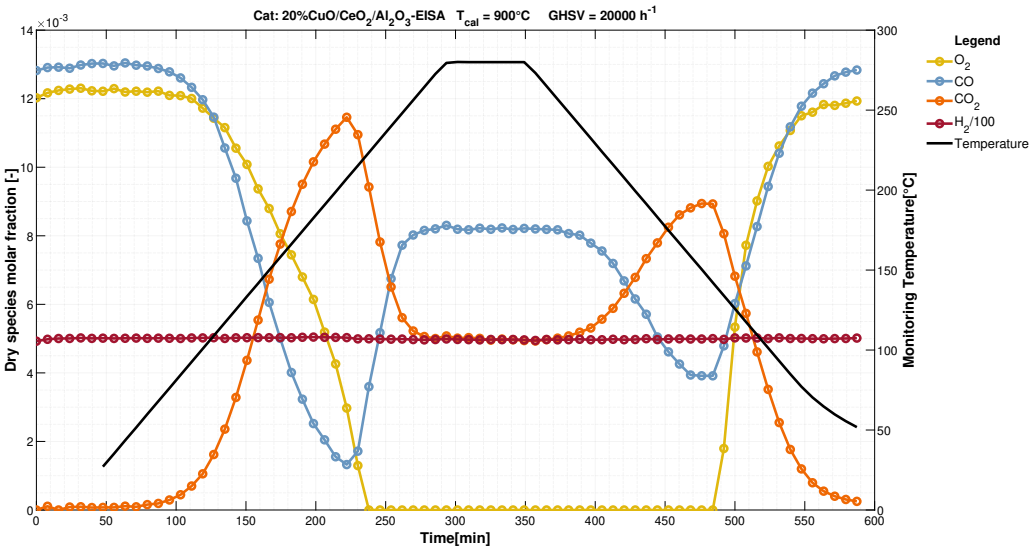

Figure 3.15: Dry species molar fraction and monitored temperature as function of time. Test:37, Cat: E-900-20

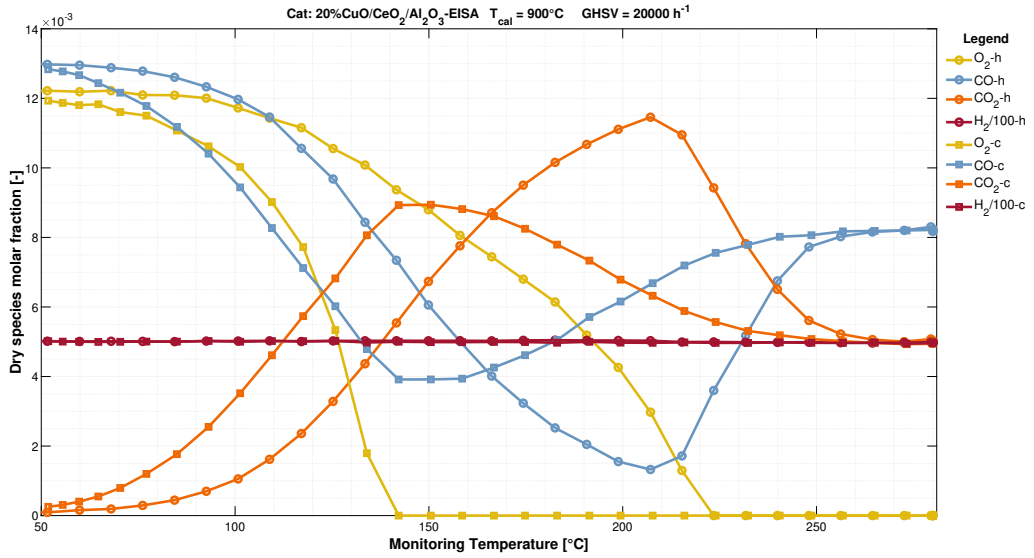

Figure 3.16: Dry species molar fraction as a function of monitoerd temperature. Test:37, Cat: E-900-20

perature the molar fraction of CO beings to decrease. At low temperatures, it can be observed that the O_2 concentration profile decreases following the stoichiometry of the CO oxidation reaction. Moreover, as the temperature increases, the oxidant concentration profile changes its slope compared to the one of the carbon monoxide

profile, indicating that the consumption of these two reagents is no longer stoichiometric. Similar to ADP catalyst, E-900-20 allow the carbon oxide contained in the reaction mixture to be completely consumed at a temperature close to 210°C and maintains this conversion level, even along the cooling section, up to 145°C.
In particular, focusing on the concentration profile of carbon monoxide, it can be observed how the mixture exiting from the reaction is less and less rich in CO as the temperature increase, reaching a fraction lower than 0.15% at 207°C. This results is feasible because, as shown in Figure 3.17, the catalyst along the test heating stage is not active toward the H_2 oxidation reaction, leaving more oxygen available in the reacting mixture, which can be used from CO molecules. Above 207°C, the CO conversion decreases because, at these operating condition, the catalyst begins to be active towards the H_2 oxidation reaction, which uses the oxygen to oxidize hydrogen and produce water. Nevertheless, in the isothermal section the conversion of carbon monoxide exceeds 30% of consumption, a much higher value than the conversion achievable by other catalysts.
Considering the cooling section in Figure 3.17, the CO conversion is lower compared to the conversion achieved during the heating section. As a matter of fact, the maximum CO consumption value is 70% and it is reached at a temperature of 150 and 140°C. This temperature range is comparable with the peak of CO conversion obtained by ADP catalyst. To define a possible explanation for the decreasing

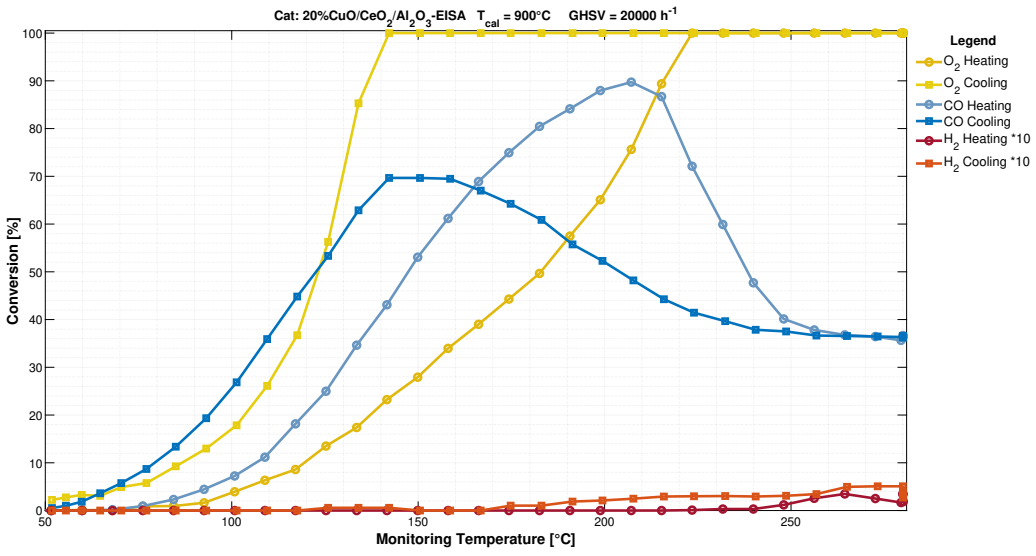

Figure 3.17: Reagents conversion as function of controlled temperature. Test:37, Cat: E-900-20

conversion achieved during the cooling ramp, the conversion profiles shown in Figure 3.14 should be considered. All the catalysts named ADP, irrespective of the

copper oxide content, in the heating stage of the test have a maximum CO consumption at 180°C, while during the cooling stage the peak shifts to lower temperatures (*i.e* between 140 and 150°C). On the contrary, in this case, the first conversion peak is observed at higher temperature (T equal to 210°C), while the second one occurs at 140-150°C. Considering the hydrogen conversion profile presented in Figure 3.17, it can be seen that the catalyst prepared using EISA method and calcination at 900°C does not show any activity towards the hydrogen oxidation reaction during the heating stage of the test, and then all the O_2 present in the mixture reacts with the CO, oxidizing it. On the other hand, during the isothermal stage and for temperatures above to 165°C of the cooling stage, the catalyst is also active towards the hydrogen reaction, leading to a decrease in the amount of O_2 available for the CO-OX reaction.This is an important conclusion since, by completely oxidizing the catalyst and maintaining the system at a temperature below 240°C, the catalyst will always almost completely consume the CO present in the reaction mixture.
It should also be noted that during the cooling cycle, oxygen conversion is higher than it should be. In particular, at 140°C the catalyst is not active towards the hydrogen oxidation reaction. For this reason, the oxygen conversion must be lower than the value shown in the figure. The reason for this higher oxygen consumption will be explained in the following sections.

3.3.2 Catalytic activity test of E-550-20

The experimental condition of the test are outlined in Table 3.5. The specific experimental conditions for this test are shown in the Test:36 row on the diary reported in the Appendix of this thesis. Figure 3.19 shows how this catalyst consumes much

Table 3.5: Experimental conditions for the catalytic test over E-550-20

Heating/cooling rate [°C/min]	**T range [°C]**	$\dot{V}_{in}$ **[ml/min]**	**GHSV [h^{-1}]**	h_{cat} **[mm]**	$\varnothing_{particle}$ **[µm]**
1	40 - 280°C	17.442	20k	1	45 - 250

less carbon monoxide during both the heating and cooling cycles. In contrast to the catalyst calcined at 900°C, this material presents a higher activation temperature. Looking for example the CO or O_2 molar fraction profiles, it is possible to observe how the slope of their curves changes for temperatures above 100°C (always considering the heating stage of the test). The lower CO conversion obtained during both the stages of the test is due to the presence of its competitive reaction (*i.e* H_2-OX reaction). In particular, the catalyst is already active towards the hydrogen oxidation reaction at 120°C, a temperature that is comparable with the activation temperature of the catalyst towards the CO-OX reaction. Comparing again the

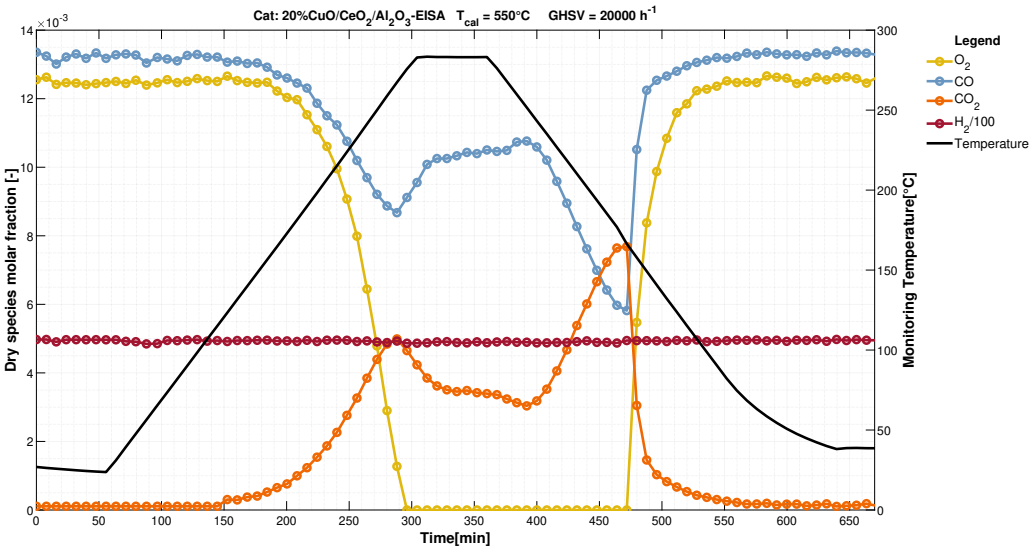

Figure 3.18: Dry species molar fraction and monitored temperature as function of time. Test:36, Cat: E-550-20

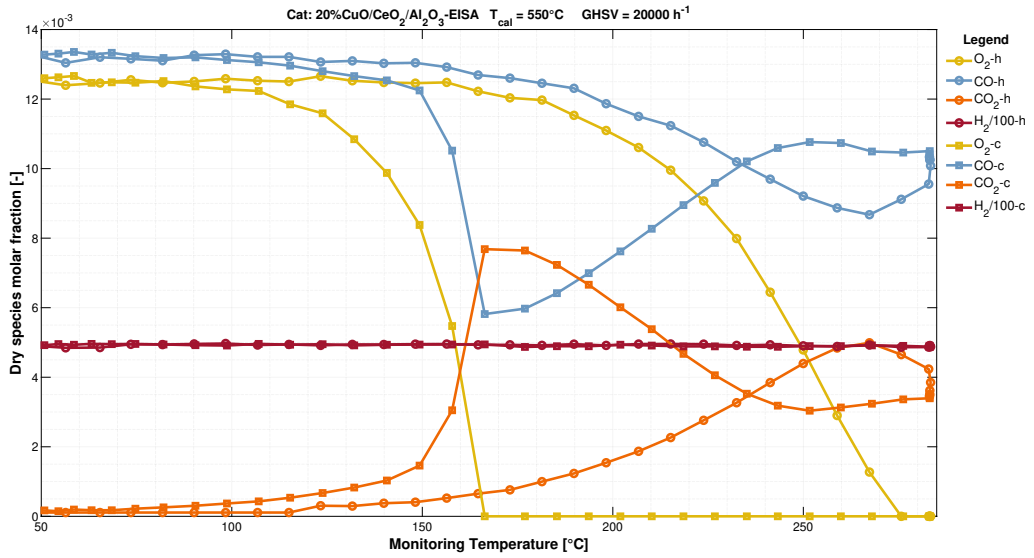

Figure 3.19: Dry species molar fraction as function of monitored temperature. Test:36, Cat: E-550-20

performance between E-900-20 and E-550-30, it is possible to observe an higher H_2 conversion by the latter, with maximum conversion values reaching 3% for temperatures above to 200°C.
A remarkable features of this catalyst is the increased conversion of CO during the cooling stage. This fact is unique, because for all the other catalyst tested (both

EISA and ADP), the performance during the second ramp was comparable or lower than the one obtained during the heating ramp. This higher activity during the cooling phase is probably due to the enhanced activity of the catalyst towards the hydrogen oxidation reaction in the heating stage. The hydrogen oxidation reaction may produce radicals which increase the activity towards the CO oxidation reaction or the R-WGS reaction.

3.3.3 Catalytic activity test of E-400-20

The experimental condition of the test are outlined in Table 3.6. The specific experimental conditions for this test are shown in the Test:11 row on the diary reported in the Appendix of this thesis. Figure 3.20 shows the concentration

Table 3.6: Experimental conditions for the catalytic test over E-400-20

Heating/cooling rate [°C/min]	T range [°C]	$\dot{V}_{in}$ [ml/min]	GHSV [h^{-1}]	h_{cat} [mm]	$\varnothing_{particle}$ [µm]
1	40 - 280°C	44	25k	1	45 - 250

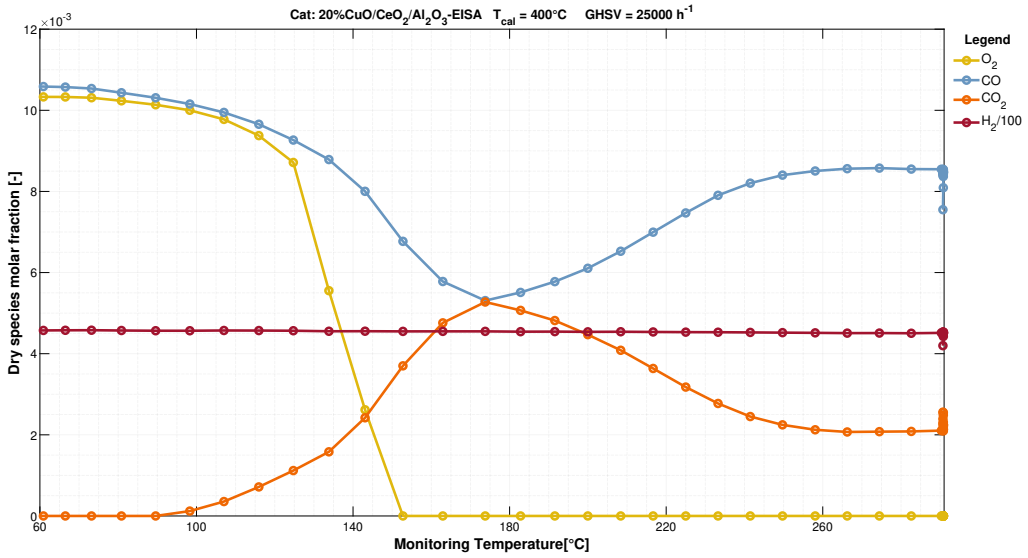

Figure 3.20: Dry species molar fraction as function of the monitored temperature. Test:11, Cat: E-400-20

curves of the species as a function of monitored temperature. As with the other two EISA catalysts, in the high-temperature isothermal stage there is a complete consumption of oxygen by the combination of both hydrogen and carbon monoxide

oxidation reactions. In particular, at 280°C, the CO concentration reaches 0.85%, corresponding to a conversion of 22%. At the same temperature there is a slight consumption of H_2, equivalent to a conversion value of 2.85%. As the temperature decreases, the catalyst is more active for CO oxidation reaction; its concentration value decrease to a minimum of 0.53%, corresponding to a maximum conversion of 52% at 157°C.
During the isothermal stage, a variation of the molar fraction of all the species can be noted. This is due to the settling of their concentrations during the high-temperature isothermal stage.

3.3.4 Conclusion

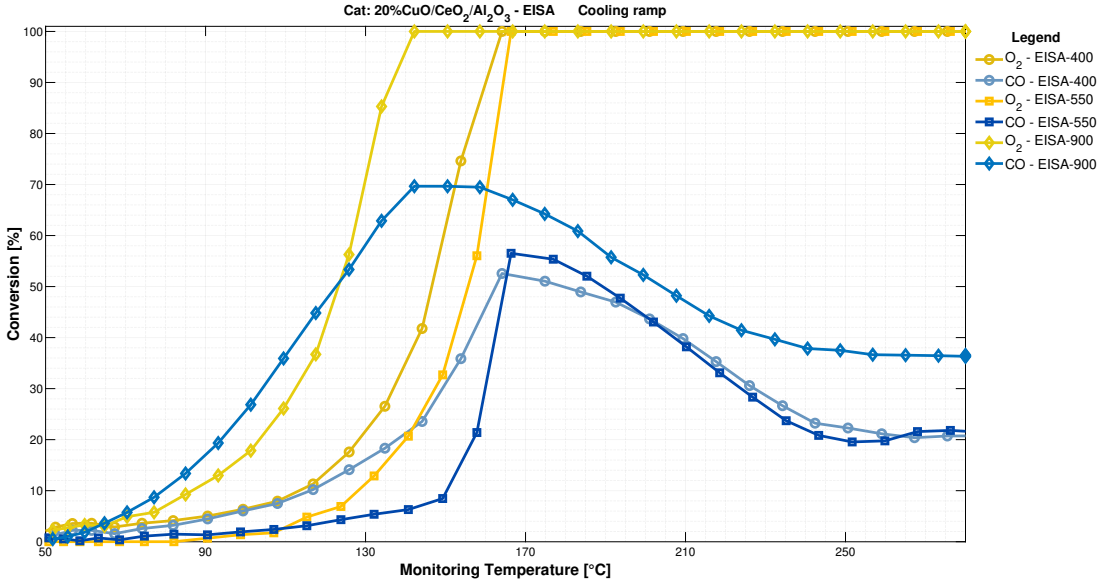

Figure 3.21: Comparison between the reagents conversion for all the tested EISA catalyst as a function of monitored temperature. Test:11 Cat: E-400-20, Test:36 Cat: E-440-20, Test:37 Cat: E-900-20

Figure 3.21 compares the conversion profiles of CO and O_2 as a function of the monitored temperature for all the calcination temperature. It can be seen that even during the cooling stage, EISA catalyst calcined at highest temperature (900°C) allows to achieve the highest conversion of carbon monoxide. It should also be noted, as shown in Figure 3.17, that this catalytic material allow almost all of the CO fed to be consumed during the heating stage of the test ($X_{CO} = 90\%$). In addition, the catalyst calcined at 900°C allow more CO to be converted at high temperature (almost twice as much compared with the catalysts calcined at lower temperatures).

In addition, it can be seen that the calcination temperature influences the activation of the hydrogen oxidation reaction. The lower the calcination temperature, the lower the temperature at which the catalyst is active for this reaction.

3.4 Comparison of catalytic performance according to synthesis method

Once the performance of the different types of catalyst has been defined it is possible to carry out a more general comparison, in which the material synthesis method is the discriminant factor. A first comparison has been made between the two catalyst which provide the best catalytic performance, while the second comparison can be made between two catalysts obtained using the two synthesis method, but calcined at the same temperature. The first comparison makes it possible to identify the best catalyst among all those tested in this work; E-900-20 is the best catalyst among those obtained using EISA synthesis method. The second comparison provides information on the only synthesis method, because both the catalyst (EISA and ADP) were calcined at the same temperature and contained the same loading of CuO.

For the first comparison, Figure 3.22 shows the CO conversion profile of the cata-

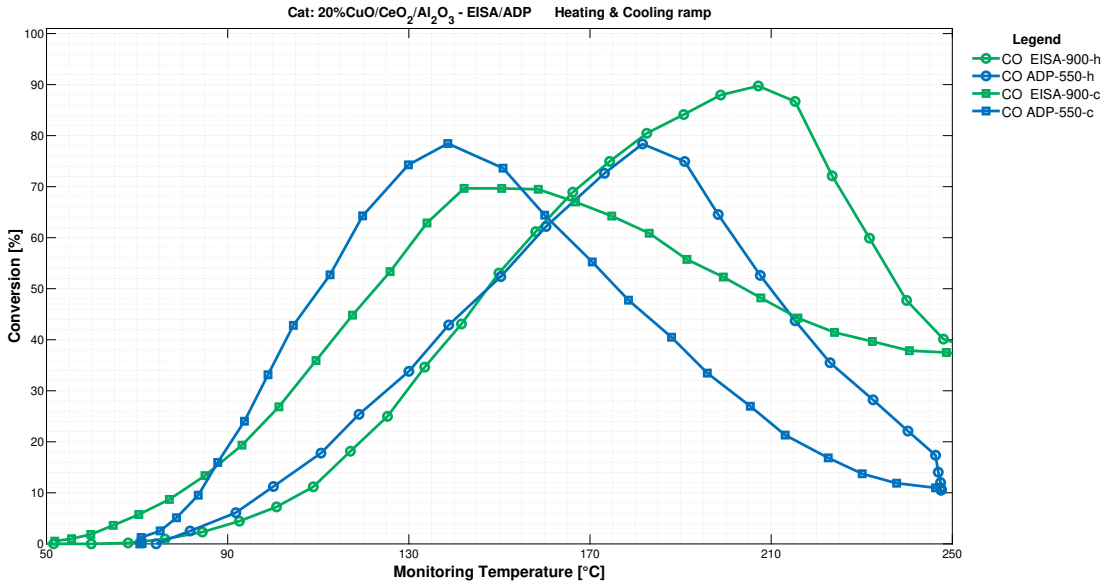

Figure 3.22: CO conversion profile as function of monitored temperature. Comparison of ADP and EISA catalyst which provide the best catalytic performance. (green line) Test:37, Cat: E-900-20, (blue line) Test:3, Cat: A-550-20

lyst which provide the best catalytic performance. Considering the heating ramp,

it is possible to observe the same activation temperature of the catalyst towards the carbon monoxide oxidation reaction (T = 70°C) and furthermore, throughout the heating cycle, the conversion profile of both the catalyst are almost overlapping. The difference between the two catalyst becomes clear for temperature above to 185°C: A-550-20 loses activity while E-900-20 continues to consume CO, achieving its maximum performance at 205°C. In addition, using E-900-20 it is possible to achieve a CO conversion of more than 40% even at high temperatures (for T greater than 250°C), whereas at the same operating condition, the catalyst synthesized by ADP method cannot convert more than 12%.
A change in performance occurs along the cooling stage: catalyst A-550-20 does not lose activity, always converting 80% of the CO present in the reactor feed mixture, while catalyst E-900-20 shows a maximum conversion of 70%. In contrast to the heating phase, along the cooling phase the temperature at which the maximum conversion occurs for both the catalyst does not differ greatly: for both of them the peaks of X_{CO} stay between 130°C and 140°C. However, the performance of the E-900-20 catalyst may have been affected by the high temperature range, in which a possible change in the physical state of the catalyst may occurred. Another reliable hypothesis could be the non-uniformity of the heat within the catalytic bed due to the high heat generation of the carbon monoxide oxidation reaction.
Figure 3.23 shows a substantial difference between the performance of the cata-

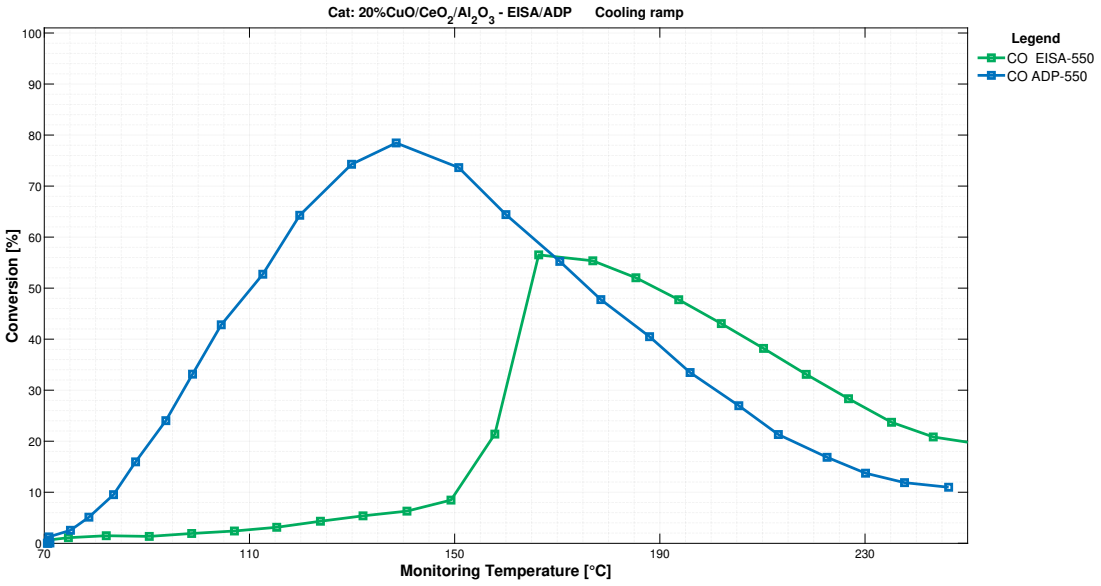

Figure 3.23: CO conversion profile as function of monitored temperature. Performance comparison between catalyst calcined at the same temperature. (green line) Test:36, Cat: E-550-20, (blue line) Test:3, Cat: A-550-20

lysts obtained using the two different synthesis methods. In particular, it can be

seen that along the cooling section catalyst synthesized by EISA methods provides significantly lower performance compared with the catalyst in which the active site was deposited using the ADP method. The differences lie both in the maximum conversion and in the activity window, that is, the temperature range at which the catalyst shows satisfactory conversion. Indeed, catalyst E-550-20 a rapid decrease in CO conversion can be observed, not due to a change in the system, such as temperature.

3.4.1 Conclusion

For catalyst with the same loading of copper oxide, the catalytic performances differs based on the type of synthesis method, including the temperature at which the material was calcined. More specifically, the effect of calcination temperature can be noticed from the conversion degree obtained by the three EISA catalyst: the catalyst calcined at 900°C was able to reach a maximum conversion of 90%, while catalyst calcined at lower temperature shows a drop in CO conversion, by more than 30%.
A positive aspect for EISA catalyst concerns their higher efficiency towards CO conversion at higher temperature (T greater than 250°C) compared to the ADP material; with EISA material, it is possible to obtain a consumption greater than 20% even at 280°C, while as shown in Figure 3.22, with a ADP catalyst, the efficiency of conversion drops very quickly for temperature higher than 200°C, reaching conversion slightly above 10% at 250°C. In contrast, a negative feature of EISA catalysts concerns the decrease in catalytic performance between the heating and cooling phases.
Ultimately, it is possible to conclude that E-900-20 catalyst provided the best performance, since it allows the conversion of almost all the CO fed at a temperature that does not differ so much compared to its rival (A-550-20). Moreover, even at high temperatures, on E-900-20, the conversion does not drop drastically but remains constant to 40%. In addition, this catalyst allows for greater variation in thermal range without incurring a steep drop in CO conversion. Regarding the conversion of hydrogen, referring to Figure 3.17, it is possible to observe how this catalyst is not very active towards its reduction and the limited consumption of H_2 is a fundamental requirement for a catalyst intended for use in the PROX process.

3.5 Specific features and effect of catalyst oxidation state on CO-PROX reaction

In section 3.2, the catalyst A-550-20 has been shown to have the highest catalytic performance towards the reaction under consideration, among ADP catalyst. However, this result is not yet sufficient, since other aspects can and should be examined

to classify this catalyst as an optimum from an operational point of view. More specifically, in addition to what has already been defined in section 2.4.1, the main features which must be verified are:

- Decay of catalytic performance depending on the prolonged use of the catalyst;
- The oxidation state of the catalyst, and its impact on catalytic activity;
- The consumption of CO occurs as a result of its oxidation reaction or also because of the WGS reaction;
- Establish how much an increase in GHSV affects catalytic performance;

Considering the first point in the preceding list, checking the catalytic activity of the catalyst according to its use is an operationally relevant factor. In continuous industrial plants, such as the Oil&Gas industry, the catalyst is used on daily basis and therefore a significant loss in catalytic performance is not acceptable. Like the life time of the catalyst, its oxidation state is also relevant here. Hydrogen and carbon monoxide are both reducing agents and therefore they spontaneously tend to reduce the catalyst. In addition, the amount of hydrogen present in a typical reacting mixture is absolutely predominant compared to the oxidant, and therefore this reducing effect is even more pronounced. In addition, high GHSV values are used in industrial plants to increase the production. The GHSV affects the catalytic performance (the reason will be discussed later in section 3.5.4), and more precisely it leads to a decrease in the catalytic performance. Therefore, determining how much the catalytic activity, and more specifically the conversion of CO decreases, is of fundamental importance for the purpose of this work.
To enable the results to be compared with the previous tests and thus to be consistent, the experimental specifications such as the fed mixture composition, the GHSV value and therefore the volumetric flow rate at the reactor inlet should be the same with respect to the first tests performed. In practice, some modifications have been made to the thermal protocol, but these do not affect the final results. This thermal protocols is shown in Figure 2.13. More specifically, the first amendment to the experimental thermal protocol is based on the following idea: observing the results of the tests reported in the previous sections, it has been noted how the A-550-20 catalyst shows the same catalytic activity between heating and cooling ramp. With this observation, it has been therefore decided to avoid carrying out test involving the monitoring of both the thermal ramps, but to consider only the cooling cycle then, reducing the analysis time. In addition to this first modification, this protocol includes an isotherm at a higher temperature compared to the isotherms used in previous tests.

3.5.1 Effect of material aging on catalytic performance

To achieve this task, results obtained from test carried out at different times have been compared. As previously mentioned, the experimental condition at which these tests have been performed were the same. The results employed to verify the possible loss of activity by the catalyst have been collected together in Figure 3.24 To derive clear information, it becomes important to define the difference between

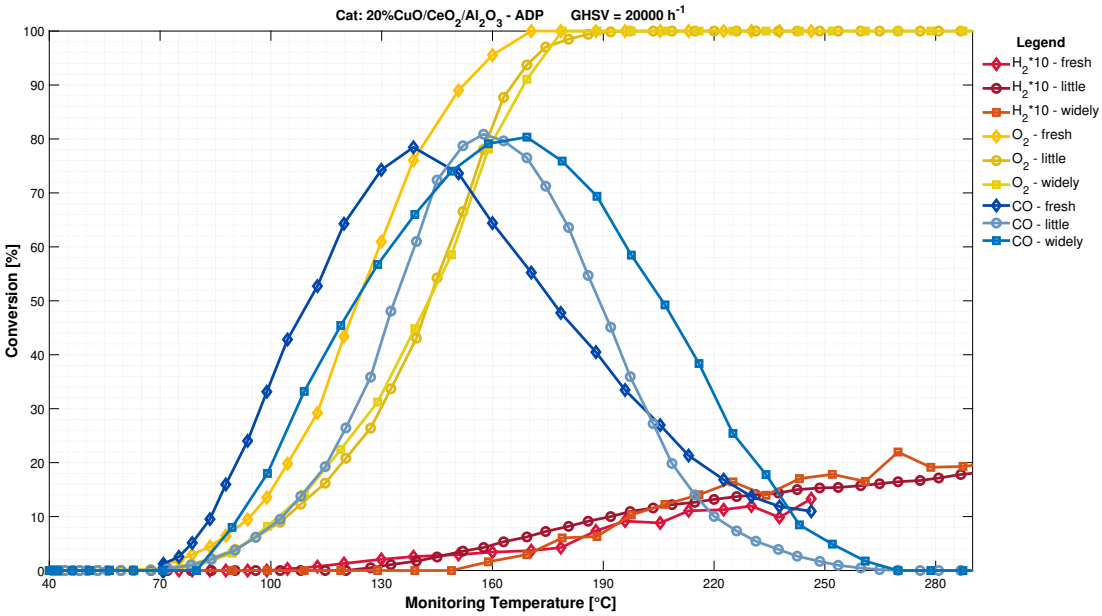

Figure 3.24: Comparison of catalytic performance as a function of catalyst aging. (◊) Test:2, (○) Test:15, (□). Stage considered: cooling, Test:31, Cat: A-550-20

the catalyst state under the respective condition. More specifically, the catalyst named *fresh* represents a new material that has undergone a single stage of air pre-treatment, which is required to perform the catalyst activity analysis. In contrast, *little* and *widely* designation identify a catalyst that has been used for many test, including many oxidations, reductions and continuous reaction, that may weaken the structure of the material itself.
The results obtained from this comparison are quite satisfactory; the catalyst does not significant lose activity (*i.e* the maximum conversion value) towards CO-OX reaction as its use increases. In particular, a slight shift towards high temperature in the material activation temperature can be noted, but this delta can be consider negligible. On the other hand, the temperature at which the catalyst achieves the same conversion changes; as the catalyst usage increase, the temperature at which the maximum CO conversion is achieved increase. The same conclusion can be drawn with regards the activation temperature of H_2-OX reaction. The difference in temperature referring to the maximum conversion of CO obtained from fresh

and used catalyst is 50°C, a fairly considerable difference considering the limited number of tests carried out.
The main cause of this ageing of the catalyst could be the continuous reductions and oxidation cycles, which may have resulted in Cu/CuO particle agglomeration on the surface.

3.5.2 Effect of the catalyst oxidation state on the activity

In the State of the Art of this work, and more specifically in section 1.3.3 of the first chapter, Polster et al. [34] stated that the catalyst is active towards the preferential oxidation of carbon monoxide whenever the active site deposited on the material is in its maximum oxidative state. Following the suggestion made by Polster et al. [34], to test the catalytic activity of our materials, with copper particle as Cu^{2+} state, an air pre-treatment stage has been carried out prior to the reaction stage.
To confirm the above point, in addition to the test involving a fully oxidized catalyst, another test has been performed, in which, contrary to the previous one, the active site was reduced, namely using a catalyst in which the active site involved metal copper particles.
The thermal protocol used for this test is shown in Figure 2.13. In contrast to air pre-treatment, a reducing flux consisting of a helium mixture containing a fixed percentage of hydrogen has been employed here. In particular, since the catalyst behavior among to reduction was unknown and to avoid possible material sintering, a low percentage of hydrogen has been used in the pre-treatment stage of this examination. H_2 and He percentage and other test specification are reported in Table 3.7. The specific experimental conditions for this test are shown in the Test:22 row on the diary reported in the Appendix of this thesis.
Figure 3.25 and Figure 3.26 show the molar fraction profiles and conversion profiles,

Table 3.7: Experimental conditions to test the catalytic activity of one reduced material. Cat: A-550-20

Pre-treatment stage

Heating rate [°C/min]	**T range [°C]**	$\dot{V}_{in}$ **[ml/min]**	y_{H_2} **[%]**
5	40 - 280°C	26.525	5

Reaction stage

Cooling rate [°C/min]	**T range [°C]**	$\dot{V}_{in}$ **[ml/min]**	**GHSV [h^{-1}]**	h_{cat} **[mm]**	$\varnothing_{particle}$ **[µm]**
1	280-40°C	26.525	20k	3	45 - 250

as a function of monitored temperature and time, respectively, on a pre-reduced A-550-20 catalyst. In particular, Figure 3.25 shows that oxygen of the reaction mixture is totally consumed at 180°C, while for lower temperatures its consumption decreases, resulting in no O_2 conversion for temperature below 65°C. Looking at the Figure 3.26, it can be seen that, apart from oxygen, the only species that undergoes a change in the isothermal stage is hydrogen. More precisely, H_2 conversion profile shows a variation in its consumption over time: in the initial period, after the switching between the reducing and reacting mixture, the value of H_2 conversion is kept around 0.9%, while after 100 minutes its value starts to increase. By keeping constant temperature for a short period of time, the conversion value should not change, unless the catalyst undergoes some alteration; in fact, an increase in hydrogen conversion after a certain time highlights that, the oxygen present in the reacting mixture is consumed by both the catalyst and hydrogen, after the switching between reducing and reaction mixture.
Still considering the isothermal stage at high temperatures,and particularly for times longer than 100 minutes, it is possible to observe a total consumption of O_2 by hydrogen, as there is no consumption of CO at these temperature (CO starts to react with O_2 only below to 280°C). Below to 280°C the species concentration profiles are similar to those obtained when the test is performed with a fully oxidized catalyst: the hydrogen conversion decrease slowly up to the reference temperature, and a CO peak appears in the temperature range between 280°C and 50°C, with a maximum of CO conversion of approximately 80% at 160°C.
Figure 3.27 compares the results obtained testing the same catalyst at two different

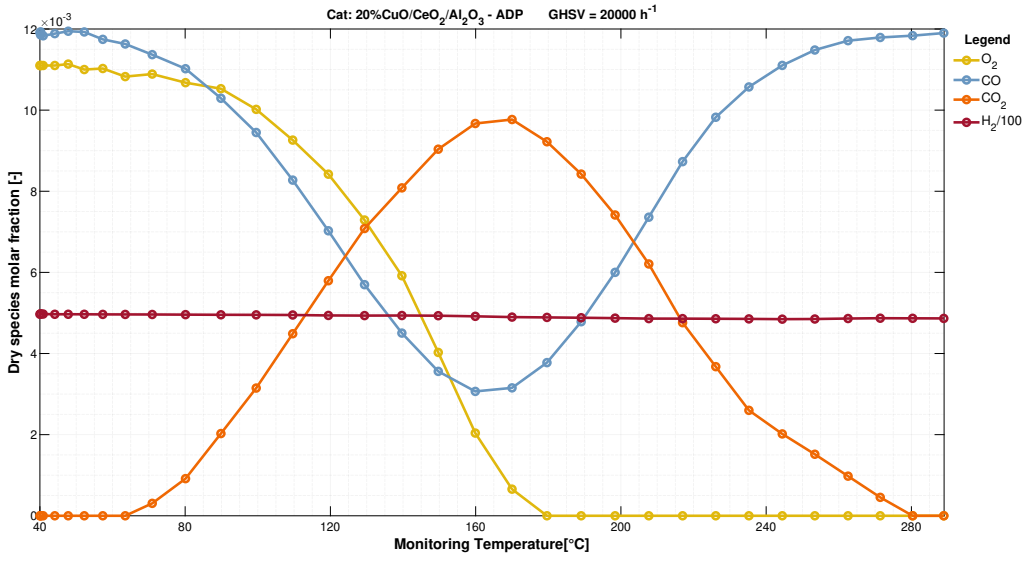

Figure 3.25: Dry species molar fraction as a function of the monitored temperature. Stage considered: cooling, Test:22, Cat: A-550-20

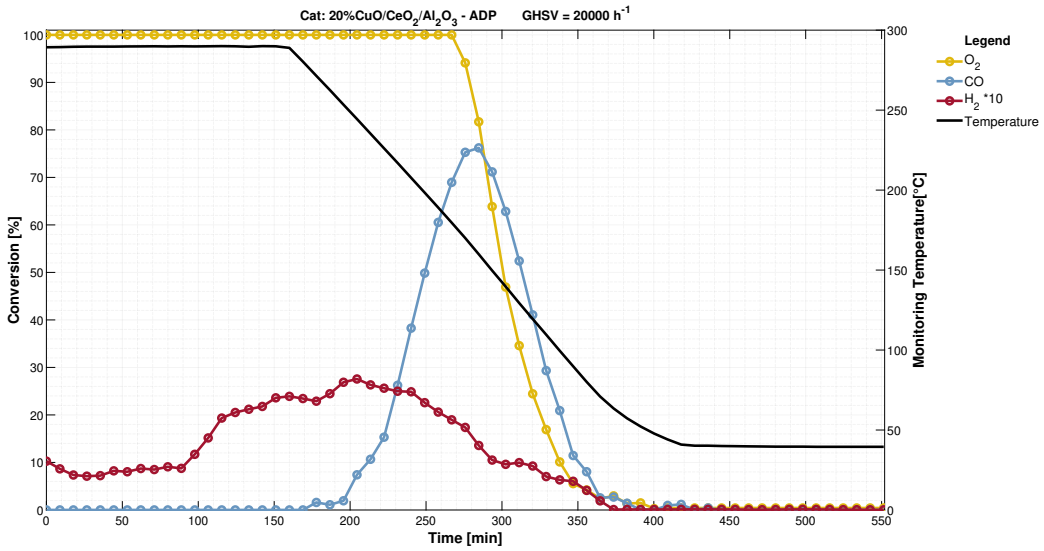

Figure 3.26: Conversion profiles and monitored temperature as a function time. Stage considered: cooling, Test:22, Cat: A-550-30

initial oxidation states. At high temperatures, a fully oxidized catalyst does not require any amount of oxygen present in the reacting mixture, so this species is totally unrestricted to be used by the hydrogen for its oxidation. On the contrary, when reduced catalyst is employed for the reaction, part of oxygen in the gas mixture is used for the catalyst oxidation, thus disadvantaging H_2-OX reaction.
In contrast to the test carried out starting with the fully oxidized catalyst, if a reduced material is employed, the hydrogen consumption little shifts to lower temperatures, reducing the quantity of oxygen available for CO oxidation reaction and thus decreasing its conversion. In particular, the two tests show a difference in CO conversion lower than 4%, but important from the point of view of catalytic activity: with fully oxidized catalyst a maximum conversion value of 80% is observed at 170°C, while with the fully reduced catalyst the CO conversion reaches at best 76.5% at 160°C.

Up to this point, the previous observations pointed out a change in the oxidation state of the catalyst, if it has previously been reduced, during the high-temperature isothermal stage. However, it must be recalled that the reaction environment is highly reductive, as the feed mixture contains carbon monoxide and a high quantity of hydrogen, which are both reducing agents. Then, at high temperature, these two compounds can again change the oxidation state of the catalyst, though a further reduction.
To highlight this aspect, the variation of concentration of the species involved in this reaction could be considered. Figure 3.28 shows the variation of concentration as function of analysis time and temperature for the test performed with pre-reduced

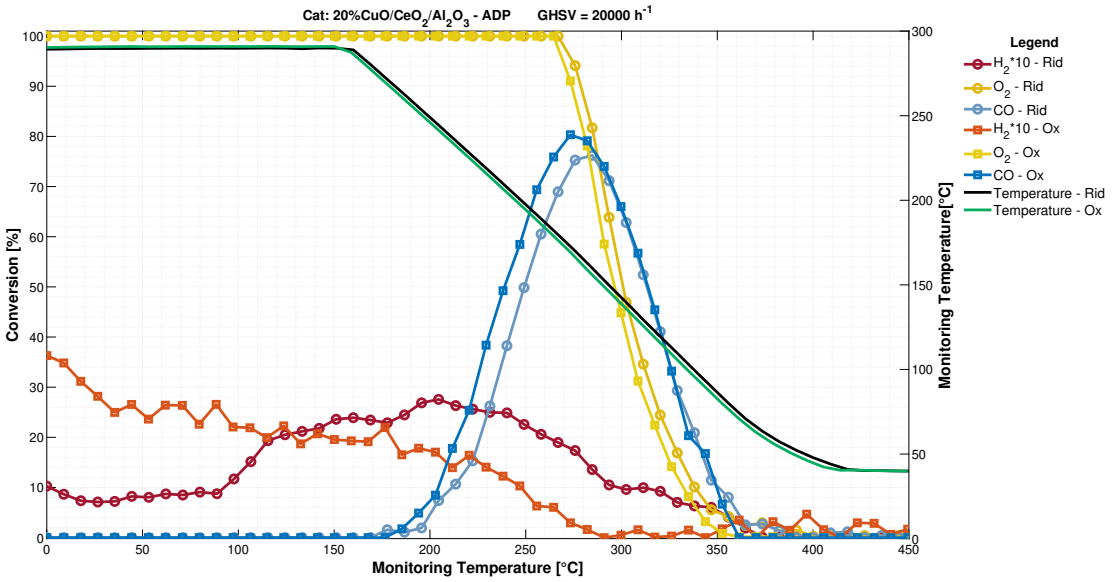

Figure 3.27: Comparison between conversion obtained with completely pre-reduced and pre-oxidized catalyst. Stage considered: cooling, (○) Test:22, (□) Test:24, Cat: A-550-20

catalyst. More specifically, throughout the isothermal period and in the first part of the cooling ramp, a quantitative discrepancy between the variation of concentration of oxygen and hydrogen can be observed: in the first period (up to 100 minutes), the oxygen consumption is predominant with respect the hydrogen one, while from the final part of the isotherm the situation changes: the H_2 consumption increase but does not reach the stoichiometric amount. In particular, during the first part of the cooling ramp there is an increase in CO consumption, which consumes a small fraction of oxygen present in the mixture, and the remaining O_2 is consumed by the hydrogen oxidation reaction and the catalyst.
The results obtained by variation of concentration alone cannot be sufficient to establish the simultaneous presence of both the catalyst oxidation and reduction whenever it is involved in a reacting system such as the one under consideration. To be sure of this, some trials must be carried out to check whether the catalyst is reduced and oxidized in the rest of the temperature range. These tests are the Temperature Programmed Reduction and Temperature Programmed Oxidation respectively, and they will be presented in section 3.7

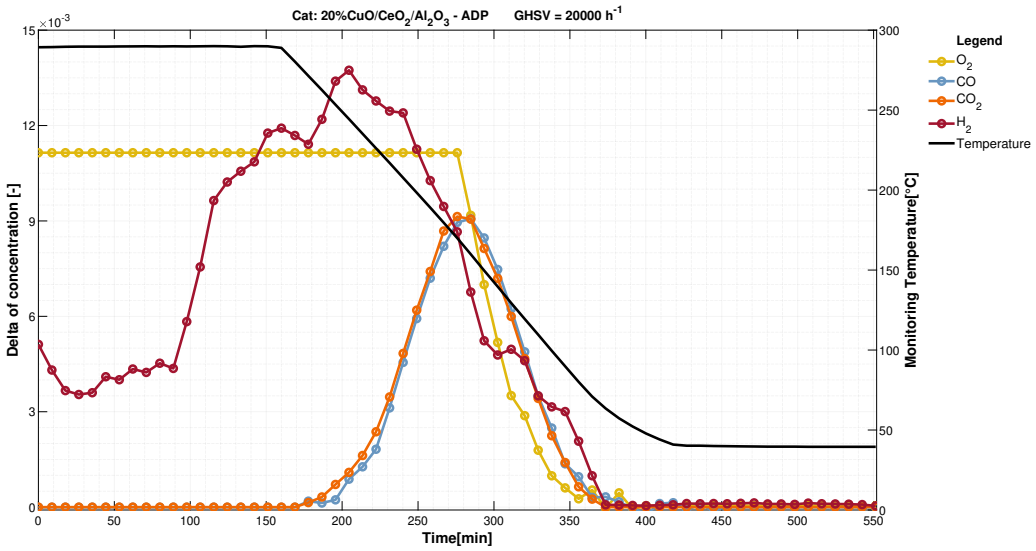

Figure 3.28: Variation of species concentration as function of time and temperature. Stage considered: cooling, Test:22, Cat: A-550-20

3.5.3 Presence of WGS reaction in the CO-PROX mechanism

It was mentioned that the likely reaction that can be take place in this reacting system are: *i* the oxidation reaction of CO *ii* the H_2 oxidation, *iii*the methanation of CO and CO_2 and *iiii* the Water Gas Shift reaction. In previous tests, it has already been shown that this catalyst is not active towards both the methanation reactions because methane was not detected by the measuring instruments. The same conclusion cannot be made for the WGS reaction since, as the reaction scheme in Eq 1.4 shows, it involves CO, H_2O, H_2 and CO_2, which are also involved in the two oxidation reactions.
More specifically, observing the delta of concentration profiles of the reacting system, it can be seen that the consumption of CO is almost equal to the CO_2 production, leading to an initial conclusion that the WGS reaction is absent. In reality this is not so obvious, because WGS may uses the water produced by the H_2-OX and the CO present in the mixture to generate H_2 and CO_2. Eq 3.6 shows the association of the two reaction involved in this described process (H_2-OX and WGS respectively) where the outcome of hydrogen oxidation and WGS is equivalent to CO-OX, and the overall reaction, with which it is possible to state that the delta of concentration is not useful in defining the presence or absence of WGS reaction

in this system.

$$\begin{gathered} \mathrm{H_2} + 1/2\ \mathrm{O_2} \longrightarrow H_2\mathrm{O} \\ \mathrm{CO} + \mathrm{H_2O} \rightleftharpoons CO_2 + \mathrm{H_2} \\ \mathrm{CO} + 1/2\ \mathrm{O_2} \longrightarrow CO_2 \end{gathered} \tag{3.6}$$

Experimentally, to highlight the presence or absence of the WGS reaction at low temperatures, a specific test has not been conducted, but on the other hand, tests aiming to define the evolution of CO-OX and H_2-OX reaction as function of temperature have been performed. In particular, if the hydrogen oxidation reaction does not take place at low temperatures, the WGS reaction will certainly not be able to take place. On the contrary, it was not necessary to carry out any tests at high temperatures because the WGS reaction is an equilibrium reaction.
The tests concerning the CO-OX and H_2-OX reaction have been carried out with the specification given in Table 3.8 and Table 3.9 respectively. The specific experimental conditions for these tests are shown in the Test:12 and Test:14 rows on the diary reported in the Appendix of this thesis. In Figure 3.29 shows the conversion

Table 3.8: Experimental conditions concerning the test conducted to verify the catalytic activity towards the CO-OX reaction alone

Cooling rate [°C/min]	**T range [°C]**	$\dot{V}_{in}$ **[ml/min]**	**GHSV [h^{-1}]**	$\mathbf{y}_{CO}$ [%]	$\mathbf{y}_{O_2}$ [%]
2	40 - 280°C	26.667	20k	1.2	1.2

Table 3.9: Experimental conditions concerning the test conducted to verify the catalytic activity towards the H_2-OX reaction alone

Cooling rate [°C/min]	**T range [°C]**	$\dot{V}_{in}$ **[ml/min]**	**GHSV [h^{-1}]**	$\mathbf{y}_{H_2}$ [%]	$\mathbf{y}_{O_2}$ [%]
2	40 - 280°C	26.432	20k	5	1.2

profile of the component involved in both the CO and H_2 oxidation reactions. The perfect oxidation stoichiometry is always strictly observed. As already shown before, the catalyst is active for CO-OX reaction at lower temperature, close to 70°C, while H_2-OX reaction does not start at temperature close to the CO-OX initiation temperature, but is active from approximately 160°C. This is enough to state that at low temperature the WGS reaction cannot take place because inside the mixture there is no water with which CO can react.

In addition, with the data obtained from these tests, some comparisons can be made with previous results. More specifically, upon to 155°C the conversion of Co obtainable in a system in which H_2 is present or absent is not identical: without hydrogen in the mixture, for the same temperature the catalyst performance obtainable are slightly better,and moreover the CO can be completely convert the CO inside the reacting mixture for temperature higher that 190°C.

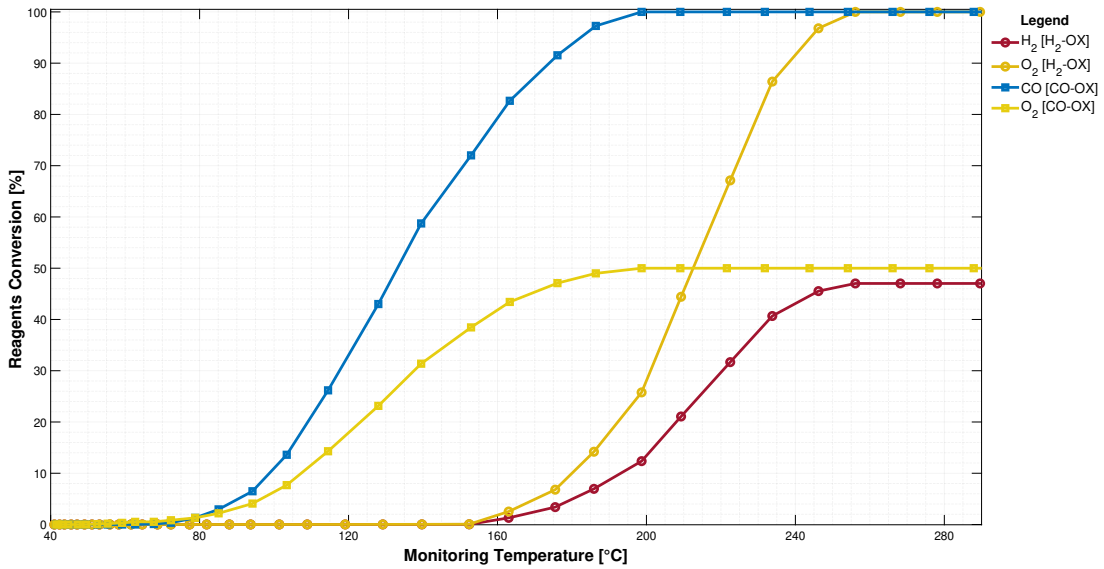

Figure 3.29: H_2-OX and CO-OX reagents conversion as function of monitored temperature. Stage considered: cooling, (○) Test:14, (□) Test:12, Cat: A-550-20

As previously mentioned, WGS is an equilibrium reaction and therefore strongly influenced by the thermodynamics of the system. Considering only the thermal aspect of the system, this reaction is favored up to 850°C (temperature at which $\Delta G^0_R < 0$), which would suggest that in present mixture, the reaction could take place because the operating temperature is lower than the threshold value. However, the reagent species concentration of the system must also be taken into account. In particular, the actual mixture has a very high quantity of hydrogen, which is a product of the WGS reaction. This amount of H_2 disadvantages the direct reaction because it shift the equilibrium towards the reactants and therefore makes the activation of this reaction practically unfeasible. The opposite reaction of WGS (*i.e* R-WGS) is not present in the reagent system, because in all tests performed no CO formation was detected at high or low temperatures

3.5.4 Catalytic activity tests at high GHSV

On an industrial scale, higher GHSV values are employed to increase productivity and thus to increase the economic gain. However, increasing the GHSV means to decrease the contact time between the gas and the catalyst, which could have a negative effect on the catalytic activity.
The test considered in this section has been performed precisely to define the impact of that operating parameter in the system being examined. The operating conditions reported in Table 3.10 has been used to carry out this test. The specific experimental conditions for this test are shown in the Test:31 row on the diary reported in the Appendix of this thesis Figure 3.30 shows the profiles of the cat-

Table 3.10: Experimental conditions for the catalytic test performed with high GHSV on A-550-20 catalyst

Heating/cooling rate [°C/min]	**T range [°C]**	$\dot{V}_{in}$ **[ml/min]**	**GHSV [h^{-1}]**	h_{cat} **[mm]**	$\varnothing_{particle}$ **[µm]**
2	40 - 300°C	46.948	40k	3	45 - 250

alytic bed temperature, the controlled temperature used as input signal to regulate the oven power, the set-point temperature and the oven heat power. Moreover, in the same picture results with lower GHSV value are reported. The profiles appear similar, but they have differences that may lead to reflections on the results of this test. In particular, from 160°C can be observed a temperature variation between the monitoring and controlling thermocouple. In section 3.2 it has been stated that this delta between the two temperatures is due to the catalytic activity, i.e. in another words, for a given temperatures the catalyst is active and it generates heat due to exothermicity of the reaction involved and the heat production is therefore detected by the monitoring thermocouple since this thermocouple is placed inside the the catalytic bed.
Comparison between the two individual plots show that GHSV and then the contact time has an effect on the activity. More precisely, the right-hand plot shows that the thermal variation occurs starting from 130°C, while as the GHSV value increases, the variation starts at 155°C. Figure 3.31 displays the conversion profiles inherent to the tests carried out with different GHSV value. Starting from Figure 3.31-a, it is clear that the operating parameter does not influence the catalyst activation temperature, but on the other hand, GHSV affects the catalytic activity, resulting in a more limited catalyst performance.
As stated in section 3.2.3, with this catalytic material, at low temperature only CO reacts with the oxygen present inside the reacting mixture, while, as the temperature (*i.e* from 110°C), the CO-OX reaction is occurs with the competitive H_2-OX, which shown an almost constant conversion up to 160°C and a slight increasing for

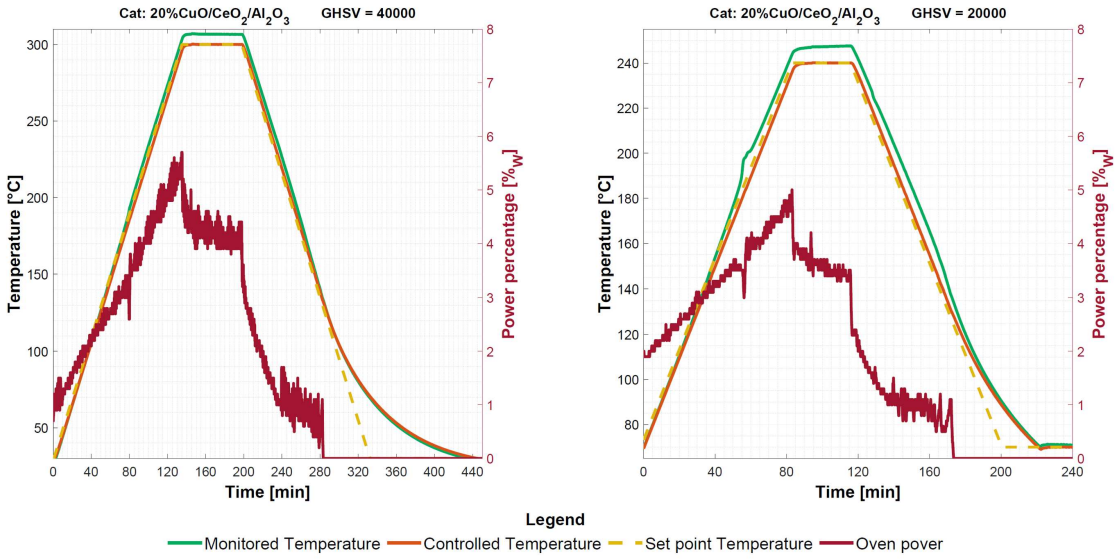

(a)

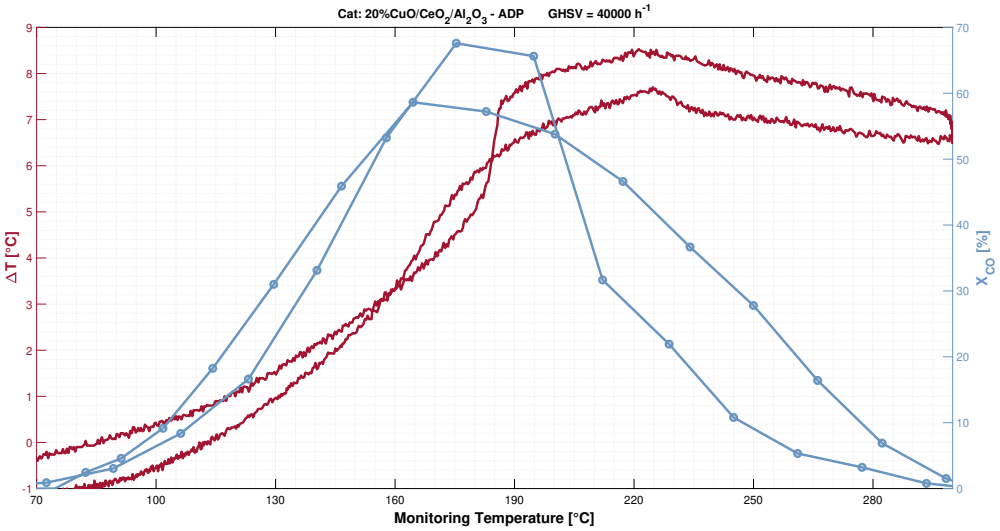

(b)

Figure 3.30: (a) Trends of monitored temperature(green line), controlled temperature (orange line), set-point temperature (yellow dashed line) and oven power (red line) as function of time. On the right Test:3 (low value of GHSV), on the left Test:31 (high value of GHSV), Cat: A-550-20; (b)Temperature variation and CO conversion as a function of the monitoring temperature. Test:31, Cat: A-550-20

higher temperatures. Furthermore, considering the cooling phase, there is no sustained decrease in the reagent conversion, but it can be noted a hysteresis if refereed

to the heating phase. For the same volume of catalyst, increasing the volumetric flow rate, the catalyst starts to be active for the CO oxidation reaction above 70°C, while the hydrogen oxidation reaction is active at higher temperature (160°C, which is comparable with the temperature at which the maximum of CO consumption occurs). Given the absence of O_2 consumption by hydrogen, it would be plausible to observe a greater conversion of CO, but this phenomenon does not occurs because, as stated at the beginning of this discussion, the greater is the value of GHSV, the lower is the contact time between the particles of catalytic material and the gas particle that make up the reacting mixture and therefore lower is the catalytic activity toward the reactions of the system. Compared to the test of GHSV of 20000 h^{-1}, a decrease in conversion is also present between the heating and the cooling phases of the test. On the other hand, the hysteresis between the two test cycles can be assumed negligible. The absence of hysteresis can be attributed to a combination of two factors, one kinetic and another physical. The chemical factor concerns the lower activity of the catalyst, while the physical one is related to the higher heat exchange within the bed: the reaction exothermicity combined with the lower activity contribute to the lower heat generation. Furthermore, considering that hysteresis is attributed to a non-uniformity of the catalytic bed temperature, which gives different activity at the same operating condition, increasing the volumetric flow rate results in a greater heat exchange which, together with the lower heat generation, makes it possible to have a greater uniformity of the temperatures inside the catalytic bed with respect the case to a lower flow rate.

3.5.5 Conclusion

A small aging on the catalytic activity was observed. As the reductions and oxidation required to occur the tests increase, a probable agglomeration of the particle occurs, which leads to the catalyst needing more energy (more heat) to achieve the same degree of conversion.
The high H_2 concentration disfavors the WGS reaction because hydrogen is a product of this reaction. In addition, for temperatures below 155°C, the catalyst is not active towards the hydrogen oxidation reaction and therefore CO does not find the second reagent necessary for the WGS.
Increasing the GHSV value adversely affects the conversion because it precludes log contact between the catalyst and gas molecules. The decrease in performance with a doubling of GHSV value is not substantial, since the conversion decreases by about 15-20%.
Tests carried out on oxidized and reduced catalysts have shown a variation in the activity at high temperatures, whereas this difference is almost negligible in the CO oxidation zone. In particular, it was known that as the initial oxidative state of the catalyst varies, hydrogen consumption changes at high temperatures.
The change in the hydrogen profile at the beginning of the test (after the switching

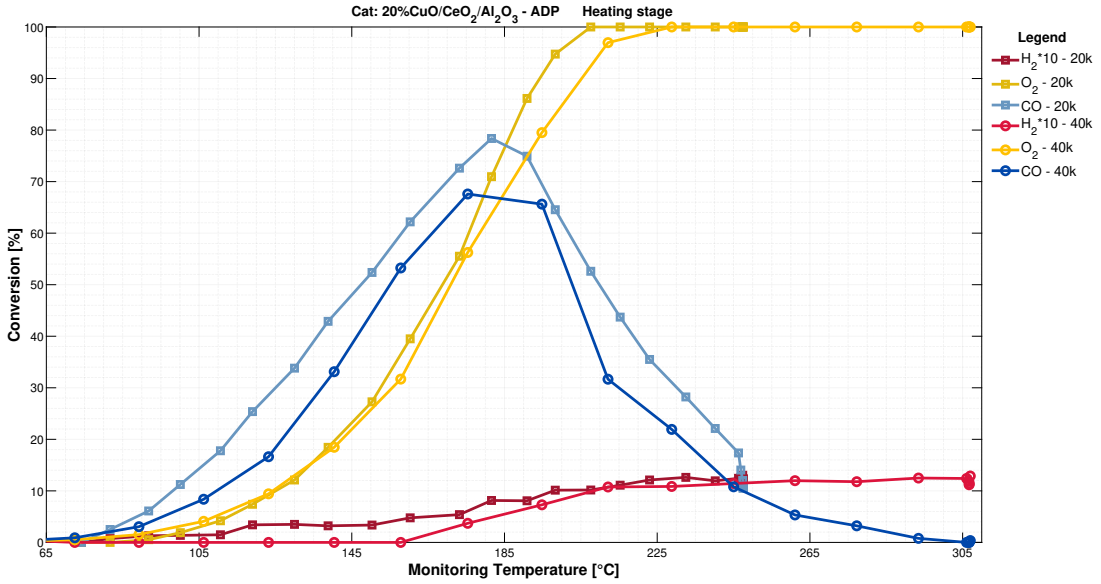

(a)

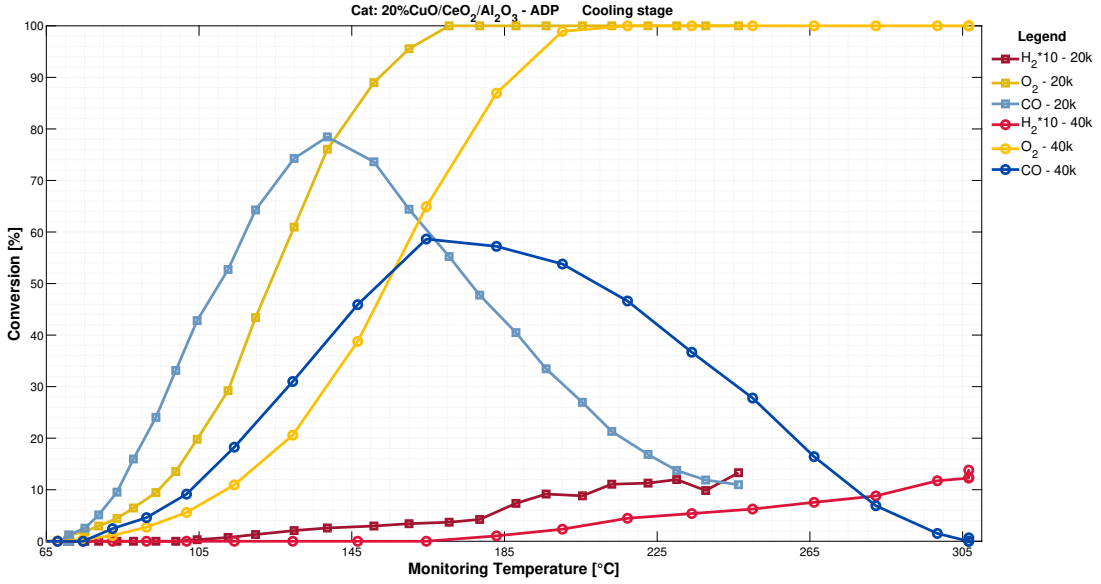

(b)

Figure 3.31: Comparison of reagents conversion profile as function of monitored temperature. (a) heating stage, (b) cooling stage. (○) GHSV=40000 h^{-1} Test:31, (□) GHSV=20000 h^{-1} Test:3; Cat: A-550-20

with the oxidizing mixture) could be due to a reduction of the catalyst at higher temperature. The results also show that the performance of the catalyst towards

the CO oxidation is almost the same, whereas a pre-oxidized or pre-reduced catalyst is used. It is therefore plausible to assume that the catalyst oxidizes at lower temperature.
Confirmation of this process and identification of reaction stability is seen in the following section.

3.6 Catalytic tests carried out with isotherms protocols

Here, two tests have been carried out using thermal protocols incorporating isotherms to asses and characterize the approach to a steady state. These analyses have been conducted to study physical aspect of the test and of the catalyst that cannot be derived using the experimental protocols described in section 2.4.1.
The first test carried out using this method involved a previously oxidized catalyst. The test has useful to define the reaction stability, since the system has not been perturbed in the isothermal period. The second test performed employing this thermal protocol involved a catalyst, which has previously undergone pre-treatment in a reducing environment. In addition to the stability of the reaction, this last test made it possible to how the catalyst change its oxidative state during a CO-PROX reaction.

3.6.1 Isotherm test performed on oxidized catalyst

This test has been carried out with the specification given in Table 3.11. The specific experimental conditions for these tests are shown in the Test:23 row on the diary reported in the Appendix of this thesis. The experimental protocol involved five

Table 3.11: Experimental conditions for reaction stage of catalytic isothermal test performed tarting from oxidized catalyst

Cooling rate [°C/min]	**T range [°C]**	$\dot{V}_{in}$ **[ml/min]**	**GHSV [h^{-1}]**	h_{cat} **[mm]**	$\varnothing_{particle}$ **[µm]**
5	40 - 280°C	25.313	20k	3	45 - 250

different isothermal stages. In particular, the first one, at 280°C, has been carried out to be able to compare these results with those of previous tests, while the other isotherms, at lower temperatures, have been defined on the basis of previous results. More precisely, an isotherm at 200°C has been chosen to better identify the point at which the maximum O_2 conversion occurs, the two isotherms at 175 and 155°C has been chosen to check more thoroughly the region at which the maximum

CO consumption and the starting H_2 oxidation reaction occurs. Finally, the last isotherm at 120°C has been considered to have a reference of what happens at very lower temperatures.

Figure 3.32 shows the species delta of concentration involved in this test. The

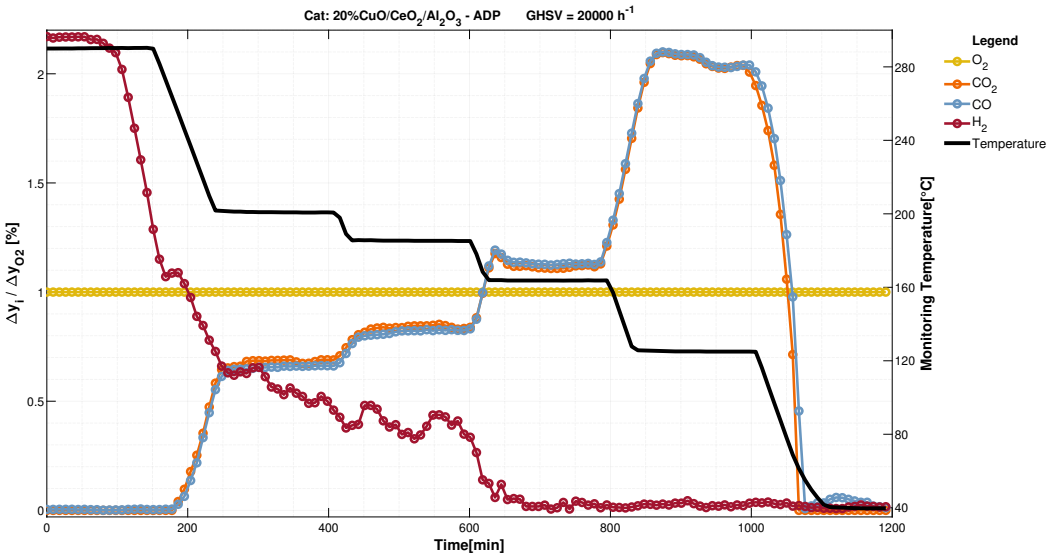

Figure 3.32: Species delta of concentration normalized to O_2 consumption and monitored temperature, as a function of time. Test:23, Cat: A-550-20

figure shows a fast stabilization of the GC-7820 signal, i.e a fast stabilization of the concentration of the species involved in the reactions, at high temperature (T>150°C). On the other hand, at low temperatures (T<120°C), concentrations reach constant values after 60 minutes.

Considering the first isothermal section (T = 280°C) and bearing in mind that *i* H_2 is fed at time zero, replacing pure inert, and *ii* at this temperature the expected reaction is only the hydrogen oxidation, H_2 delta of concentration is greater than its stoichiometry. This statement can confirm what was stated earlier, namely, the catalyst reduction by means to the reducing environment resulting from the high amount of hydrogen in the reacting mixture. The catalyst reduction can be taken as a valid hypothesis by observing how between 200 and 155°C, the amount of O_2 is greater than the one needed for H_2 and CO oxidation reaction. Further confirmation of the reduction at high temperature is given by considering the stoichiometry of the oxidation of CuO with hydrogen, in Eq 3.7. In particular, it has been calculated through the stoichiometry of the reaction, the time required to just reduce the known moles of CuO to Cu, which should equivalent to the moles of H_2 consumed. This calculation showed the time required for reduction to be equal to 160 min. The time shown in the figure is not extremely precise, but is comparable, as the

order of magnitude, with the theoretical time.

$$\mathrm{CuO}_{(s)} + H_{2(g)} \longrightarrow Cu_{(s)} + H_2O_{(g)} \tag{3.7}$$

Intersecting the results shown in Figure 3.32 and Figure 3.33, it is possible to

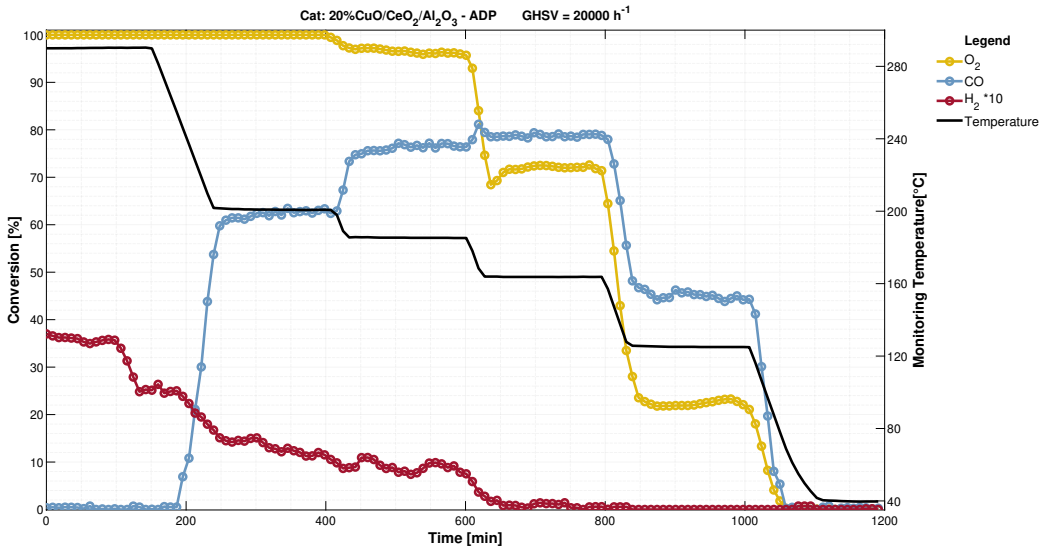

Figure 3.33: Reagents conversion profile as a function of time and monitored temperature. Test:23, Cat: A-550-20

obtain further reactions about the system, namely to compare the reagent conversion profiles obtained from this test with the same profiles obtained from previous test performed without a thermal protocol involving isothermal stages and to define for each temperature the reaction degree taking place. In particular, during the isotherm at 200°C, a complete oxygen conversion is still observed due to the competitive consumption between hydrogen and carbon monoxide, which reach an average conversion value of 1.4% and 62% respectively. By decreasing the operating temperature and reaching the isotherm conducted at 175°C and 155°C, the consumption of O_2 declines because the catalytic material decreases its activity towards the H_2-OX and in favors of CO oxidation reaction. At these temperatures, the maximum conversion of the CO and a substantial drop in the H_2 conversion, which reaches approximately a zero value (during the isotherm conducted at 150°C), can be observed. At these temperatures it is also possible to define that the CO is completely converted to CO_2 since the species delta of concentration of the reagent is comparable to the same parameter of the product, and because of that, WGS reaction does not occur .
In conclusion, a good stabilization of the reaction can be deduced from this test, since in the isothermal sections, beside the concentration of hydrogen, the other species' concentrations settle around an average value and do not show significant

oscillations. The fluctuations present in the hydrogen profile are not due to the chemistry of the reaction but to the precision of the analysis. Figure 3.34 shows

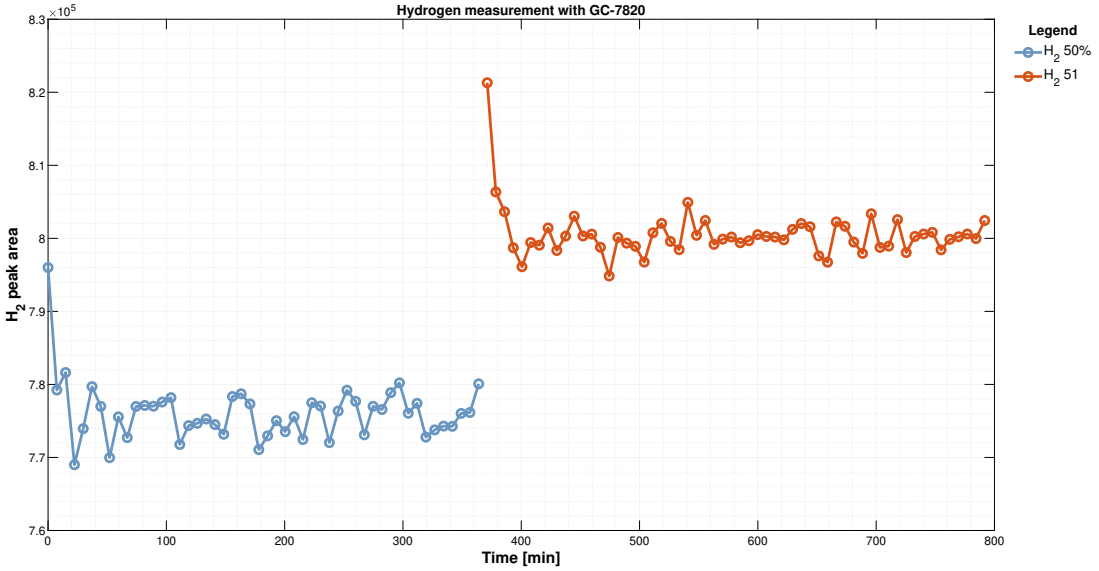

Figure 3.34: Measurement of hydrogen peaks with 50 % and 51%, as a function of time

the hydrogen measurements of a test. The figure shows a variation of the peak areas, even if the concentration of H_2 sending to the GC did not change. The subplots (a) and subplots (b), in Figure 3.35, show the width of the confidence intervals in terms of percentages compared to the mean, as the number of measurements increases, for both hydrogen concentrations. These last plots show that with only a few measurements (2-3 readings), there is an uncertainty of ±3%. This is not permissible since, in the tests performed, the hydrogen variation is about 4%. In order to obtain precise hydrogen measurements, it is therefore necessary to increase the number of measurements (e.g. about ten) for each experimental condition.

3.6.2 Isotherm test on reduced catalyst

This test has been carried out with the specification given in Table 3.12. The specific experimental conditions for this test are shown in the Test:30 row on the diary reported in the Appendix of this thesis.
Contrary to the previous test, here the thermal protocol, or rather the temperature at which the isothermal system is to be maintained, has not been chosen on the basis of preceding results, but it has been decided to divide the temperature range at which the catalyst exhibits relevant activity into three different isothermal stages. In particular, as defined in Table 3.12, the thermal protocol provides for four different isothermal stages, at each 50°C over the temperature range between 100°C and

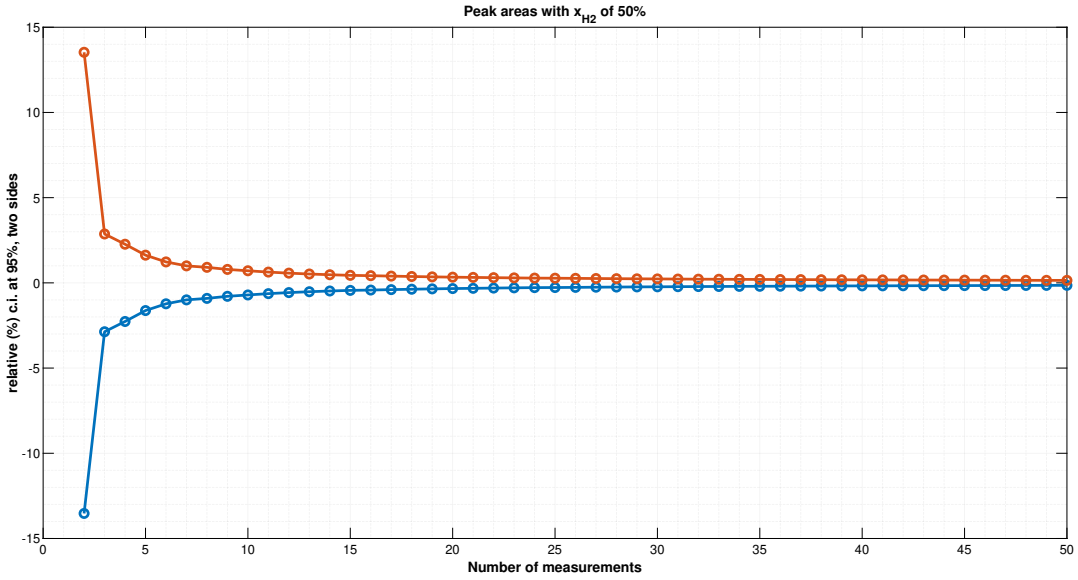

(a)

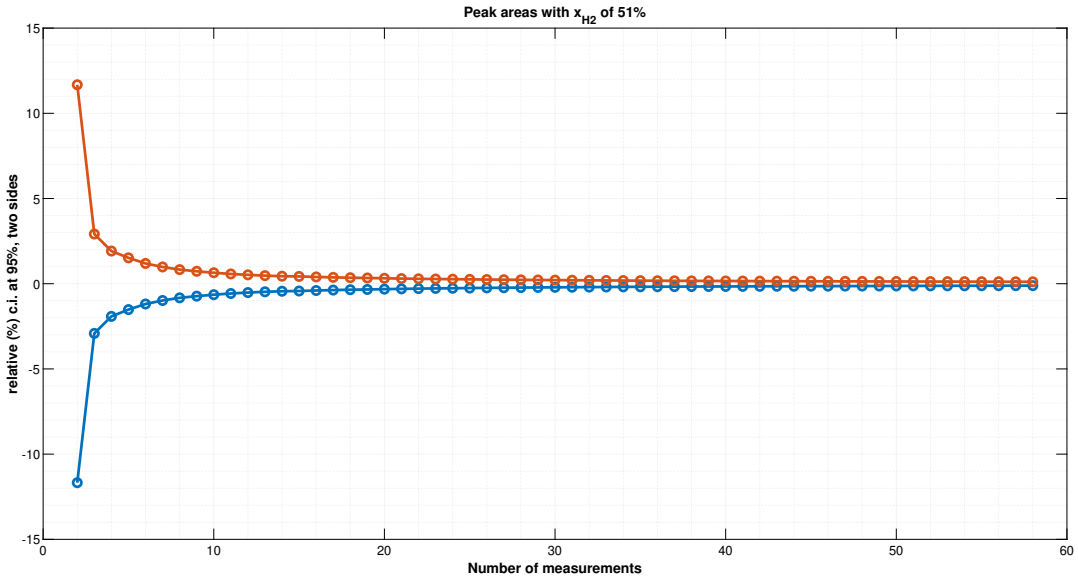

(b)

Figure 3.35: Width of confidence intervals in terms of percentages compared to the mean as a function of the number of measures

250°C. This choice has been made because no previous significant number of test starting from a reduced catalyst have been carried out. In addition to identifying the stability of the reaction, the aim of this test was to identify an approximate

Table 3.12: Experimental conditions for reaction stage of catalytic isothermal test performed tarting from reduced catalyst

Heating/cooling rate [°C/min]	**T range [°C]**	$\dot{V}_{in}$ **[ml/min]**	**GHSV [h^{-1}]**	h_{cat} **[mm]**	$\varnothing_{particle}$ **[µm]**
10	100 - 250°C	27.599	20k	3	45 - 250

temperature at which the catalyst would reduce. A further difference in this experimental protocol is the actual reduction stage. In contrast to the tests focused on identifying the specific properties of CO-PROX starting from a reduced catalyst, in which the pre-treatment step was performed by sending a dilute mixture of H_2 in a inert and with a heating ramp, here the same stage has been carried out at the same temperature as the reaction and with a reducing mixture consisting of H_2 and CO at the respective concentration of the reacting mixture. This effect has been ibtained by runaway O_2 from the feed an the onset of a new isotherm.In this case we started with low temperatures because we wanted to identify at what temperature the catalyst reduces. If the test had started with high temperatures, this effect would not have been visible as the catalyst would reduce immediately.
Figure 3.36 shows the results, in terms of the conversion as function of time and both the controlled and monitored temperatures. The chart highlights how the isotherms do not have the same duration because, by means of a Matlab code which, in real time, exported the output data from each instrument employed to perform the test allowing to monitor the process of reaction almost in real time, it was possible to identify when the system stabilized.

One important features obtained from the chart is the difference of temperature between the catalytic bed and the one measured by the controlled thermocouple (positioned below the bed). The delta of temperature is negligible during all the reduction stages (first point, at wach temperature), while it is noticeable during the reaction (*i.e* oxidative) stages and this delta increase with the operating temperature reaching a constant value of about 10°C from 200°C. From 150°C the higher temperature variation is due to the greater catalytic activity towards hydrogen and carbon monoxide oxidation reactions. The same reactions occur during the reduction stages, but in this specific case the oxygen consumed is the one present in the catalyst lattice. The absence of temperature variation does not mean the absence of reduction, but probably the amount of oxygen present in the catalytic matrix is low enough to limit the temperature rise detectable by the thermocouples.
To be able to identify specific features of the catalyst, this test involved a first air pre-treatment (not monitored) and a second phase which is depicted in Figure 3.36. At the beginning of this second stage (at 100°C and reduction step) a slight consumption of CO is observed, and this usage can only be attributed to the

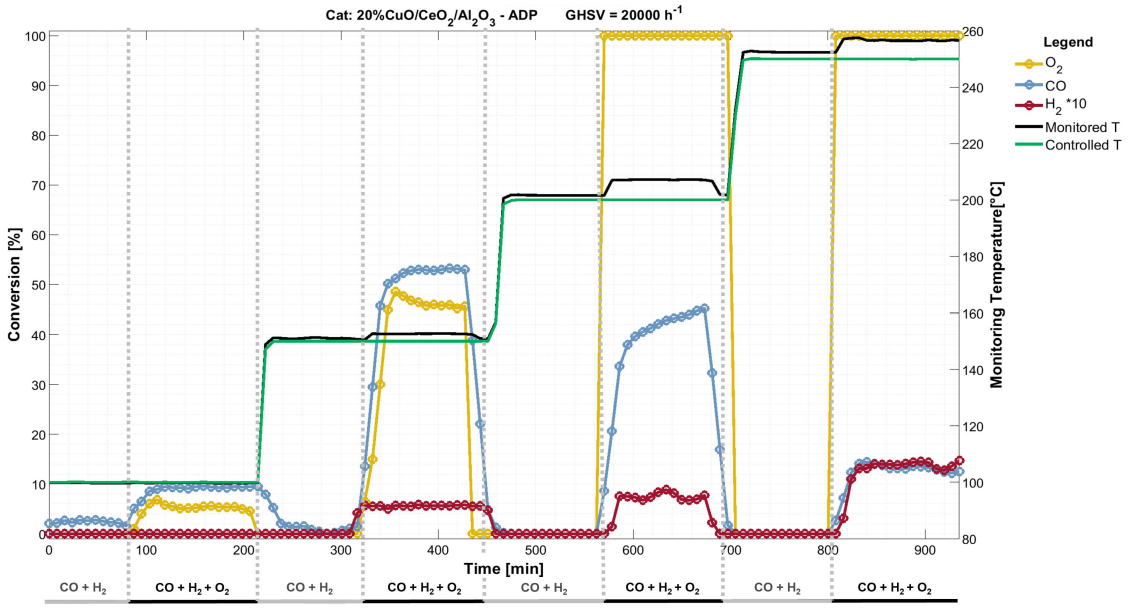

Figure 3.36: Reagent conversion profile as a function of time and monitored temperature. Test:30, Cat: A-550-20

consumption of O_2 trapped in the catalyst lattice, since at this moment, no oxygen was present in the mixture sent to the reactor. Upon the introduction of oxygen in the reacting mixture, an increase in CO conversion is observed, while there is no change in the hydrogen conversion profile. The CO conversion value is around 10%, which is lower than the conversion obtained in the test with a previously reduced catalyst (Figure 3.26 in which $X_{CO} = 21.5\%$). In particular, this value is comparable to the conversion obtained with an oxidized catalyst(and subject to a heating ramp), and then it is possible to say that at 100°C the reduction does not take place.
Similar considerations to those just stated can be made about the stage at 150°C, whereas a change in the catalytic state is observed as the temperature increases. From 200°C the conversion profiles can be compared with those obtained from a test carried out with a reduced catalyst. This shows that between 150°C and 200°C the catalyst is reduced, but this reduction is not detected by the analysis instrument, since probably at these temperature the reducing agent is hydrogen and given its high concentration, a small variation is not significant as for CO and therefore cannot be represented in the figure. In addition, if the catalyst reduction occurred during the transient stage, i.e during the heating ramp, the heating rate accelerated the reduction, which was not detected by GC-7820.
A further important observation can be made at temperatures above 200°C: the conversions of CO and H_2 suggest that only 79% of the entire oxygen present in the reaction mixture is utilized by the carbon monoxide and hydrogen. The remaining

O_2 concentration, knowing that the catalyst is reduced at these temperatures, is then used by the catalyst for its oxidation. To be able to confirm these results, programmed reduction test with both the reducing agent must be made on the catalyst. In addition, to be ale to identify the temperature at which oxygen present can oxidize the catalyst, a programmed oxidation test must be performed. These analyses are set out below in section 3.7

3.6.3 Conclusion

Considering the test carried out with a oxidized catalyst and without an intermediate reduction stage, it is possible to state that the molar fractions are coare stable at all isothermal stages because there is no excessive change in the mole fractions. In addition, it is possible to observe a probable reduction at high temperatures (isotherm at 280°C), which then implies a partial oxidation at lower temperatures, since part of the oxygen in the mixture is used by the catalyst for its oxidation. However, if we consider the test carried out with intermediate reduction, it can be seen that the catalyst is reduced between 155 and 200°C, since at lower temperatures the profiles can be compared with those of a test carried out with an oxidised catalyst, while at higher temperatures the performance is similar to that of a reduced catalyst. However, as the temperature increases, part of the oxygen is consumed by the catalyst for its oxidation.
It is therefore possible to state that whatever the initial stage of the catalyst, the high quantity of hydrogen present in the system leads to a total reduction of the catalyst. However, since the reduced stage of the catalyst is unstable, the catalyst will tend to oxidize again, slightly reducing the amount of O_2 available for CO oxidation.

3.7 Temperature Programmed Reduction and Oxidation

Earlier section reported the results of some tests comparing the catalytic performance of the same material by varing its state of oxidation. The results showed that the reaction mixture, or rather apparently CO and H_2 can reduce the catalyst. In particular, in paragraph 3.6.2 was concluded that at low temperature CO slightly reduces the catalyst, while H_2 causes a reduction at higher temperature.
The aim of this section is to provide the results obtained from temperature programmed oxidation (TPO) and temperature programmed reduction (TPR) tests, which may prove the hypotheses made previously. The thermal protocol used to carried out these tests has already been defined on paragraph 2.4.1 of Chapter2. Table 3.13 and Table 3.14 show the experimental specification used for TPR and TPO analysis respectively. In particular, each table indicated the mixture used

to carry out the test, their respective composition, the heating rate employed and the catalytic material on which the test was carried out. The specific experimental conditions for these tests are shown in the Test: 32, Test: 33 and Test: 34 rows on the diary reported in the Appendix of this thesis. In particular, two different

Table 3.13: Mixture composition and heating rate used in TPR analyses

Test	Reducing mix	Composition [$\%_{H_2/CO}$]	Heating rate [°C/min]	Catalyst
1	H_2 in Ar	5	0.5	A-550-20
2	H_2 in Ar	5	1	A-550-20
3	H_2 in Ar	5	2	A-550-20
4	H_2 in Ar	50	1	A-550-20
5	CO in N_2	5	1	A-550-20

Table 3.14: Mixture composition and heating rate used in TPO analyses

Test	Oxidizing mix	Composition [$\%_{O_2}$]	Heating rate [°C/min]	Catalyst
1	O_2 in He	5	2	A-550-20
2	O_2 in He	5	0.5	A-550-20

TPO analysis have been carried out, the first one focused to determine the oxidizing peaks and the amount of oxygen present inside the catalyst lattice, while the second TPO analysis is carried out to pinpoint the reduction during a standard CO-PROX test and then to determine the amount of oxygen of the lattice consumed during the test.

3.7.1 Temperature Programmed Reduction (TPR)

The temperature at which the catalyst reduction occurs, as a function of the reducing species, was determined by means Temperature Programmed reduction analysis. In addition, from the same test, the amount of hydrogen consumed along all the reduction period can be determined through an integration of the reduction peak. As well as identifying the reduction temperature, the effect of the concentration of the reducing agent in the mixture and of the heating rate subjects to the catalyst affect the reduction peak, the TPR is further investigated.
The TCD was used to monitor TPR with hydrogen as reducing species, because the water present in the stream leaving to the reactor was condensed before the analysis instrument. On the contrary, FTIR was the analytical too employed to determine

the concentration of the species developed inside the system during TPR with CO as reducing compound. In contrast to H_2-TPR, during CO-TPR the CO binds with the oxygen in the catalytic lactate to form CO_2, which cannot be condensed by a simple passage through the condenser.

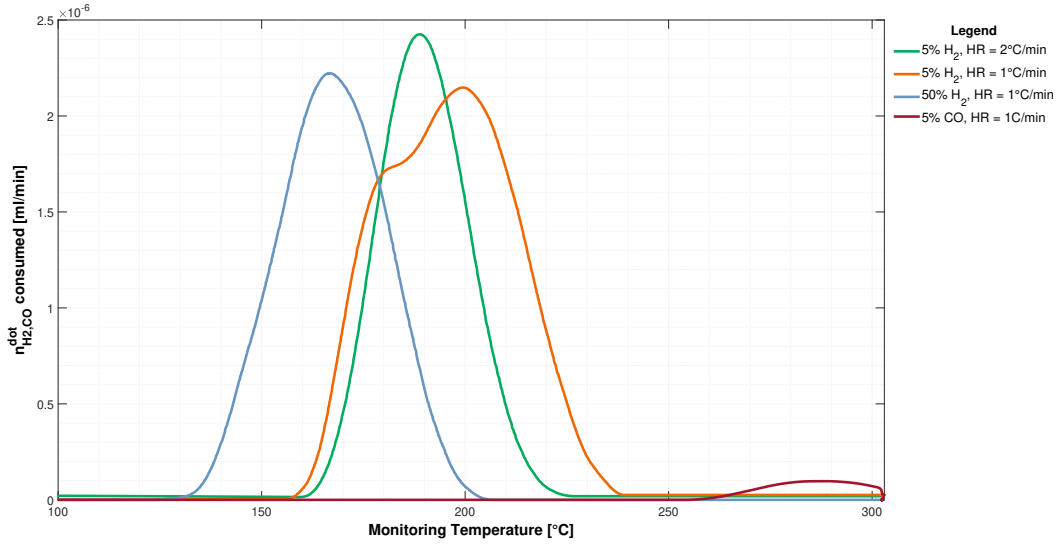

Figure 3.37: Consumed molar flow rate of H_2 and CO during TPR analysis as a function of monitored temperature. (orange and green line) Test:32, (blue line) Test:33, Cat: A-550-20

Figure 3.37 shows the molar flow profiles of the two reducing agents as a function of monitoring temperature. The reduction temperature of the catalyst appears influenced by the concentration of reducing agent in the mixture. By supplying a mixture consisting of 5% hydrogen to the catalytic bed, a first reductive activity is shown for temperatures above 160°C. On the contrary, increasing the mole fraction of H_2, the temperature decreases: a mixture containing 50% of H_2 leads the catalyst to reduce at temperatures above 130°C. The heating rate slightly influence the onset of reduction, by increasing or decreasing the temperature at which the catalyst changes its oxidation state, but it has an effect on the heating rate itself: the higher the reduction rate, the faster the catalyst goes from being fully oxidized to being fully reduced.
Considering the curve regarding the TPR carried out with a mixture containing 5% of H_2 and low heating rate (orange line), it is possible to observed two different peaks: the first is visible at slightly lower temperature which indicates the transition from CuO to Cu_2O, while the second is visible at slightly higher temperature and indicates the transition between Cu_2O and metallic copper. The resolution of these details is lost by increasing the heating rate or the concentration of the reducing agent.

Carbon monoxide does not show an high reducing power. In contrast to hydrogen, CO is consumed for catalyst reduction at temperatures close to 300°C, and the molar flow rate consumed is almost one order of magnitude lower than the flow rate of H_2 consumed. In addition, it can be assumed that the peak shown in the figure is related to the first oxidation step (*i.e* the transition between CuO to Cu_2O) and the second peak is only visible at higher temperatures.

3.7.2 Temperature Programmed Oxidation (TPO)

As shown in Figure 2.14, two instruments in series have been used to perform the TPO analysis: TCD and O_2 sensor. Due to the high noise present in the output signal of the oxygen sensor, this instrument has been considered only to check the data obtained from TCD and therefore no results inherent to the O_2 sensor will be present here.

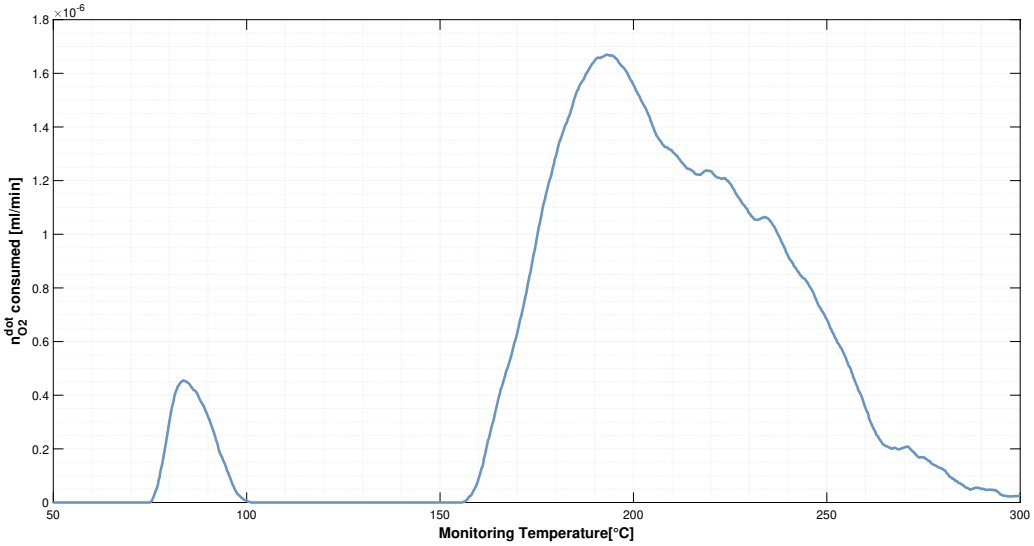

Figure 3.38: Profile of molar flow rate of O_2 consumed as a function of monitored temperature, Test:10, Cat: A-550-20

Figure 3.38 shows the oxidation peaks of the catalyst as a function of time and monitored temperature. On the figure, a drift of O_2 mole flow rate profile during the temperature ramp can be observed. This signal variation is derived from the small TCD signal variation, which is slightly influenced by the heating rate. Contrary to the profile shown in Figure 3.37, in which it is not possible to clearly define the two reduction peaks of the catalytic material, in this case the TPO highlights with high detail the two oxidation peaks. In particular, the first oxidation peak, which defines the oxidation of Cu metal particles to copper oxide (I), is visible at low

temperatures (in the temperature range between 75°c and 100°C), while the second peak, which indicates the transition of the material to its maximum oxidative state occurs at higher temperature (*i.e* for temperature above 156°C). The two profiles do not show the same amplitude. The first profile (Cu to Cu_2O) is more sharped, while the second (Cu_2O to CuO) is more dispersed. One possible explanation for this phenomena could be the greater time required to fully oxidize the catalyst compared to the one needed for the transition between the completely reduced state and the first oxidative state. Another possibility could be the formation of some agglomerates between the oxygen and the copper particles when Cu_2O is formed, which hinder the diffusion of other O_2 particles inside the lattice needed to complete the material oxidative cycle.

As mentioned above, in addition to the TPO carried out from fully reduced

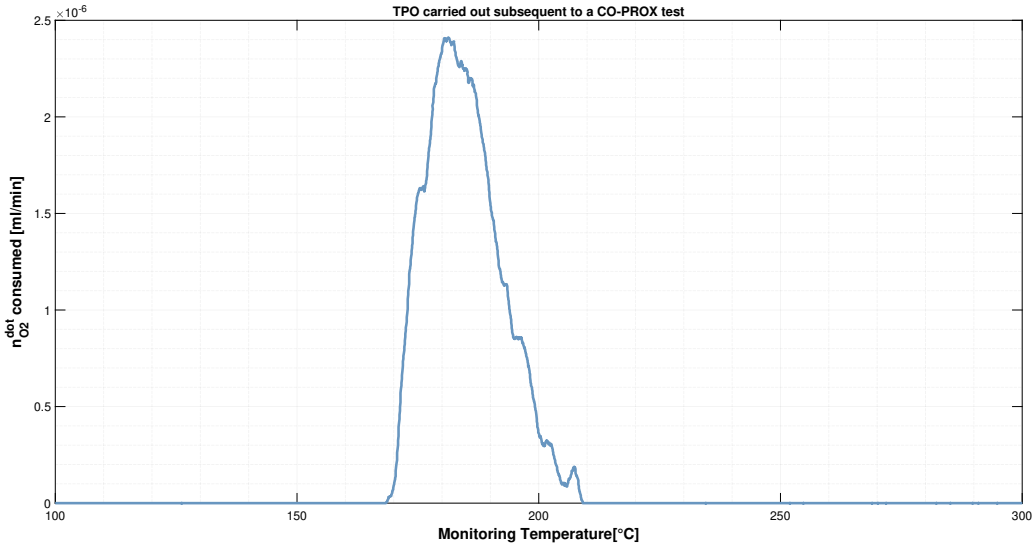

Figure 3.39: Profile of molar flow rate of O_2 consumed as a function of monitored temperature, Test:24, Cat: A-550-20

catalyst, another TPO was also conducted in series to the standard CO-PROX test. In contrast to the previous figure, only one oxidation peak is present in Figure 3.39. Observing the operating temperature, it can be assumed that the oxygen consumption at higher temperature is due to the second oxidation stage of copper oxide material (*i.e* the stage in which the coprous oxide oxides to cupric oxide).

Form this test, it can be concluded that during the reaction stage of a generic preferential oxidation test, the high amount of hydrogen present in the reacting mixture and the high temperature reduce the catalyst, but the reduction does not appear to be complete because only one oxidation peak is present in the chart. In addition, the effect that the heating rate has on the reduction rate can also observed

here. In particular, the increase of 1.5°C/min creates a substantial shortening of oxidation.

3.7.3 Conclusion

TPR analysis confirmed what was said in the section on tests with isotherms. between 155 and 200°C the catalyst starts to reduce. In particular, the TPR analysis showed that with the percentage of hydrogen present in the mixture of the catalytic tests, the catalyst begins to reduce from 130°C, while with a smaller quantity of the same reducing agent, the reduction begins at higher temperatures (160°C). In addition, TPR analysis shows the effect of heating rate. The higher the heating rate the shorter the reduction time, but with high heating rates there is a loss in the resolution of the reduction, i.e. the two reduction peaks cannot be seen. On the other hand, TPO analyses show that the catalyst can be completely reduced over the thermal range of the CO-PROX reaction, with both oxidation peaks being evident. In particular, the first oxidation peak is noted for temperatures between 70 and 100°C, while the second peak is more distributed and is observed at higher temperatures (T> 155°C). A final conclusion of the re-dox process that take place during the reaction phases is the following: as a result of the reduction of the catalyst at high temperatures, the catalyst will tend to oxidize using the oxygen present in the mixture. Due to the low temperature (below 250°C), the catalyst can only complete the first oxidation stage by changing from metallic Cu to CuO. To complete its oxidation, as shown in Figure 3.39, a higher temperature is required.

Chapter 4

Conclusions

The objective of this thesis was to test supported CeO_2/Al_2O_3-based catalysts containing different copper loading, prepared with ADP and EISA synthesis methods, and different oxidation state of the active site. The purpose of these tests was to obtain information on the overall activity of the catalyst in the CO-PROX process and then to hypothesize a specific reaction mechanism. Identifying a valid catalyst for PROX reaction is important because with this process it is possible to purify the H_2 streams from CO and then to use this stream as fuel cell feed.
The thermodynamic model built with NASA software showed that between 50 and 450°C, the methanation of CO is favored over its oxidation because oxygen is completely consumed in hydrogen oxidation and thus it is not available for CO oxidation. The use of a suitable catalysts is crucial to limit hydrogen consumption through its oxidation and methanation and obtain high-purity hydrogen stream without CO.
Six catalysts based on CeO_2 and Al_2O_3 as supported and Cu-CuO redox couple as active compound were synthesized with two methods: Ammonia-driven Deposition Precipitation (ADP) and Evaporation-Induced Self-Assembly (EISA). The optimization of the synthesis procedure and its realization was carried out by National Center for Scientific Research "Dumokritos" (NCSRD).
CO-PROX activity experiments on ADP samples showed a higher CO conversion (80% at 185°C) for 20%-CuO sample while the maximum CO conversion for the 15% and 30% sample was 62% at 172°C and 53% at 170°C, respectively. Additionally, selectivity profiles showed two distinct temperature ranges for oxygen consumption: between 70 and 150-160°C oxygen is fully employed in CO oxidation while at temperatures higher than 160°C, carbon monoxide and hydrogen competes for oxygen consumption. The same reaction protocol was applied to EISA catalysts calcined at different temperatures (E-900-20, E550-20 and E-400-20). The E-900-20 sample was capable of converting 90% of CO at 210°C. The calcination temperature of EISA materials influenced the catalytic performance because, as the calcined temperature increase, the CO conversion increase as well. Comparing the most active

samples for ADP and EISA method, it is clear that 20%Cu/Ce/Al-EISA-900 has the highest performance in terms of CO conversion (90% at 205°C versus 80% at 185°C for the ADP case). Also, maximum H_2 conversion is lower for the EISA sample (lower than 0.5% for temperature higher than 250°C), identifying the E-900-20 sample as the most promising for practical applications.
20%Cu/Ce/Al-ADP-550 catalyst was further tested to correlate the catalyst properties (aging, catalyst oxidation state and WGS presence) to its activity towards CO-PROX reaction. Long-term performance was retrieved from different experiments carried out at difference catalyst state (after 1, 15 and 31 tests) and conversion profiles showed a small decrease of activity at increased time-on-stream (80% at 145°C for the first test, and at 170°C in the last test). Deactivation is likely to occur as higher temperatures are required to obtain the same performance.
The initial copper oxidation state did not influence the overall catalytic activity, as the CO-PROX reaction was tested with pre-reduced and oxidized state. The oxidized A-550-20 sample showed a CO conversion equal to 80 % at 170°C, while the reduced catalyst showed 76% in conversion at 160°C. The slightly lower activity associated to the reduced state is correlated to an increased activity towards H_2 oxidation.
A change in the oxidation state during the CO-PROX reaction is likely to happen as the mixture is prevalently composed by reducing gases (50%H_2 and 1.2% of CO) and this result was proven by isothermal reaction steps at different temperatures (100°C, 150°C, 200°C and 250°C) with a reducing gas mixture (only H_2 and CO) and an initial oxidized sample. The activity at different temperatures in this isothermal steps experiment, and the previous ramping test are reproducible and it corresponds to the expected copper state, with a probable catalyst reduction between 155 and 200°C.
This result was further confirmed by Temperature-Programmed Reduction (TPR) and Oxidation (TPO) through which it was possible to identify the change in oxidation state from +2 (CuO) to 0 (Cu). However, TPR analyses are strongly influenced by the experimental parameters applied in the analysis and thus the same condition applied in the activity tests have been kept in the TPR, to obtain a reliable comparison between the results. Specifically, the reduction temperature depends on the concentration of the reducing agent and heating rate. Using 50% H_2 at 1°C/min, the CuO on the support is reduced with a single-step to Cu between 145°C and 210°C. Conversely, TPO analyses showed two peaks (at 70°C and a broad peak between 150 ans 290°C) as the Cu oxidation is a double-step process in which Cu undergoes to Cu_2O and then CuO.
Experimental results demonstrated the effective role of the catalyst to limit the most thermodynamically favorable reaction (CO methanation) as no traces of CH_4 were detected in the outlet stream. Also WGS reaction is not occurring as H_2 oxidation is not taking place at low temperatures (T<155°C), and it is also an equilibrium-controlled reaction in which H_2 (WGS product) shifts the equilibrium

towards CO and H_2O.
The increase of GHSV obtained by a higher volumetric flowrate with a fixed catalyst volume worsens A-550-20 performance as the contact time between the catalyst particles and gas phase is reduced. The shorter contact time,(*i.e* lower activity), accompanied by the greater heat exchange due to the higher gas convective motion, increases the thermal uniformity within the catalytic bed, reducing the hysteresis phenomenon observed for lower GHSV value.

Future works

Different issues have not been fully clarified in this work;

- Based on section 3.2, a first relevant problem is the non-uniformity of the temperature inside the catalytic bed, probably due to the very exothermic reactions considered in this system. In particular, is has been said that exothermic reactions, from their activation temperature, generate heat in locally in the catalytic bed, which take time to uniform. However, this slow process is in contrast with the chosen thermal protocol (heating ramps) since the heatinf is always too fast compared with the time required for the bed temperature to settle. A possible option to remedy this problem could be the use of a thermal protocol consisting of long-testing isothermal stages, at different temperatures. In particular, with this new experimental protocol, it is possible to wait until the heat generated by the reaction is uniform throughout the bed and observe how long it takes the system to reach a steady state, thus obtaining more precise results for the concentration of the species involved.

- Another problem encountered is the difficulty in detecting very small variation of the hydrogen concentration, such as those due to the catalyst reduction. In the work carried out, hydrogen concentration has to reflect, as closely as possible, the industrial conditions because different catalyst that could be used on this industrial scale has to be tested. In contrast, a lower H_2 concentration could be used to identify the mechanism of the PROX reaction and thus determine very precisely what is happening within the system. To achieves the same objective, it is therefore necessary to define a precise experimental procedure.

- In section 3.5.2 and section 3.6, it was noted that the initial conditions of the catalyst (*i.e* its oxidative state) do not particularly affect the performance of the material itself. During the reaction it change its oxidation state due to the reduction by means of hydrogen, and a subsequent oxidation (due to the presence of O_2) to return to its maximum oxidative state (*i.e* its maximum stability). To avoid further damaging the catalyst, with continuous reductions

or oxidations, it would be advisable to establish an experimental procedure, i.e. a policy defining that all tests are carried out from reduced or oxidized catalysts. In addition, the inert flow in the transient thermal regions could be used so that there is less influence on the reactions in the first isothermal stage.

- another possible experience would be to investigate what happens inside the reacting system when there is no O_2 flow in it. In particular, in this way it would be possible to truly understand if the catalyst used is abe to activate the methanation reaction.

- It would be possible to fed a reaction stream comparable to the industrial one, namely containing CO_2 and steam. In this way, it would be possible to see whether the presence of these two other species influences the performance of the catalyst, or support other reaction, such as WGS or methanation reaction.

Bibliography

[1] Rodolfo M. Antoniassi, Arthur P. Machado, Ana Rita N. Paiva, Carla M.S. Queiroz, Jorge M. Vaz, Estevam V. Spinacé, Julio Cesar M. Silva, Eduardo Carmine, Pedro H.C. Camargo, and Roberto M. Torresi. One-step synthesis of ptfe/ceo2 catalyst for the co-preferential oxidation reaction at low temperatures. *International Journal of Hydrogen Energy*, 46(34):17751–17762, 2021.

[2] A. Arango-Díaz, E. Moretti, A. Talon, L. Storaro, M. Lenarda, P. Núñez, J. Marrero-Jerez, J. Jiménez-Jiménez, A. Jiménez-López, and E. Rodríguez-Castellón. Preferential co oxidation (co-prox) catalyzed by cuo supported on nanocrystalline ceo2 prepared by a freeze-drying method. *Applied Catalysis A: General*, 477:54–63, 2014.

[3] G. Avgouropoulos and T. Ioannides. Effect of synthesis parameters on catalytic properties of cuo-ceo2. *Applied Catalysis B: Environmental*, 67(1-2):1–11, 2006.

[4] G. Avgouropoulos, T. Ioannides, and H. Matralis. Influence of the preparation method on the performance of cuo-ceo 2 catalysts for the selective oxidation of co. *Applied Catalysis B: Environmental*, 56(1-2 SPEC. ISS.):87–93, 2005.

[5] G. Avgouropoulos, T. Ioannides, H.K. Matralis, J. Batista, and S. Hocevar. Cuo-ceo2 mixed oxide catalysts for the selective oxidation of carbon monoxide in excess hydrogen. *Catalysis Letters*, 73(1):33–40, 2001.

[6] C. Bas, N.D. Albérola, and L. Flandin. Effects of contaminant on thermal properties in perfluorinated sulfonic acid membranes. *Journal of Membrane Science*, 363(1-2):67–71, 2010.

[7] J. J. Baschuk and Xianguo Li. Carbon monoxide poisoning of proton exchange membrane fuel cells. *International Journal of Energy Research*, 25(8):695–713, 2001.

[8] Nicolas Bion, Florence Epron, Maximo Moreno, Fernando Mariño, and Daniel Duprez. Preferential oxidation of carbon monoxide in the presence of hydrogen (prox) over noble metals and transition metal oxides: Advantages and drawbacks. *Topics in Catalysis*, 51:76–88, 12 2008.

[9] Marion Brown, Albert Green, Gunther Cohn, and Holger Andersen. Purifying hydrogen by selective oxidation of carbon monoxide. *Industrial & Engineering Chemistry*, 52(10):841–844, 1960.

[10] Tiziana Caputo. *CuO/CeO2 Catalysts for the Preferential Oxidation of CO in H2 rich mixture for fuel cell applications*. Dottato di ricerca ingegneria chimica, dei materiali e della produzione, Università degli studi di Napoli Ferderico II, 2005.

[11] Xuan Cheng, Zheng Shi, Nancy Glass, Lu Zhang, Jiujun Zhang, Datong Song, Zhong-Sheng Liu, Haijiang Wang, and Jun Shen. A review of pem hydrogen fuel cell contamination: Impacts, mechanisms, and mitigation. *Journal of Power Sources*, 165(2):739–756, 2007.

[12] Barbera Davide. *Innovative Processes for Syngas Production*. Dottato di ricerca in chmica industriale, Università degli Studi di Bologna, 2013.

[13] C Doornkamp and V Ponec. The universal character of the mars and van krevelen mechanism. *Journal of Molecular Catalysis A: Chemical*, 162(1):19–32, 2000.

[14] Perry's Chemical Engineers'Handbook 8TH Edition. *Don W. Green, Robert H. Perry*. The MCGraw-Hill Companies, 2007. 8TH Edition.

[15] N. Edwards, S.R. Ellis, J.C. Frost, S.E. Golunski, A.N.J. Van Keulen, N.G. Lindewald, and J.G. Reinkingh. On-board hydrogen generation for transport applications: The hotspot™ methanol processor. *Journal of Power Sources*, 71(1-2):123–128, 1998.

[16] Frank A. de Bruijn Gaby Janssen. Pem fuel cell materials: Costs, performance and durability. *Encyclopedia of Sustainability Science and Technology*, pages 7694–7725, 2012.

[17] Yuxian Gao, Wendong Wang, Sujie Chang, and Weixin Huang. Morphology effect of ceo2 support in the preparation, metal–support interaction, and catalytic performance of pt/ceo2 catalysts. *ChemCatChem*, 5:3610, 12 2013.

[18] Preshit Gawade, Burcu Bayram, Anne-Marie C. Alexander, and Umit S. Ozkan. Preferential oxidation of co (prox) over coox/ceo2 in hydrogen-rich streams: Effect of cobalt loading. *Applied Catalysis B: Environmental*, 128:21–30, 2012.

[19] M. Haruta, N. Yamada, T. Kobayashi, and S. Iijima. Gold catalysts prepared by coprecipitation for low-temperature oxidation of hydrogen and of carbon monoxide. *Journal of Catalysis*, 115(2):301–309, 1989.

[20] K. Jiao, I.E. Alaefour, and X. Li. Three-dimensional non-isothermal modeling of carbon monoxide poisoning in high temperature proton exchange membrane fuel cells with phosphoric acid doped polybenzimidazole membranes. *Fuel*, 90(2):568–582, 2011.

[21] M.J. Kahlich, H.A. Gasteiger, and R.J. Behm. Kinetics of the selective co oxidation in h2-rich gas on pt/al2o3. *Journal of Catalysis*, 171(1):93–105, 1997.

[22] JR Ladebeck and JP Wagner. Catalyst development for water-gas shift, 2003.

[23] O.H. Laguna, W.Y. Hernández, G. Arzamendi, L.M. Gandía, M.A. Centeno, and J.A. Odriozola. Gold supported on cuox/ceo2 catalyst for the purification

of hydrogen by the co preferential oxidation reaction (prox). *Fuel*, 118:176–185, 2014.

[24] K. Liu, A. Wang, and T. Zhang. Recent advances in preferential oxidation of co reaction over platinum group metal catalysts. *ACS Catalysis*, 2(6):1165–1178, 2012.

[25] N. Lopez, T.V.W. Janssens, B.S. Clausen, Y. Xu, M. Mavrikakis, T. Bligaard, and J.K. Nørskov. On the origin of the catalytic activity of gold nanoparticles for low-temperature co oxidation. *Journal of Catalysis*, 223(1):232–235, 2004.

[26] F. Mariño, C. Descorme, and D. Duprez. Supported base metal catalysts for the preferential oxidation of carbon monoxide in the presence of excess hydrogen (prox). *Applied Catalysis B: Environmental*, 58(3-4):175–183, 2005.

[27] M.S. Mikkola, T. Rockward, F.A. Uribe, and B.S. Pivovar. The effect of nacl in the cathode air stream on pemfc performance. *Fuel Cells*, 7(2):153–158, 2007.

[28] A. Mishra and R. Prasad. A review on preferential oxidation of carbon monoxide in hydrogen rich gases. *Bulletin of Chemical Reaction Engineering and Catalysis*, 6(1):1–14, 2011.

[29] Sutarawadee Monyanon, Sangobtip Pongstabodee, and Apanee Luengnaruemitchai. Preferential oxidation of carbon monoxide over pt, au monometallic catalyst, and pt–au bimetallic catalyst supported on ceria in hydrogen-rich reformate. *Journal of the Chinese Institute of Chemical Engineers*, 38:435–441, 09 2007.

[30] David S. Newsome. The water-gas shift reaction. *Catalysis Reviews*, 21(2):275–318, 1980.

[31] J.-W. Park, J.-H. Jeong, W.-L. Yoon, H. Jung, H.-T. Lee, D.K. Lee, Y.-K. Park, and Y.-W. Rhee. Activity and characterization of the co-promoted cuoceo2/γ-al2o3 catalyst for the selective oxidation of co in excess hydrogen. *Applied Catalysis A: General*, 274(1-2):25–32, 2004.

[32] Prakash Parthasarathy and Sheeba Narayanan. Hydrogen production from steam gasification of biomass: Influence of process parameters on hydrogen yield – a review. *Renewable Energy*, 66:570–579, 06 2014.

[33] Jing Peng, Xia Gong, Baocang Liu, and Jun Zhang. Recent advances of synergistic effects promoted catalysts for preferential oxidation of carbon monoxide. *Catalysis Science Technology*, 10, 02 2020.

[34] C.S. Polster, H. Nair, and C.D. Baertsch. Study of active sites and mechanism responsible for highly selective co oxidation in h2 rich atmospheres on a mixed cu and ce oxide catalyst. *Journal of Catalysis*, 266(2):308–319, 2009.

[35] Whitney G.Colella Fritz B. Prinz Ryan O'Hayre, Sunk-Won Cha. *Fuel Cells Fundament*. Wiley, 2016. Third Edition.

[36] J.G. Seo, J.T. Kwon, J. Kim, W.S. Kim, and J.T. Jung. Impurity effect on proton exchange membrane fuel cell. pages 484–487, 2007.

[37] D. Shekhawat, J.J. Spivey, and D.A. Berry. *Fuel Cells: Technologies for Fuel Processing*. Elsevier, 2011.

[38] Adam Z.Weber Timothy E.Lipman. *Fuel Cells and Hydrogen Production*. Springer, 2018. Second Edition.

[39] A. Wootsch, C. Descorme, and D. Duprez. Preferential oxidation of carbon monoxide in the presence of hydrogen (prox) over ceria-zirconia and alumina-supported pt catalysts. *Journal of Catalysis*, 225(2):259–266, 2004.

[40] Zhiwei Wu, Huaqing Zhu, Zhangfeng Qin, Hui Wang, Jianfei Ding, Lichun Huang, and Jianguo Wang. Co preferential oxidation in h2-rich stream over a cuo/ceo2 catalyst with high h2o and co2 tolerance. *Fuel*, 104:41–45, 2013.

[41] Qi Xin, Antonella Glisenti, Constantine Philippopoulos, Evangelos Poulakis, Myrjam Mertens, Jeff L. Nyalosaso, Vera Meynen, and Pegie Cool. Comparison between a water-based and a solvent-based impregnation method towards dispersed cuo/sba-15 catalysts: Texture, structure and catalytic performance in automotive exhaust gas abatement. *Catalysts*, 6(10), 2016.

[42] Quan Yuan, Haifeng Duan, Le-Le Li, Zhenxing Li, Wen-Tao Duan, Lesheng Zhang, Wei-Guo Song, and Chun-Hua Yan. Ceria nanocatalysts: Homogeneously dispersed ceria nanocatalyst stabilized with ordered mesoporous alumina. *Advanced materials*, 22, 04 2010.

Ringraziamenti

A conclusione di questo elaborato, desidero ringraziare vivamente tutte le persone che mi hanno aiutato ad arrivare a questo importante traguardo.

Vorrei ringraziare il Professor Paolo Canu per avermi dato la possibilità di partecipare a questo progetto e per avermi seguito durante tutto il suo svolgimento.
Ringrazio la mia correlatrice, l'*Ing.* Benedetta Oliani per la sua immensa disponibilità, i preziosi consigli e per le indicazioni essenziali sulle varie prove. La vorrei inoltre ringraziare per le correzioni della tesi e della presentazione finale.
Vorrei inoltre ringraziare tutti i membri del gruppo K-Inntech: l'*Ing.* Micol Della Zassa, l'*Ing.* Jessica Fabro, l'*Ing.* Nicola Zanetti e l'*Ing.* Luca Da Lio, per avermi fatto da subito sentire parte del gruppo e per il costante supporto. Un particolare ringraziamento è dovuto all' *Ing.* Mattia Pagin e l'*Ing.* Marco Mantovani per la loro immensa disponibilità e per aver rallegrato tutte le giornate di questo bel periodo con del buon degrado(.cit).
Il più grande ringraziamento è dedicato ai miei genitori ed a mio fratello, per aver sempre creduto in me e per aver sostenuto la realizzazione dei miei progetti. Senza di loro tutto questo non sarebbe avvenuto.

Appendix

Diary

n°	**Cat.**	**An.**	**HR** $[\frac{C}{min}]$	$\dot{V}_{in}$ $[\frac{ml}{min}]$	$\mathbf{y}_{He}$ [%]	$\mathbf{y}_{H_2}$ [%]	$\mathbf{y}_{O_2}$ [%]	$\mathbf{y}_{CO}$ [%]	$\mathbf{h}_{bed}$ **[mm]**	**GHSV** $[\mathbf{h}^{-1}]$
2	ADP-550-30	µGC	2	47.022	47.6	50	1.2	1.2	5	20k
3	ADP-550-20	µGC	2	38.316	47.6	50	1.2	1.2	4	20k
4	ADP-550-15	µGC	2	38.482	47.6	50	1.2	1.2	4	20k
10	ADP-550-20	GC-6890	2	50	95		1.2		4	28k
11	EISA-400-20	GC-7820	1	44	47.6	50	1.2	1.2	4	20k
12	ADP-550-20	GC-7820	1	26.667	97.6		1.2	1.2	3	20k
14	ADP-550-20	GC-7820	1	26.432	93.8	5	1.2		3	20k
15	ADP-550-20	GC-7820	1	26.446	47.6	50	1.2	1.2	3	20k
22	ADP-550-20	GC-7820	1	26.525	47.6	50	1.2	1.2	3	20k
23	ADP-550-20	GC-7820	5	26.315	47.6	50	1.2	1.2	3	20k
24	ADP-550-20	GC-7820	1	26.189	47.6	50	1.2	1.2	3	20k
24	ADP-550-20	GC-6890	0.5	26.189	95		5		3	20k
30	ADP-550-20	GC-7820	10	27.599	47.6	50	1.2	1.2	3	20k
31	ADP-550-20	GC-7820	1	29.268	47.6	50	1.2	1.2	3	40k
32	ADP-550-20	GC-7820	2	50	85	5			3	38k
33	ADP-550-20	GC-6890	1	50	50	50			3	38k
34	ADP-550-20	FT-IR	1	50	95			5	3	38k
36	EISA-550-20	GC-7820	1	17.442	47.6	50	1.2	1.2	2	20k
37	EISA-900-20	GC-7820	1	17.611	47.6	50	1.2	1.2	2	20k
39		GC-7820			50	50				
40		GC-7820			49	51				

Matlab code used for post-processing

```
clear all; clc; close all

%% Informazioni da specificare necessarie per l'analisi
numberTest = 30; % Numero del test
n0 = 3; % Numero della prima run considerata
Rid = 0; % 0 se catalizzatore ridotto, 1 altrimenti
Riscaldamento_Raffreddamento = 0; % 1 se Test con risc/raffr, 0 altrimenti
title_on = 0; % 1 se inserire il titolo, 0 altrimenti
row_Vdot_in = 395; % Riga lettura portata volumetrica totale e calibrazioni
row_cal_slope_GC = 37; row_cal_int_GC = row_cal_slope_GC+1; % Riga di m e q nel file excel delle calibrazioni
if numberTest == 31 || numberTest == 27; row_cal_slope_GC = 5; row_cal_int_GC = row_cal_slope_GC+1; end
if numberTest == 38; ow_cal_slope_GC = 73; row_cal_int_GC = row_cal_slope_GC+1; end
row_cal_slope_GC = num2str(row_cal_slope_GC); row_cal_int_GC = num2str(row_cal_int_GC);
rowExcel = num2str(numberTest+1);

species = ["H2" "O2" "CO" "CO2" "H2O"];% Specie coinvolte
reacting_mixture = "1.2%CO + 1.2%O2 + 50%H2"; % composizione della miscela
obj_Test = 'Test CO_PROX da catalizzatore ridotto'; % Obiettivo del test
% Scelta lettura termocoppia || TC = 1; % 2 se legge Tin8, 1 se legge Cx-thermo
if numberTest == 37 || numberTest == 30; TC = 1; else TC = 2; end
nTC = 4; % colonna lettura termperatura per Tin8
save_fig = 0; % 0 per non salvare le figure, 1 altrimenti
save_data = 0; % 0 per non salvare i dati, 1 altrimenti
mis_w = 0; % 0 se H2O non misurata, 1 altrimenti
Stag =  1;  % 0 se estate, 1 se inverno
% Definizioni valori per grafici
f_title = 15; f_subtitle = 13; f_leg = 15; lw = 3; f_label = 17; ms = 8;

%% Directory dei file
%== Directory GC-7820
Dir_7820 = 'C:\Users\danie\Google Drive\CreaLabDrive\PROX\PROX_MS\Data\GC7820\Test\';
Dir_7820_1 = [Dir_7820 'Test_', num2str(numberTest),'\'];
```

```
33 Dir_7820_2 = [Dir_7820_1 'METODO_PROX_0211.met-Back Signal.
       Area'];
34 fid1 = fopen(Dir_7820_2);
35 %== Directory Tin8
36 Dir_T= 'C:\Users\danie\Google Drive\CreaLabDrive\PROX\PROX_MS\
       Data\Temperature_Data\';
37 Dir_T_Tin8 = [Dir_T 'Test_',num2str(numberTest),'\'];
38 Temperature_file = [Dir_T_Tin8 'Dati_temp_Tin8.dat'];
39 DirCX_thermo = [Dir_T 'Test_',num2str(numberTest),'\','Omron\'
       ];
40 %== Directory Excel
41 % Dir_excel = 'G:\Il mio Drive\CreaLabDrive\PROX\PROX_MS\Data\
       Excel\';
42 Dir_excel = 'C:\Users\danie\Google Drive\CreaLabDrive\PROX\
       PROX_MS\File_Excel\';
43 file_diario = 'Diario PROX_MS.xlsx';
44 file_calibrazioni = 'File_CALIBRAZIONI.xlsx';
45 file_test = 'TEST_ESEGUITI.xlsx';
46 %== Directory salvataggio dati e figure
47 Dirfig = 'C:\Users\danie\Google Drive\CreaLabDrive\PROX\
       PROX_MS\Processing\Figure\';
48 Dirfig = strcat([Dirfig 'Test_',num2str(numberTest),'\']);
49 Dirdata = 'C:\Users\danie\Google Drive\CreaLabDrive\PROX\
       PROX_MS\Processing\Data_Test\';
50 Dirdata = strcat([Dirdata 'Test_',num2str(numberTest),'\']);
51
52 %% Lettura dati da Excel
53 dum_1 = xlsread([Dir_excel file_diario],'Diario',['AE',
       rowExcel,':AL',rowExcel]);
54 h_cat = dum_1(1)*10; m_cat = dum_1(2); % h_cat [mm]; m_cat [mg
       ];
55 nsamples = dum_1(5); nwhite_in = dum_1(6); nwhite_end = dum_1
       (7); nend = dum_1(8);
56 [canc,cat] = xlsread([Dir_excel file_diario],'Diario',strcat('
       C',num2str(rowExcel)));
57 catalyst = string(cat);
58 if numberTest == 37
59     catalyst = '20%CuO/CeO_2/Al_2O_3-EISA T_c_a_l_c = 900 C ';
60 end
61 if numberTest == 36
62     catalyst = '20%CuO/CeO_2/Al_2O_3-EISA T_c_a_l_c = 550 C ';
63 end
64
```

```
65 hydrogen = xlsread([Dir_excel file_calibrazioni],'H2',['S',
       row_cal_slope_GC, ':S',row_cal_int_GC]);
66 m_H2 = hydrogen(1); q_H2 = hydrogen(2);
67 oxygen = xlsread([Dir_excel file_calibrazioni],'O2',['S',
       row_cal_slope_GC, ':S',row_cal_int_GC]);
68 m_O2 = oxygen(1); q_O2 = oxygen(2);
69 carbon_monoxide = xlsread([Dir_excel file_calibrazioni],'CO',[
       'S',row_cal_slope_GC, ':S',row_cal_int_GC]);
70 m_CO = carbon_monoxide(1); q_CO = carbon_monoxide(2);
71 carbon_dioxide = xlsread([Dir_excel file_calibrazioni],'CO2',[
       'S',row_cal_slope_GC, ':S',row_cal_int_GC]);
72 m_CO2 = carbon_dioxide(1); q_CO2 = carbon_dioxide(2);
73 Vdot_in = xlsread([Dir_excel file_test],'Test',strcat('D',
       num2str(row_Vdot_in))); % [ml/min];
74
75 %% Lettura dati da GC-7820
76 tline = fgetl(fid1); tline = fgetl(fid1); dum = strread(tline,
       '%s');
77 Nrec = str2num(cell2mat(dum(4))); tline = fgetl(fid1);
78 dum = strread(tline,'%s','delimiter','\t');
79 Ncol = length(dum); Nc = Ncol-10; Nomi_tcd = dum(11:end);
80
81 for i = 1 : Nrec-1
82     tline = fgetl(fid1); tline = strrep(tline,':','.');
83     dum = strread(tline,'%s','delimiter','\t');
84
85     if length(dum) < Ncol || length(tline) == Ncol
86         dum(Ncol) = {''};
87     end
88
89     d = strread(char(dum(1)),'%d','delimiter','/');
90     h = strread(char(dum(2)),'%s','delimiter',' ');
91     t = strread(char(h(1)),'%d','delimiter','.');
92
93     if length(h) > 1
94         if strcmp(h(2),'PM') && t(1) ~= 12
95             t(1) = t(1) + 12;
96         end
97         if strcmp(h(2),'AM') && t(1) == 12
98             t(1) = 0;
99         end
100    end
101
102    tGC(i) =datenum([d(3),d(2),d(1),t']);
```

```
103
104     for j = 1 : Nc
105         a = str2num(cell2mat(dum(10+j)));
106         if isempty(a)
107             Areas(i,j) = 0;
108         else
109             Areas(i,j) = a;
110         end
111     end
112 end
113 fclose(fid1)
114 Areas_tcd = Areas; tGC_tcd = tGC; Nc_tcd = Nc;
115 pH2 = Areas_tcd(:,1); pCO2 = Areas_tcd(:,2); pCO = Areas_tcd
    (:,4); pO2 = Areas_tcd(:,3);
116 p = [pH2 pO2 pCO pCO2];
117 clear Areas a tGC
118 tGC = tGC_tcd; t_GC_noser = datetime(tGC,'ConvertFrom','
    datenum');
119 if Stag == 1
120     t_GC_noser = t_GC_noser + minutes(60);
121 else
122     t_GC_noser = t_GC_noser + minutes(120);
123 end
124 tGC = datenum(t_GC_noser); tGCin = min(min(tGC_tcd),min(
    tGC_tcd));
125 tGCfin = max(max(tGC_tcd),max(tGC_tcd)); tGC_tcd = (tGC_tcd-
    tGCin)*1440;
126
127 %% Lettura dati da Ti8 o Cx-Thermo
128 if TC == 1
129     d_CX_Thermo = dir(DirCX_thermo);
130     filenames = char(d_CX_Thermo.name);
131     f = cellstr(filenames);
132     nfile = length(f);
133     if nfile > 2
134         tcx_ciclo = []; Treg_ciclo = []; Tsp_ciclo = [];
            MVheat_ciclo = [];
135         for j = 3 : nfile
136             ff = char(f(j));
137             fid_Ti = fopen([DirCX_thermo ff]);
138             if fid_Ti > 0
139                 for j = 1 : 8
140                     tline = fgetl(fid_Ti);
141                 end
```

```
142                 while 1
143                     tline = fgetl(fid_Ti);
144                     if tline == -1
145                         break
146                     end
147                     dum_cx_thermo = strread(tline,'%s','
                           delimiter','\t');
148                     tcx = datenum(tline(1:19),'yyyy/mm/dd_HH:
                           MM:SS');
149                     i = i+1;
150                     tcx_ciclo   = [tcx_ciclo tcx];
151                     Treg_ciclo  = [Treg_ciclo str2num(cell2mat
                           (dum_cx_thermo(3)))];
152                     Tsp_ciclo   = [Tsp_ciclo str2num(cell2mat(
                           dum_cx_thermo(4)))];
153                     MVheat_ciclo = [MVheat_ciclo str2num(
                           cell2mat(dum_cx_thermo(5)))];
154                 end
155             end
156         end
157         fclose(fid_Ti);
158         tT = tcx_ciclo; T = Treg_ciclo; Tsp = Tsp_ciclo;
               MVheat = MVheat_ciclo;
159     end
160 end
161 if numberTest == 30; TCX = Treg_ciclo; end
162
163 if numberTest == 30; TC = 2;end
164 if TC == 2
165     Tdata = fopen(Temperature_file);
166     ant = 6.7024;
167     i = 0;
168     while 1
169         tline = fgetl(Tdata);
170         if tline == -1
171             break
172         end
173         dum = strread(tline,'%s');
174         dum = strrep(dum,',','.');
175         d1  = strread(char(dum(1)),'%d','delimiter','/'); %
               date d/m/y
176         t   = strread(char(dum(2)),'%d','delimiter','.'); %
               time h.m.s
```

```
177         t    = datenum([d1(3),d1(2),d1(1),t']);              %
               time as serial
178          if t > min(tGC)-ant/1440
179             i = i + 1;
180             tT(i)= t;
181             T(i) = str2num(cell2mat(dum(1+nTC)));
182             if t > max(tGC)
183                 break
184             end
185         end
186     end
187 end
188 t_GC = (tGC - tGC(1))*1400; tTemp = (tT - tGC(1))*1440;
189 T_tot = interp1(tTemp,T,t_GC); T_GC = interp1(tTemp,T,tGC_tcd)
    ; T_GC = T_GC';
190 if numberTest == 30
191     t_GC = (tGC - tGC(1))*1400; tTempCX = (tcx_ciclo - tGC(1))
        *1440;
192     T_totCX = interp1(tTempCX,TCX,t_GC); T_GCCX = interp1(
        tTempCX,TCX,tGC_tcd); T_GCCX = T_GCCX';
193 end
194
195 %% Calcolo delle frazioni e portate molari, bilancio di
    materia, conversione, delta di concentrazione e
    selettivit
196 %Frazioni molari
197 xH2 = q_H2 + m_H2*p(:,1); xO2 = q_O2 + m_O2*p(:,2);
198 xCO = q_CO + m_CO*p(:,3); xCO2 = q_CO2 + m_CO2*p(:,4);
199 x_tot = [xH2 xO2 xCO xCO2];
200 for i = 1: length(x_tot(:,1))
201     for j = 1:4
202         if x_tot(i,j) < 0
203            x_tot(i,j) = 0;
204         end
205     end
206 end
207
208 x_ref = (x_tot(nwhite_in:nwhite_end,:))/100;
209 xref_mean = mean(x_ref);
210 x = (x_tot(n0:nend,:))/100;
211
212 % portate molari
213 T_ref = 273.15;                                          % [K]
214 T_in = 25;                                               % [ C ]
```

```
215 n_in = 1*101325/8.314/(T_ref+T_in)*Vdot_in/1e6;      % [mol/min
    ]
216 n_ref = (n_in*(xref_mean));
217 n_i = n_in*x;
218
219 % Bilanci di materia
220 Cbal_err = []; Obal_err = [];
221 for i = 1 : length(n_i)
222     Cbal_err(i) = (((n_ref(3) + n_ref(4)) - (n_i(i,3)+n_i(i,4)
        ))./(n_ref(3) + n_ref(4)))*100;
223     Cbal_err(i) = (((n_ref(3) + n_ref(4))- (n_i(i,3)+n_i(i,4))
        )./...
224         ((n_ref(3) + n_ref(4)))).*100;
225     Obal_err(i) = (((2*n_ref(2) + n_ref(3) + 2*n_ref(4))-(2*
        n_i(i,2) + ...
226         n_i(i,3) + 2*n_i(i,4))./(2*n_ref(2) + n_ref(3) + 2*
            n_ref(4))).*100;
227 end
228 Cbal_err = smooth(Cbal_err,3);
229 Obal_err = smooth(Obal_err,3);
230
231 % Conversione
232 X = zeros(size(x));
233 for i = 1 : length(n_i(:,1))
234     for j = 1 : 3
235         X(i,j) = ((n_ref(j)-n_i(i,j))/(n_ref(j))).*100;
236     end
237 end
238 for i = 1 : length(X(:,1))
239     for j = 1 : length(X(1,:))
240         if X(i,j) < 0
241             X(i,j) = 0;
242         end
243     end
244 end
245
246 % Delta di concentrazione
247 x_delta = x*100; % PERCENTUALE
248 deltaCO = xref_mean(3)*100 - x_delta(:,3);
249 deltaH2 = xref_mean(1)*100 - x_delta(:,1);
250 deltaO2 = xref_mean(2)*100 - x_delta(:,2);
251 deltaCO2 = x_delta(:,4) - xref_mean(4)*100;
252
253 % Selettivit
```

```
254 S_CO2 = zeros(length(n_i),1);                nu_CO_OX = [0 0.5 1
    1 0];
255 S_CO2 = 100*(((n_i(:,4) - n_ref(4))./(n_ref(2) - n_i(:,2)))*(
    nu_CO_OX(2)/nu_CO_OX(4)));
256 S = S_CO2;
257 for i = 1 : length(S(:,1))
258     for j = 1 : length(S(1,:))
259         if S(i,j) < 0
260             S(i,j) = 0;
261         end
262         if (S(i,j) > 100) && (S(i,j) <= 130)
263             S(i,j) = 100;
264         end
265     end
266 end
267
268 %% Grafici dei risultati ottenuti
269 close all
270 if Rid == 1
271     reaction = string(['Test ', num2str(numberTest) ':CO-PROX
        da Cat Ossidato']);
272 end
273 if Rid == 0
274     reaction  = string(['Test ', num2str(numberTest) ':CO-PROX
         da Cat Ridotto']);
275 end
276 set(0,'DefaultFigureWindowStyle','docked','DefaultAxesFontSize
    ',f_label)
277 colors = [0 0.6745 0.3686; 0.850 0.325 0.098; 0.4078 0.5882
    0.7529;...
278     0.9373 0.4078 0.01176; 0.8784 0.7216 0.0549; 0.6350 0.0780
         0.1840; 0 0 0];
279 colors_1 = ['#E6CD10';'#0072BD';'#D95319'];
280
281 figure('NumberTitle','on')
282 yyaxis left
283 plot(t_GC(n0:nend)-t_GC(n0), X(:,2),'-o','MarkerSize',ms,'
    LineWidth',lw,'Color',colors(5,:)); hold on
284 plot(t_GC(n0:nend)-t_GC(n0), X(:,3),'-o','MarkerSize',ms,'
    LineWidth',lw,'Color',colors(3,:)); hold on
285 plot(t_GC(n0:nend)-t_GC(n0), X(:,1)*10,'-o','MarkerSize',ms,'
    LineWidth',lw,'Color',colors(6,:)); hold off
286 set(gca,'xcolor',colors(7,:),'FontSize',14); set(gca,'ycolor',
    colors(7,:),'FontSize',14);
```

```
287 if numberTest == 22; ylim([-0.014 101]); end
288 if numberTest == 27; ylim([-0.002 100.5]); end
289 if numberTest == 23; ylim([-0.1 101]); end
290 grid on; grid minor;set(gca,'MinorGridAlpha', 0.15);set(gca,'
    GridAlpha', 0.05)
291 yyaxis right
292 plot(t_GC(n0:nend)-t_GC(n0), T_GC(n0:nend),'LineWidth',lw,'
    Color',colors(7,:));
293 set(gca,'xcolor',colors(7,:),'FontSize',14); set(gca,'ycolor',
    colors(7,:),'FontSize',14);
294 lgd = legend('O_2','CO','H_2 *10','Temperature','location','
    bestoutside',...
295          'FontSize',f_leg);legend('boxoff'); title(lgd,'Legend'
             )
296 if numberTest == 22; xlim([0 552]);set(gca,'XTick', 0:50:552);
     end
297 if numberTest == 27; xlim([0 440]);set(gca,'XTick', 0:50:440);
     end
298 if numberTest == 36; xlim([71 720]);set(gca,'XTick', 0:50:720)
    ; end
299 if numberTest == 37; xlim([0 600]);set(gca,'XTick', 0:50:600);
     end
300 if  numberTest == 23;xlim([-0.0006 1200]);set(gca,'XTick',
    0:200:1200); ylim([35 300]);set(gca,'yTick', 40:40:300);
    end
301 if numberTest == 30; xlim([0 935]);set(gca,'XTick', 0:100:935)
    ; ylim([-1 101]); end
302 yyaxis left
303 xlabel('Time [min]','FontSize',f_label,'FontWeight','bold','
    Color',colors(7,:))
304 ylabel('Conversion [%]','FontSize',f_label,'FontWeight','bold'
    ,'Color',colors(7,:))
305 yyaxis right
306 ylabel('Monitoring Temperature[ C ]','FontSize',f_label,'
    FontWeight','bold','Color',colors(7,:))
307 if numberTest == 22 || numberTest == 23 || numberTest == 30
308     subtitle('Cat: 20%CuO/CeO_2/Al_2O_3 - ADP       GHSV =
        20000 h^-^1','FontSize',15,'FontWeight','bold')
309 end
310   %% Ulteriori grafici non riportati
311
312
313 %% Grafici separati tra rampa di riscaldamento e rampa di
    raffreddamento
```

```
314 if Riscaldamento_Raffreddamento == 1
315     T_i = T_GC(n0:nend);
316     ind = find(T_i > 280); ind = ind(end); ind_2 = find(x == x
           (end,1)); ind_2 = ind_2(end);
317
318     if numberTest == 27; ind = 25; end
319     if numberTest == 36; ind = 44; end
320     if numberTest == 37; ind = 41; end
321
322     range_R = [1 : ind]; range_C = [ind+1 : ind_2];
323
324     if Rid == 1
325         reaction_H = string(['Heating ramp with reduced
               catalyst']);
326         reaction_C = string(['Cooling ramp with reduced
               catalyst']);
327     end
328     if Rid == 0
329         reaction_H = string(['Heating ramp with oxidised
               catalyst']);
330         reaction_C = string(['Cooling ramp with oxidised
               catalyst']);
331     end
332
333     figure('NumberTitle','on')
334     plot(T_i(range_R),x(range_R,2),'-o','MarkerSize',ms,'
           LineWidth',lw,'Color',colors(5,:)); hold on
335     plot(T_i(range_R),x(range_R,3),'-o','MarkerSize',ms,'
           LineWidth',lw,'Color',colors(3,:)); hold on
336     plot(T_i(range_R),x(range_R,4),'-o','MarkerSize',ms,'
           LineWidth',lw,'Color',colors(4,:)); hold on
337     plot(T_i(range_R),x(range_R,1)/100,'-o','MarkerSize',ms,'
           LineWidth',lw,'Color',colors(6,:)); hold off
338     set(gca,'xcolor',colors(7,:),'FontSize',13); set(gca,'
           ycolor',colors(7,:),'FontSize',13);
339     xlabel('Monitoring Temperature [ C ]','FontSize',f_label,'
           FontWeight','bold','Color',colors(7,:))
340     ylabel('Species molar fraction [-]','FontSize',f_label,'
           FontWeight','bold','Color',colors(7,:))
341     lgd = legend('O_2','CO ','CO_2','H_2/100','location','
           bestoutside',...
342         'FontSize',f_leg);legend('boxoff'); title(lgd,'Legend'
               )
```

```
343     if numberTest == 27; xlim([40 307]);set(gca,'XTick',
            40:40:307); ylim([-0.0000002 0.015]); end
344     grid on; grid minor;set(gca,'MinorGridAlpha', 0.15);set(
            gca,'GridAlpha', 0.05)
345     subtitle({strcat("",reaction_H,'')},'FontSize',f_subtitle,
            'FontWeight','bold')
346
347     %% Ulteriori grafici non riportati
348
349 end
350
351 j = findobj('type','figure');
352 totalfig = length(j);
353 for i = 1 : totalfig
354     figure(i)
355     if title_on == 1
356         title(catalyst,'FontSize',f_subtitle,'FontWeight','
                bold')
357     end
358
359 end
360
361
362 %% Salvataggio dei dati e delle figure
363 %Salvataggio dati
364 Dati.ID=5.9; Dati.cat=catalyst; Dati.d_p = "45-200" ; Dati.
        h_cat = h_cat;
365 Dati.V_dot_IN = Vdot_in; Dati.WHSV = 35000; DAti.GHSV = 20000;
366 Dati.reacting_mixture = reacting_mixture;Nomi_tcd = [{'H2'} {'
        CO2'} {'O2'} {'CO'} ];
367 Dati.Nomi=Nomi_tcd;Dati.t=t_GC ; cal =[m_H2 m_CO2 m_O2 m_CO];
        int = [0 0 0 0];
368 Dati.calib_gas_slope= cal; Dati.calib_gas_offset = int;
369 Dati.Aree= p ; Dati.y_in = x_ref; Dati.y_out= x ; Dati.X=X;
370 Dati.T_in= T_GC(n0:nend);
371 Dati.n0 = n0; Dati.nend = nend;
372 Dati.t_plot = t_GC(n0:nend)-t_GC(n0);
373 %dati per confronto X
374 if  Riscaldamento_Raffreddamento == 1
375     Dati.XR = X(range_R,:);Dati.XC = X(range_C,:);
376     Dati.TR = T_i(range_R);Dati.TC = T_i(range_C);
377 end
378
```

```
Dati.UdM=["ID [mm]","MW_cat [g/mol]","d_p [um]","h_letto [mm
    ]",...
     "V_dot_IN [cm3/min]","WHSV [cm3/g_cat h]","t [min]", "y
        [-]",",X [-]","T [ C ]"];

save_fig = 1; save_data = 1;

if save_fig == 1
    h = findobj('type','figure');
    totalfig = length(h);
    set(h, 'Units', 'Inches');
    pos = get(h, 'Position');
    set(h,'PaperPositionMode','Auto','PaperUnits','Inches','
       PaperSize',[18, 9])
    [status_Data, mgs_Data, mgsID_Data] = mkdir(Dirfig);
    disp('Status_Data');disp(status_Data);disp('Message_Data')
       ;disp(mgs_Data);
    for i = 1 : totalfig
        figure(i)
        print('-dpng','-noui',[Dirfig 'Test' num2str(
           numberTest) '_' num2str(i)])
        savefig([Dirfig 'Test' num2str(numberTest) '_' num2str
           (i)]);
        h = gcf;
        print('-dpdf',[Dirfig 'Test' num2str(numberTest) '_'
           num2str(i)])
    end
end
if save_data == 1
    mkdir(Dirdata)
    save(strcat(Dirdata,'Test_',num2str(numberTest),'.mat'));
end
```